Choice of a unicellular organism: *Physarum polycephalum*

Dissertation submitted towards the degree
Doctor of Natural Sciences
– Dr. rer. nat. –

Jonghyun Lee

Bremen, August 26, 2019

Referees: Prof. Dr. Hans-Günther Döbereiner
Prof. Dr. Wolfgang Marwan

Universität Bremen

Abstract

Physarum polycephalum, a slime mould, is a unicellular organism with unique biological characteristics. One of its characteristics is the plasmodium, a vegetative state of *P. polycephalum*, which can be fragmented into microplasmodia and fuse back while maintaining its integrity as a unicellular organism. Starvation and a lack of glucose resulted in the formation of globular motile bodies that radially expanded, named 'Satellites', from microplasmodia, instead of a network. How these isolated fragments coordinate and reconstitute larger structures, and how this occurs without a centralized control were the main focus of this thesis.

Two different approaches were taken to investigate satellite growth. The first approach was to construct models to describe the satellite growth pattern with physical parameters. The distance travelled by the satellites showed a saturating increase and was consistent between the satellites from the same patch. Therefore, negative chemotaxis from a signal molecule was considered as a mechanism of propagation. The model was constructed based on diffusion of a signal molecule from the patch, and the length scale of the diffusion front as a function of the patch size matched the displacement of the satellites. Using this model, the diffusion coefficient of the signal molecule was calculated, which was within the range of known biological signalling molecules.

Also, a scaling relationship was derived based on the maximization principle, assuming that a starving organism would maximize the search area. This assumption is influenced by the optimal foraging theory, which predicts the foraging behaviour of organisms by assuming that the net energy intake is maximized. This scaling was refined with a fusion probability function, calculated based on diffusion and a typical distance between microplasmodia, as well as possible collisions between satellites. The refined scaling equations accurately described the observed number and the sizes of satellites. Based on these models, it is shown that a unicellular organism maximizes the search area even when they are fragmented, and uses a signal molecule to coordinate their behaviour.

Acknowledgments

I would first like to thank Dr. Hans-Günther Döbereiner. He has introduced me to the world of biophysics and has guided me throughout my Master's and PhD studies. He helped me to broaden my views on topics and gave the courage to try and tackle unconventional problems, and for that, I am a better scientific researcher today.

I would like to thank Dr. Adrian Fessel, who has helped a biologist with minimal physics background through extensive theories and models to analyse data. His advice and counsel made the experiments as well as the thesis much better.

I would like to thank Dr. Wolfgang Marwan for initiating the *Physarum polycephalum* research in our laboratory by providing the strains, as well as deep discussion and assistance in setting up and interpreting the growth of the organism.

I would also like to thank Anja Bammann, who kept the laboratory in pristine condition and prepared reagents for all my experiments. Without her, the quality of the data would not be so excellent and the experiment schedule not so fluid.

Special thanks to Christina Oettmeier, who had started the *P. polycephalum* work in the laboratory, established protocols and investigated optimal culture conditions for macro- and microplasmodia. Without her, this work would not have been possible.

Special thanks to the colleagues Malte Ohmstede, Julia Lange, Tanja Huxoll, Holger Doschke, Anna Piorecka-Ecken and for constant assistance and making every day enjoyable.

Changes and amendments

As discussed per the dissertation defence, Chapter 5: Complex behaviours have been removed. Instead, two chapters are added.

Chapter 5: Discussion, summarizes results from Part III: Results and evaluate whether the original hypothesis has been proven. Moreover, it explores some of the intriguing implications of the experimental observations and analytical results.

Chapter 6: Outlook builds on from the results and discussion to outline future experiments. This chapter is divided into three sections, detailing biochemical, biological, and biophysical investigations. The experimental designs and examples are given and cited, along with background information cross-referenced to the results section. The Author hopes that future researchers working on *P. polycephalum* find these helpful.

Contents

List of Figures

List of Tables

Part I

Introduction

Chapter 1

Introduction

Foraging is an essential behaviour of the living organism, as it directly determines the energy intake for survival and reproduction. It is integrated within the concept of natural selection, both as a selection pressure and the resulting adaptation, and it is also related to the niche of the organism [1,2]. Without proper foraging strategies, an organism would not survive.

To better explain and predict the foraging behaviour of organisms, a theory called Optimal foraging theory (OFT) based on natural selection was developed in the 1960s. Proponents of the theory assumed that efficient and effective foraging strategies would result in more energy gain, and therefore advantageous. This 'advantage' was characterized as Darwinian fitness, which reflected the ability to survive, produce and care for offspring. This foraging strategy was assumed to be heritable. Therefore, foraging strategies that gave a competitive advantage, or in other words, maximizing the Darwinian fitness were selected and passed down, while ineffective strategies died out. The organism, under the assumption of OFT, either maximizes the net energy intake or minimize the time of foraging to reach the required energy intake. The models based on OFT predicts optimal behaviour and the observed behaviours are compared to this optimum.

These foraging strategies may be present within us, without us even realizing it. For example, when foraging for berries in a farm, humans tend to move from bushes to bushes, without exhausting the berries in one bush [3]. This process of harvesting 'low hanging fruit' is intuitive and seem obvious when one wants to maximize the berries harvested per time spent. However, humans do not consciously calculate the rate of taking berries, nor do they attempt to estimate the quantity of the remaining berries. However, the berry foraging behaviour can be described, and predicted by a model based on OFT, which mathematically calculates the optimal behaviour. Therefore, some of the foraging patterns are optimized to maximize the energy intake, and in this particular case, the number of berries harvested.

One of the pioneering work based on the optimal foraging is the Marginal value theorem (MVT) by Charnov in 1976 [4]. He assumed a heterogeneous distribution of numerous patches where preys are found and calculated the optimal foraging behaviour of a predator. Since the predator consumes the prey in the patch, the rate of energy gain de-

preciates as the predator resides and exploits the same patch. Therefore, to optimize the foraging, the predator must decide when to leave the patch and explore the environment. The optimum is found when the predator leaves the patch when the rate of energy intake from the patch is equal to the rate of energy intake from the environment as a whole.

This formulation allows us to predict foraging behaviours, based on the quality of the individual food patches, or the environment as a whole. Locally, if the food quality is higher, i.e. a patch contains a lot of prey, predator should stay for a long time under MVT, as one intuitively expects. However, if the food quality is high overall, i.e. an environment contains a lot of high-quality food patches, then the optimal behaviour is to spend a little time on each patch, and quickly depart to look for another. This relationship between the food quality and the exploitation time based on MVT is seen in both controlled and natural environment, from various organisms [3, 5, 6]. The foraging of berries by humans, as described above, is one of the examples [3]. Therefore, based on OFT, these foraging behaviours are developed to maximize energy gain.

In developing MVT, Charnov assumed that the forager has prior knowledge of the environment and is capable of assessing the quality of the food patch. Based on these assumptions, optimal foraging behaviour was calculated. However, in most cases, the location of the prey, as well as the density of preys, are unknown to the forager. For example, even with technological innovations, there is no clear indication of where the fish are located in a sea. Therefore, fishing vessels cannot plan the paths to a voyage, but search as they explore. At the same time, fishermen also want to minimize the travel length to minimize the cost of operation, while maximizing the fish captured to maximize the financial gain [7]. These are the same line of assumptions that OFT takes, as the goal of both processes is to optimize the target currency.

However, instead of starting with a hypothetical optimal behaviour to analyze the foraging behaviour, the behaviour of an agent can also be described in detail first. The paths these fishing boats take during 'foraging' can be divided into turns and step lengths. Then, these type of movements can be simulated in various environments to assess its effectiveness as well as efficiency.

When the foraging paths of different organisms were analyzed this way, a common type of the step length distribution was found. This distribution, mathematically, is called Lévy distribution. In this distribution, the tail is heavier than the Gaussian distribution. Therefore, in Lévy distribution, the probability of longer steps are higher. This results in the movement of many small steps with infrequent, longer steps. This type of movement is observed from microswimmers to large birds, humans, and even fishing vessels, as described above [7–9]. When this type of step distribution was simulated and tested for its efficiency against a movement that has a Gaussian distribution, the Lévy distribution showed higher efficiency in finding food with fewer steps taken. Moreover, the analysis shows that this type of movement is the most efficient method of foraging in a wide range of environmental conditions, when it was compared with other movement types [8, 10].

Both the behavioural predictions from MVT and the Lévy distribution of step length are observed from a wide range of organisms, from humans to unicellular organisms. The prevalence of these traits is intuitively understandable, as these behaviours are shown to optimize the net energy gain and therefore maximize Darwinian fitness. However, does this mean that all the underlying assumptions of the OFT are true? MVT assumes that the forager has prior knowledge of the environment, and can quickly estimate the quality of the food patch. This would be a difficult task for a human, and likely improbable for simple, unicellular organisms. Do organisms consciously make large steps after many small steps, to fit their movement into Lévy distribution? How are these strategies exhibited in such a wide range of organisms with varying degrees of differentiation?

On this end, we are far away from a molecular understanding of complex behaviour. However, optimal foraging of simpler organisms provides hints that the optimality does not necessarily require a high level of differentiation and development. To make optimal decisions, an organism must be able to assess and evaluate information. The complex cognitive abilities are associated with neurons and brains, and therefore it was previously assumed that only organisms with brains were capable of complex behaviours [11–13]. However, simple organisms are also capable of detecting and responding to signals that are present in the environment. A growing number of publications also describe the complex behaviours of simple organisms [14–19].

Therefore, an investigation of foraging strategies of a model organism provides ample opportunities to clarify how the foraging behaviours are generated. If a simple model organism can react to an environment and alter its behaviour to optimize its survival, there must be mechanisms which allow these type of optimization within the model organism.

Physarum polycephalum therefore provides researchers with a unique avenue into the evolutionary adaptation of survival and foraging. The slime mould separated from humans, as early as one billion years ago, and is a unicellular organism. However, this slime mould exhibited some complex behavioural patterns that were only expected from highly evolved organisms. One of this behaviour is a speed-accuracy tradeoff, where the accuracy of the decision is reduced when less time is given to make a decision [20, 21]. Another is that given a choice with multiple options, the slime mould can make an irrational choice [22].

Understanding the underlying mechanics of the foraging and decision-making of a simple organism has a significant implication on a wide range of disciplines that investigates any type of animal behaviour. There are three main advantages of working with a simple model organism to study decision-making. First, a mechanism utilized by *P. polycephalum* should be simpler to describe due to the relative biological simplicity of this model organism. Second, efficiency or capability of this decision-making mechanism can be tested more easily, and applicable tests can be developed to quantitatively measure how good this mechanism is. Third, the possibility of universality in a decision-making mechanism can be explored. If a certain property of decision-making is shared between an organism of the highest and lowest complexity, it would be worth investigating why

this is so.

1.1 Motivation

The field of biology began with observations. Advancements of optics brought on the discovery of the cell through a microscope, which visualized the length scales that were not visible to the naked eye. Voyage to the previously uncharted territories, such as Galapagos islands, inspired natural selection theory. Techniques are concurrently and continuously improved and innovated to make what previously unseen to the visual realm.

However, the data collected with these techniques are also becoming more and more unintuitive. Now we observe electric signals on membranes, fluorescence, and fragment patterns of small molecules that require interpretations to have any biological relevance. Quantitative and rigorous analyses are required to detect small changes that may be hidden under noises.

A field of biophysics utilizes methods of physics to study biological systems. It categorizes and quantifies the observations into variables and parameters, find relationships and correlations, and construct models to describe the observation. A model can be constructed to purely describe the outcome of the behaviour without any underlying biological implications. A model can be also conceived based on known processes, such as a laminar flow or chemical reaction to produce a mechanistic model. The latter model produces parameters that can be altered and make predictions on the outcome, which then can be tested on the biological model.

These models help predict future behaviours and discover hidden implications within the behaviour that are not obvious. A simple observation of the behaviour does not infer any intent or goal of an organism, nor does it assess whether this behaviour is good or bad. However, by simplifying these observations into parameters, one can attempt to describe the trend of the behaviour, and predict future behaviours from it. The relationship between the variables and parameters may provide hints to infer mechanisms that drive the behaviour. This is the case of Lévy walk distribution, where the movement of the organisms was described first, and then the usefulness of this movement was identified subsequently.

Not only the description of the behaviour can lead to the identification of the mechanism, but also appropriate assumptions on its behaviour may reveal different characteristics of the behaviour. This is the case of OFT, where assumptions based on maximization predicted certain behavioural characteristics of foraging, such as leaving the patch sooner when the food quality is very high. When these trends from the model fit the observed behaviour, then one can also infer that the observed behaviour is consistent with the underlying assumptions of the model. When a model constructed based on the OFT accurately matches the observations made from an organism, one can argue that this particular organism is foraging optimally.

Recently, an alternative growth of *P. polycephalum* was observed [23], which had not been documented before. A typical network formation was bypassed in favour of motile fragments, which moved away from each other. The pattern was visually striking due to the temporal coordination of fragments. To better understand why this alternative growth occurs, and what type of possible benefits it provides to an organism, a biophysical approach was considered most appropriate. By constructing models to describe the alternative growth of *P. polycephalum*, and examining the principles behind the models, one can reveal why this alternative behaviour occurs instead of the typical network growth.

One does not usually think of microorganisms and complex and intelligent behaviours. However, bacteria and other microorganisms are capable of adapting to an environment and cooperating to demonstrate complex behaviour [24]. It is highly intriguing that these traits, typically associated with multicellular organisms with specialized organs, can be seen from the entities without it. How can a simple organism take different information, process it, and make a decision that is comparable with organisms with dedicated sensory organs and brains?

One of the characteristics shared between the unicellular and the multicellular organism is a decision of differentiation [25]. In multicellular organisms, an undifferentiated cell divides and produces a wide array of specialized cells that becomes different organs. However, this is also seen in a slime mould, a unicellular organism. For example, a cellular slime mould *Dictyostelium discoidium* generally forages as a single cell, but upon certain types of signals, cells aggregate and form a multicellular structure to produce spores [26]. A true slime mould, *P. polycephalum* also differentiates to form stalks and spores, but in this case, one cell is divided and differentiated to give a complex structure [27]. Many of the differentiation and cell division studies were conducted on *P. polycephalum* as a model organism. Therefore, not only investigating the complex behaviours from a simple organism worthwhile, it seems even advantageous due to the simplicity.

Moreover, the growing number of evidence on complex behaviours from *P. polycephalum* is staggering [20,22,28–35]. Some of these behaviours and characteristics were previously attributed to organisms with neurons and brains since it was assumed that these organs were needed to process information and make decisions. However, while there have been many parallels drawn between the behaviours of a single-cell organism and more 'evolved' organisms such as mammals, no systematic approaches have been taken to compare and assess the complexity of these behaviours.

Therefore, the alternative growth of *P. polycephalum* provided an opportunity to assess whether this unicellular organism possesses cognitive abilities. Based on biophysical modelling approaches, one can infer the mechanisms and advantages of alternative growth. Detailed understanding of these mechanisms in a simple model organism would further aid in investigating complex behaviours in other organisms.

1.2 Objectives

The primary objective of the thesis is to investigate and gain insight on a foraging behavioural spectrum of our model organism, *Physarum polycephalum*. Specifically, the work is focused on an alternative growth pattern occurring near nutrient depletion, where instead of forming a network, *P. polycephalum* forms local aggregates and exhibits directed motility with stable morphology. These motile fragments are termed 'satellites', and the growth that produces satellites are referred to as a 'satellite growth', to differentiate from a 'network growth'. The change from network to local aggregate is observed systematically as a function of microplasmodial age and nutrient availability.

The satellite growth was modelled with two different approaches. First, the characteristics of the behaviour were captured, and the correlations between variables and factors were sought. Based on this description, a possible mechanism was inferred that caused alternative behaviour. Different aspects of growth were characterized, including the change in the area, the change in the number of objects, and the movement of the organism. Based on the correlation between the variables, parameters are identified, such as the decay constant to describe the change in the number of objects, and the diffusion coefficient to describe how fast the slime mould moved. These parameters are used to infer possible mechanisms that caused certain aspect of the satellite growth, and used to construct and refine the subsequent model based on maximization.

Second, a model was established based on a maximization principle. Then, the observed behaviour was compared with the prediction from the model. Since the satellite growth was observed during starvation, it was considered a foraging behaviour. Therefore, it was assumed that by maximizing the search area, the probability of encountering a new food source was also maximized. Based on this model, scaling relationships are derived that describe the satellite growth, which is then compared with the observation. The agreement between the observed and the predicted outcome validated our underlying assumption of maximization.

1.3 Outline

The thesis first reviews an optimal foraging theory, which inspiration for a model to assess the foraging efficiency was drawn from. The history of how this theory has come to be implemented in biological systems, as well as main assumptions and the validity and successes of models, are discussed. Marginal value theorem (MVT), as well as Lévy walks, are discussed as a part of describing foraging behaviours.

Then, the model organism *P. polycephalum* is reviewed, beginning with biological classification and characteristics unique to the model organism. The life cycle, as well as the unique characteristics that allow the experimental design of the thesis is explained. Previous studies on *P. polycephalum* are also highlighted, with a focus on the description of foraging and modelling.

The alternative growth pattern, which is named 'satellite growth' is then introduced. In the typical growth, small fragments called microplasmodia come together to form one giant network. In the satellite growth, these fragments create local motile aggregates, which is termed 'satellites'. Some works regarding the discovery and initial characterization of the growth were performed as a part of the author's Master's thesis and are briefly reviewed to aid in readers' understanding.

The characteristics of the satellite growth is described in both qualitative and quantitative manner. Different phases of the alternative growth are defined first qualitatively based on observation based on the publication by the author [23]. How the satellite growth is affected by the age, as well as the environmental conditions, are shown.

Then, the satellite growth is analyzed with image processing and digitization and reduction of information. In here, the growth is described in numbers and parameters, such as area and growth rate. The phases defined with qualitative observation is matched with the change in the variables and parameters. The satellite growth is differentiated from the other growths based on these parameters. A preliminary investigation on the motility of the microplasmodia, their diffusivity, as well as their step length distribution, is also stated.

The satellite growth is analyzed in two different time and length scales. From initial conditions to the building of satellites, the behaviour and the movement are characterized in the level of microplasmodia. Each microplasmodium of *P. polycephalum* is measured in its steps, angles as well as its mean squared displacements. These measurements are used to calculate diffusive properties and step length distribution, to determine whether *P. polycephalum* performs a Lévy walk. Moreover, these parameters are compared between satellite and network growth to determine how the different growth is initiated from a similar initial condition.

The macroscopic perspective analyzes the entirety of the satellite growth from the start to end. Two models are introduced to describe the satellite growth pattern. The first model is based on the diffusion of a signal molecule, and it describes how far the satellite travels. The second model is based on the maximization principle, and it describes the number and size of the satellites. Both models are compared with empirical data, and goodness of fit and the implications of the assumptions behind the models are discussed.

Finally, the satellite growth is discussed as a whole, and further investigative points are given.

Part II

Background

Chapter 2

Optimal foraging theory

2.1 Inception

Mathematically, an optimization problem can be approached by first choosing an appropriate currency. Then, cost-benefit functions are established and an optimum is sought [36]. These optimizations, originally utilized in engineering and economics, were imported to biology to explain the diversity of life in the 1960s. The logic behind the application of optimization into biology stems from natural selection, where complex behaviours and characteristics all contribute to survival and reproduction. It is assumed that these behaviours are heritable and better and more efficient behaviours for survival are more likely to be passed down, eventually becoming a dominant behaviour. The 'currency' to be optimized is called 'Darwinian Fitness', which is the contribution of an individual to the next generation [37, 38] Specifically, feeding and foraging behaviours were considered particularly appropriate for such an analysis, since they were directly involved in energy gain for the organism. This approach of mathematical and analytical maximization falls under optimal foraging theory (OFT).

To apply an optimization method to model foraging, several assumptions are made for an optimization process to be applicable.

- Darwinian fitness of an organism depends on its behaviour while foraging [38]. This contribution to fitness may be genetic, or cultural.
- A foraging behaviour is heritable, whether it is genetically inherited to offspring or learned from parents [37, 38]. Therefore, based on the first two assumptions, the fitness of the population tends to increase over generations.
- The relationship between fitness and foraging behaviour is known. This is the currency of fitness [38] and is the target of optimization.
- The foraging behaviour reaches near optimum before the relevant constraints change. Therefore, it is assumed that a foraging behaviour is optimal.

Therefore, models were constructed based on optimizing an energy gain, which maximizes Darwinian fitness. A point of contention is that this implicitly makes an assumption that the complex behaviour has already become prevalent because it contributed to

Darwinian fitness, and is not testable [37]. The criticisms and counterpoints of optimal foraging are covered in detail in a subsequent section (Section 2.2).

Analyses on optimal foraging can be divided into 5 categories [38, 39]:

1. Diet
2. Patch choice
3. When to leave a patch
4. Movement
5. Central place foraging

Generally, these optimal foraging theory concerns with the behaviour of one predator while they are foraging [38]. An optimal behaviour between individuals and species where competition influences the behaviour led to the application of the game theory in biology [40, 41].

2.1.1 Marginal value theorem

One of the earliest, and most widely utilized model based on the OFT is the Marginal value theorem (MVT) proposed by Charnov [4–6]. The theorem defines an optimal time a forager should spend exploiting a food patch before leaving to achieve maximum energy intake. It assumes that food items are distributed in patches, and it is limited and non-regenerating. Therefore, as a predator exploits the patch, the rate of food intake decreases, which results in a diminishing return. Therefore, the energy intake as a function of time while predator remains in the patch rises to an asymptote. There are different types of patches with different qualities, i.e. a different asymptote. MVT then finds the behaviour of the predator that maximizes the energy gain. Based on the calculation, Charnov concluded that the maximum energy gain is achieved if the predator leaves the patch when the 'marginal' rate of energy gain from the current source is equal to the average rate of energy gain of the entire system.

The model is interesting and useful in that it leads to testable predictions of behavioural characteristics [38, 42]. It gives a quantitative prediction on exploitation time as a function of food quality. If a patch quality is increased, then the time spent exploiting a patch, or in other words, a giving-up time of a predator to abandon the present patch is also increased. However, an increase in the overall quality of the system decreases the exploitation time of a patch. Therefore, when there are high-quality food sources everywhere, a forager would quickly move from one patch to the other. Moreover, exploited patches in a sufficiently large system would have the same amount of food remaining after foraging.

The MVT has been extensively tested in both controlled and natural habitat. One of the earliest supporting evidence was gathered from chickadees, where higher quality patches resulted in lower exploitation time of the patches [43]. The researchers have

constructed artificial trees with cones that contain worms, and grouped the cones based on the number of worms, then defined a giving-up time as an interval between the last consumption of the worm from the patch and leaving the patch. The giving up time was consistently shorter in food-rich patches than the food-poor patches. Moreover, the giving-up time was quantitatively predicted based on the ratio of energy intake rate, or in this case, a capture rate. They found that the giving-up times indeed matched the ratio between the patch qualities. Intriguingly, the foraging method with certain giving-up times can also be described in simple heuristics, which is discussed later (Section **??**).

An extensive review of MVT was performed in 2001, in which previous studies were examined to see how well the theory was supported with experimental data [6]. The study found a general trend that the organisms stay in the patch longer than predicted by the MVT. There are several factors not considered in MVT, such as predation risk, mating and reproduction. The MVT model was compared with the more complex state-dependent model based on its state determined by the internal energy. The simulations showed that the state-dependent models performed better than the MVT in optimizing the fitness of the organism. Moreover, there was only a narrow range of environmental conditions where MVT performed optimally. It was concluded that optimal behaviour was not 'synonymous with net intake-rate maximization'. However, the researcher also noted that MVT was a reasonable starting point, and qualitative predictions will continue to remain valid.

Most recently, foraging of Adelie penguins was observed to test the MVT [5]. Authors were able to capture an individual prey capture event by the acceleration of the penguin's head relative to the body. Also, the prey in this study is distributed as patches with different prey densities in the water, matching the assumptions of the MVT. Penguins only performed a dive to forage and could capture multiple preys during a dive. They also found that penguins made successive dives, which they termed a dive bout. With successive prey capture event, they sought to validate the assumption of diminishing return of the same patch. They found that the diminishing return was also seen in the observation. However, the curves were not a simple decelerating curve with an asymptote as MVT assumed, but close to a sigmoid function.

Moreover, they plotted the dive length against the quality of the patch and the system. To do this, they first calculated the quality of the patch from an individual dive, and the quality of the system from a dive bout. The results supported the prediction from the MVT and showed a positive correlation between the dive length and the patch quality, and negative correlation between the dive length and the system quality. They also tested the MVT model against other models derived based on experience, which showed that the MVT better explained the trends in the dive duration.

The MVT model assumes that the fitness increases linearly with the energy intake, as well as a priori knowledge of the system by the predator. Further theories were developed to account for random variables and unknown patch qualities [38].

2.1.2 Lévy flight and Lévy walk

To study the movement of the organism, a common method is to study its move length and how it is distributed [7]. To this end, the movement data is generally broken into steps and turns. The angles can determine whether the movement is truly random, or there is a preferential direction of turns. The distribution of the step length and the probability can show a typical length the organism explores the environment. The step length distribution can be fitted to a general power law, where the exponent μ describes the shape of the distribution. Lévy flight describes a family of random walk with a characteristic distribution of step length l defined by:

$$P(l_j) \sim l_j^{-\mu} \tag{2.1}$$

with $1 < \mu < 3$, where $P(l_j)$ is the probability of a given step length l_j to occur.

The mathematical definition of the Lévy flights originates from Paul Lévy in 1930s [44, 45]. He investigated the distribution of sums of random variables p_n with infinite moments, i.e. the expected value of the random variable is infinite. Lévy wanted to find distributions where the sum of n steps $p_n(x)$ would be the same as the $p(x)$, with some scale factors. This is the same property shared by fractals, where parts of the whole resemble each other. He found a simple form in a Fourier space where this is true: $p_n(k) = exp(-const \times n|k|^\alpha)$ for $0 < \alpha \leq 2$. Inverse Fourier transformation results in equation 2.1. It becomes a Gaussian distribution if $\alpha > 2$, due to the central limit theorem [8]. However, the distributions have infinite second moments when $0 < \alpha \leq 2$. This property describes the family of Lévy distributions.

Lévy flight is a type of a movement called a random walk, where the step length is defined by the Lévy distribution, with directions of each turn being randomly chosen. However, in that case, the average step length is infinite, as it has infinite moments. Moreover, in the description of the Lévy flight, steps occur instantaneously, which is physically implausible. One way to circumvent the infinite length steps is to couple the steps with the time that it requires to complete the step. The derivation of the dynamics of random walker which performs Lévy flight, based on time instead of the number of steps is called Lévy walk [46].

One may also introduce a detection radius which an organism can detect the presence of food along the step lengths, and stops and turns towards the food once the food is detected within the radius. This also limits the length of the step, leading to a truncated Lévy distribution [8, 47]. The distribution arising from this truncation is called a truncated Lévy flight, and this distribution eventually converges to a Gaussian distribution due to the central limit theorem. However, this convergence takes a large number of independent variables, or in this case, steps. Without convergence, the truncated Lévy flights are effectively indistinguishable from Lévy flights in terms of statistical properties [47]. Due to the limitations of physiological and temporal limitations, a truncated distribution is thought to be more appropriate in describing the biological system [9].

It has been suggested that the Lévy walk may be observed in a wide range of organisms [8, 44, 48]. Due to the fractal property of the Lévy walk, it is advantageous during searching to reduce revisiting, and therefore may be positively selected by natural selection [7]. This may also be interpreted as an adaptation to the fractal properties of the ecosystem, as the prey distribution may also be fractal. Some seed dispersal under specific weather conditions fit the Lévy distribution [45]. Moreover, Lévy flight exhibits superdiffusive property, which may reduce competition between foragers [7].

Viswanathan et al. demonstrated in 1999 that the Lévy flight is an optimal foraging strategy for an organism under certain conditions [8]. The researchers constructed an idealized model of a forager in an environment where food is randomly distributed. A forager has a vision distance r_v and moved towards a target if there is food within this radius. If there is no food within r_v, the forager moves with a step length chosen from a Lévy distribution. A forager can search for food as they move along and terminates its step if food is detected to move towards the target. In this model, the forager did not perform Lévy flight when food was plentiful since long steps were practically non-existent. If the foraging was destructive and the food site could not be revisited, the forager performed ballistic motion until it encounters food. Under the conditions of non-destructive foraging with sparsely located food, foraging efficiency was the highest when $\mu = 2$. Therefore, Lévy foraging is most advantageous in an unknown environment with non-destructive foraging.

This hypothesis was tested on the Hazda tribe from Tanzania that maintained traditional hunting and gathering lifestyle without technological aid. After monitoring their foraging bouts with GPS, researchers found that humans indeed exhibited Lévy walk during foraging [9]. However, the parameters for the Lévy walk differed between men and women, and researchers attributed this to a different target of foraging. Men hunted wildlife and searched for honey, whereas women foraged berries and other plant foods, which were distributed with different densities in the environment.

Lévy flight was not exclusive to a direct foraging movement from an organism, but also other types of movement such as from a fishing vessel [7]. Utilizing satellite vessel monitoring systems to monitor the movement of the fishing boats, they found the step distribution of the vessels can be described with Lévy distribution. Moreover, the mean of the Lévy exponent μ from the fishing vessels was 2, the same optimum obtained from [8]. Researchers suggested several reasons why the fishing vessels may have similar foraging behaviour as natural predators. First, the locations of the fishing schools are, even with the advancement of technologies, are unknown to the forager. Second, both foraging maximizes the currency. While natural predators maximize energy intake, while the fishing vessels attempt to maximize financial gain. Therefore, even though the length scale of the foraging via a fishing vessel is much larger, the Lévy flight was still the optimal movement pattern.

However, it is not to say that the organism purposely exhibits random walk with step lengths of Lévy distribution, rather than organisms in some circumstances have movement patterns that resemble Lévy flight [45]. Moreover, OFT may not be the sole reason

that Lévy walk was developed. This movement pattern can be observed in situations not related to foraging, and some cases may be a byproduct of the mechanism of movement. Distribution resulting from random diffusion may naturally create Lévy distribution. Seeds and spores may also be distributed as a fractal-like spatial structures [45]. One of the most intriguing utilization of the Lévy distribution properties is observed from *Chamydomonas reinhardtii* [45, 49]. This alga used flagella to cause nearby particles to acquire Lévy characteristics. Since algae inhabit in a low Reynolds number environment, the movement of the algae is not as crucial since most of the surrounding environment moves with the algae. Therefore, the enhancement of diffusion allows algae to increase its foraging efficiency.

Overall, Lévy walks have been observed from the following organisms: albatross [50], reindeer, jackals, microzooplankton, seals, spider monkeys [7, 51], protein motors, fossil traces, bacteria, T cells, molluscs, bees, and human hunter-gatherers [45]. It was also demonstrated in our model organism, *P. polycephalum* [52]. The widespread demonstration of this type of movement has caused a debate on the origin of this foraging movement. There are two arguments over the origin, one arguing that it is an emergent property in response to the natural environment, while the other side argues that it was developed through evolution and natural selection [10].

Wosniack et al. in 2017 showed through extensive modelling of various type of food distributions, that the Lévy walk emerged as the best strategy in majority of these environments [10]. As long as the target density is low and the forager's information is limited to its vicinity, the Lévy walk was optimal in finding food. The other emergent strategy was the random walk when the density of the food patches was high. The researchers have measured the search efficiency in various landscapes, with different step length distribution of movement defined by the Lévy parameter μ. The ballistic and random movements were represented with μ of 1 and 3, respectively. They found, that only in the cases of landscapes with high-density food sources, the search efficiency was maximum in random movements, and in all other cases the Lévy walks with $\mu \approx 2$ demonstrated the highest efficiency. Researchers therefore argued, the robustness of the Lévy strategies favours evolutionary origin hypothesis. Moreover, the Lévy walk can essentially assume characteristics of a random walk with frequent encounters of food causing truncation of the long steps.

One can analyze and describe the diffusive properties of the movement [7, 53], with equations such as:

$$< R^2(t) > \propto t^c \tag{2.2}$$

where $< R^2(t) >$ is the mean squared displacement. In random walks with diffusive properties, the exponent c is expected to be 1. However, in a Lévy walk the mean squared displacement increases faster than a normal diffusion, with an exponent between 1 and 2 [51].

Based on an Einstein relation, it is known that in a Brownian motion the mean squared displacement is proportional to the time squared [53]. This is also the case when

$\mu \geq 3$ for equation 2.1, where step lengths fit the Gaussian distribution. When $\mu \leq 1$, the motion is ballistic, and the displacement is proportional to the time, instead of time squared [54]. Lévy walks lie in between the ballistic and Brownian motion.

2.2 Criticisms and validity

There have been many criticisms on the optimal foraging approach. One of the most prominent paper that faults the OFT is from Gould and Lewontin [55]. In the paper, they list four arguments typically used by researchers when the OFT fails:

1. Attempt another explanation from optimal foraging. The paper did not fault or discourage newer interpretation of old results. However, it suggested that the focus should be widened to consider alternatives.

2. Assume that an explanation exists that can be explained with OFT.

3. Assume that imperfect understanding of the organism and its surrounding is the main reason why OFT could not be applied.

4. Focus on immediate usefulness of the form or function, and disregard other possible advantages.

They suggest that rather than observing a trait of an organism as an individual entity, a holistic approach must be taken to understand the behaviour and characteristics of the organism.

In response to these criticisms, Parker and Maynard Smith [56] have rebuked in a review that OFT does not assume nor trying to prove that an organism is optimally adapted. Rather, it is to understand a specific example of adaptation through an explicit model. The model produces predictions based on a set of assumptions. A model can be inappropriate if the assumptions are false or not well-grounded, and its predictions are not absolute. When consistency is found between the model and observation, then the underlying assumptions may be consistent with what occurs.

As stated above from a review [6], even the most prominent theory from the OFT fails to predict quantitatively the behaviour of organisms. Although Lévy walks can demonstrate good performance in many different environments, more specific models based on environmental conditions can be constructed that can outperform Lévy walks. However, under the conditions where those assumptions about the environment and the behaviour of the organism are correct, then the model may produce a result that is consistent with the observation.

Two models, the MVT and (truncated) Lévy walks, represent the two ends of the optimal foraging modelling. The MVT presupposes all the knowledge and solves for a mathematical optimum from a theoretical perspective, and its applications in biological systems have been successful only in a qualitative sense, leaving a room for practical and biological considerations. Lévy walks, first observed from a wide range of biological

systems and fitted to a physical model, assumes that the forager has limited knowledge. The strategy appears to be always beneficial, albeit seldom optimal, in a wide range of landscape owing to its property of superdiffusion and scale-invariability. Nonetheless, relative successes of both models suggest that the foraging behaviour is under natural selection and is being influenced by natural selection pressure.

Chapter 3

Physarum polycephalum

Physarum polycephalum is a unicellular organism, commonly referred to as a slime mould. Its morphology, as well as its developmental cycle, is similar to that of a common fungus, which led to the misnomer as well as the initial false classification.

In this chapter, the biological characteristics and the previous studies that utilized *P. polycephalum* are reviewed. These serve as a basis of the experimental design of the thesis and interpreting the observed behaviour of experiments.

3.1 Biology

P. polycephalum is a unique unicellular organism that exists in a wide range of length scales. Most, if not all of the experiments conducted for this work simply cannot be performed with other model organisms. To clarify and explain why this is so, this section is dedicated to describing the biological properties of *P. polycephalum*.

3.1.1 Classification

The goal of this section is to state how *P. polycephalum* is defined and classified biologically, with important evolutionary diversions. This will aid in understanding the uniqueness of *P. polycephalum*, as well as to bolster the argument regarding the universality of the aspects investigated in this study.

Current classification of the *P. polycephalum* is based on the publication of Adl et al. from 2012 [57]. Following is the name of each classification with small descriptions.

Eukaryota (Domain)

Amorphea (Super-group) This group, just below the Domain, is the least inclusive clade containing: *Homo sapiens*, *Neurospora crassa*, *Dictyostelium discoideum* and *Physarum polycephalum*. Cells belonging to this clade do not have a fixed form unless restricted by an external layer. This is the last common ancestor of *P. polycephalum* and

Homo sapiens.

Amoebozoa (Super-group / Phylum) The fossil record of Amoebozoa can be traced back up to 750 million years ago [58]. This implies that *P. polycephalum* as well as other slime moulds have already diverged from other animals, including humans at this point.

Conosa (Subphylum) These organisms have complex microtubular skeleton structures at some point in their life cycles. Some Conosa (e.g. *Dictyostelium*) have extensive cytoplasmoic microtubules [59].

Mycetozoa (Infraphylum) This clade specifically groups all slime moulds. This infraphylum contains *Myxogastria* and *Dictyostelia*. This is the last common ancestor of *P. polycephalum*, a true slime mould, and *D. discoideum*, a cellular slime mould [60]. A cellular slime mould is unicellular, and differentiation occurs when multiple of these cells are aggregated and interact with one another. In a case of a true slime mould, a single cell differentiates, more akin to the development of embryos.

Myxogastria (Class) These organisms are free-living amoebae. They perform cell division without cytokinesis, which leads to multiple nuclei in one cell called plasmodium. They take nutrients by decomposing dead matters. This class is further divided into orders, based on the colour of the spores they produce.

Physareles (Order) These organisms produce dark-coloured spores, and lime deposits are found in parts of the fructification [61]. This order contains family *Physaraceae*, genus *Physarum*, and finally, species *Polycephalum*.

3.1.2 Life cycle

Organisms commonly known as slime moulds have a complex life cycle spanning both diploid and haploid states. *P. polycephalum*, a true slime mould (*Myxogastria*), forms a large coenocyte called plasmodium. Coenocyte describes a multinucleated cell that does not undergo cell division, resulting in multiple nuclei housed in a single membrane. Phaneroplasmodium, or a plasmodium, is the dominant and most prevalent form of *P. polycephalum*. At this diploid stage, *P. polycephalum* propagates and constructs a network, which many of the studies take advantage of its efficient and robust design [34]. Plasmodia grow indefinitely, as long as nutrients are supplied [62]. The number of nuclei is proportional to the size of the plasmodium, and all nuclei in a plasmodium are synchronized in cell cycle [27,63].

Under certain conditions, a plasmodium differentiates into spores. There are specific signals that the organism requires to commit to the sporulation. These are starvation, activation of blue light photoreceptor, and red light photoreceptor [27]. The sequential event of sporulation has been investigated in detail. The commitment to sporulate occurs much earlier than any of the visual differences are exhibited. After all the signals are received and maintained for at least 3 to 6 hours, then the organism commits to sporu-

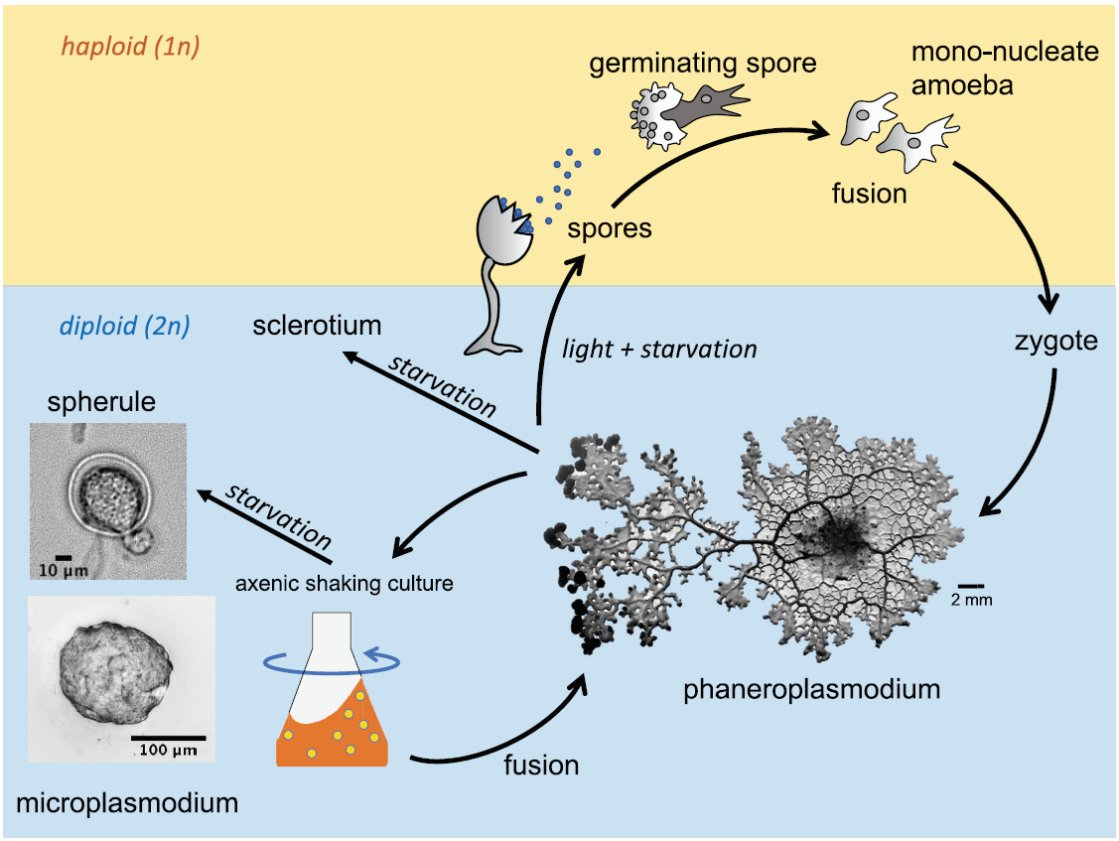

Figure 3.1: Life cycle of *P. polycephalum*, adapted from [25]. The vegetative form, the phanero- or macroplasmodium is generally arranged as a network. With appropriate signals, macroplasmodia differentiates into fruiting bodies and spores. Spores are then released, becoming haploid amoebae. When two amoebae fuse, then a diploid zygote is formed. This zygote then grows to become a plasmodium, completing the life cycle. Artificially, macroplasmodia can be broken down into microplasmodia by submerging a plasmodium into the liquid culture and applying a shear force via shaking. These microplasmodia, when placed back on a solid substrate, fuse to form macroplasmodia, thus completing an 'artificial' life cycle. At any point, macroplasmodia and microplasmodia can assume a dormant form when the surrounding environment is unfavourable to growth. These are called sclerotium and spherule, respectively.

lation. Then, after 10 hours from the initial onset of the signals, the plasmodial body breaks into smaller nodular structures. These structures differentiate into fruiting bodies, and haploid spores are formed within these structures. The entire process throughout the plasmodial body is synchronized within 15 minutes [64].

The resulting amoebae are haploid with a diameter of 10-20 µm. These amoebae can also undergo mitosis and increase their population. When they are subjected to a moist environment, they develop two flagella and swim. In a flagellated form, they cannot undergo mitosis. In a dry environment, the flagella are retracted and amoeboid movements are resumed. They can also assume a dormant form called cysts when they are faced with harsh conditions. Two amoebae fuse to give rise back to a plasmodium, which completes the life cycle [65].

3.2 Microplasmodia

Although an uncontaminated culture of *P. polycephalum* has been reported as early as 1939, these early cultures were only maintained in insoluble natural media such as oat flakes.

First reported *P. polycephalum* culture in liquid, and therefore the first creation of microplasmodia is reported by Daniel and Rusch in 1961 [66]. Originally, it was not the researchers' intention to establish a *P. polycephalum* culture in a liquid, but rather for detailed nutritional and biochemical investigations. A macroplasmodium was submerged in a liquid medium and constantly shaken, which caused fragmentation and produced microplasmodia. The size of microplasmodia varied from a fragment containing a few nuclei to a fragment with thousands of nuclei [67]. Extensive studies on microplasmodia were published from 1979 to 1991, detailing classification, morphology, locomotion and more [68–73].

According to Gawlitta et al. [68], microplasmodia are divided into three groups based on morphology:

1. Spherical (100 - 150 µm in diameter) and rod (10 µm in diameter, 50 µm in length). These do not exhibit vigorous protoplasmic streaming.
2. Amoeboid (50 - 100 µm in diameter).
3. Symmetrical (200 - 400 µm in length). These exhibit regular protoplasmic streaming

High rotation frequency of the shaking favours the creation of spherical microplasmodia, while in lower rotation frequency small networks of microplasmodia are found. The difference is likely caused by the difference in shear force which fragments the large components. The researchers noted that the amoeboid microplasmodia bear similarities with another protist, *Amoeba proteus* in structural organization and movement. The dumbbell-shaped microplasmodia were more similar to macroplasmodia, with regular shuttle streaming. Both types of microplasmodia lacked cortical filament layer, which is required for motility [74].

Microplasmodia exhibited reduced endocytotic activity compared to other plasmodia grown on solid surface [69]. Possible reasons of this reduction may be the need to make close contact to a solid substrate so that food can be ingested, or extensive slime layer produced during the submerged stage of the microplasmodia reducing the efficiency of endocytosis.

Microplasmodia in suspension lacks a fibrillar actin system, but after 30 minutes of incubation on a solid surface, tiny spikes begin to form at the surface of the cell. After 60 minutes these spikes turn into small pseudopodia, and the number of fibrils reaches

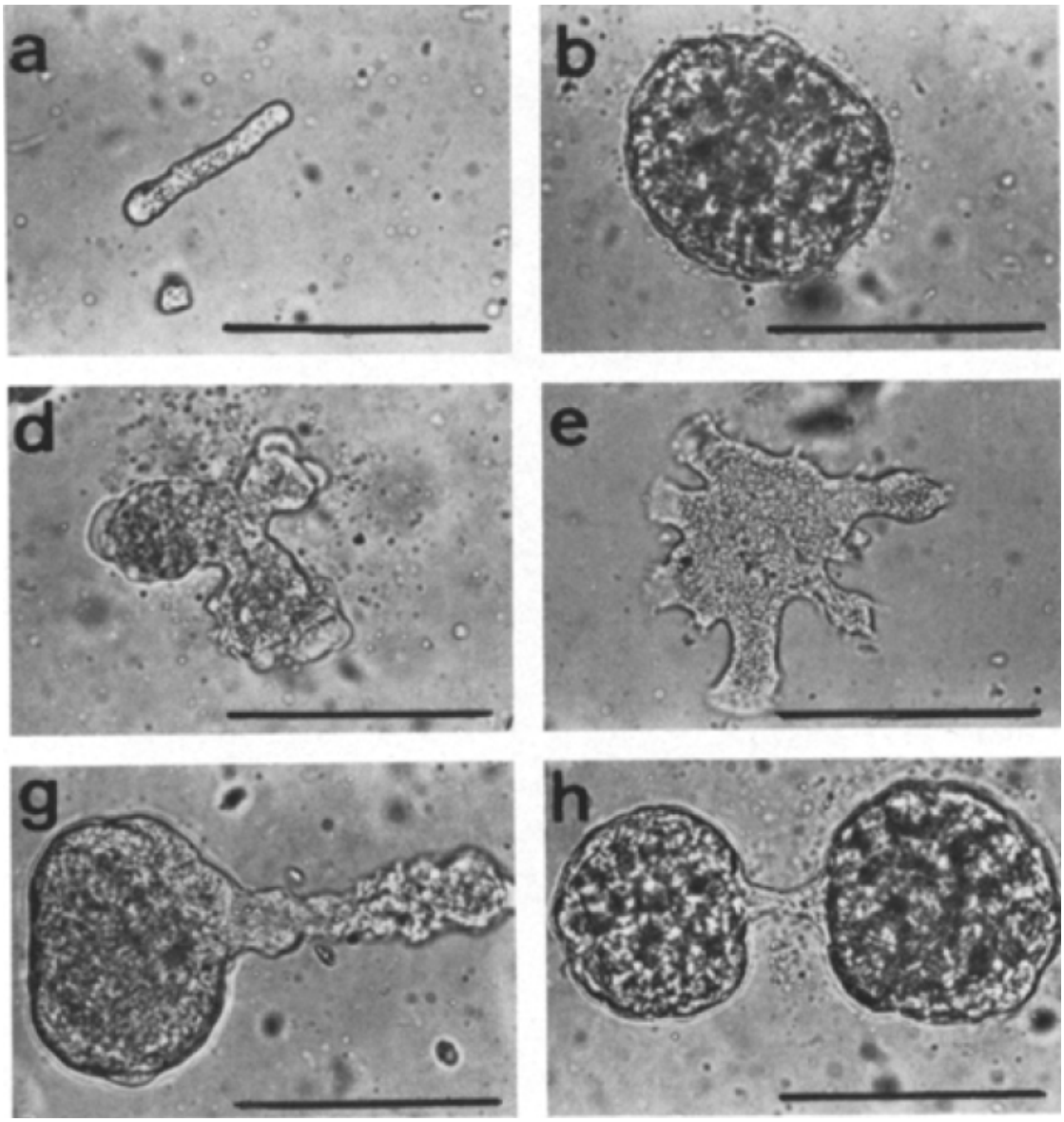

Figure 3.2: Different morphologies of microplasmodia, from [68]. **a** and **b** represents rod and spherical types, respectively. **d** and **e** represent amoeboid morphology, and **g** and **h** represent a symmetrical morphology. Typically a spherical type of microplasmodia dominated in a satellite experiment. Scale bar represents 100 µm.

a maximum after 120 minutes, where a dense network of fibrils are established within microplasmodia [71].

Many studies utilized microplasmodia as a means of maintaining *P. polycephalum* culture, even if experiments utilized macroplasmodia [75,76]. Gawlitta et al. [68] utilized microplasmodia for *in vivo* experiments under the microscope due to its suitable size. Moreover, if the nutrients are replenished, microplasmodia continue to grow and can be maintained indefinitely, unlike macroplasmodia [69, 77]. The researchers suspected

that due to the quick fragmentation caused by the external force, damaged and dead organelles are quickly isolated to preserve the integrity of the organism.

Microplasmodia, when placed back on a solid surface, fuse with one another to form macroplasmodia. A typical morphology at the end of fusion is an extended network, which is a subject of various investigations on network formation and network properties. Specifically, this transition from fragments to a large component was found to be of a percolation transition [75], and resembles angiogenesis in cancer cells.

Although microplasmodia may be from the same plasmodium, mitosis is not synchronous between the microplasmodia. It is only when these fragments fuse, the nuclear division is synchronized [78].

3.3 Previous research

3.3.1 Biological and biochemical properties

Physarum polycephalum has been a model organism for diverse biological investigations due to its size, unicellular simplicity and ease of culture. It has been utilized to study the cell cycle regulation, cell differentiation via spherulation and sporulation, cell fusion, DNA replication, histone modification and chemotaxis [25,60]. There are several unique characteristics of *P.polycephalum*, which can be exploited to further the understanding of cellular functions.

1. Mitosis, a division of nucleus, is synchoronus in the plasmodium [66]. A growing plasmodium on a solid medium synchronously undergoes mitosis every 8 - 12 hours, and phases of mitosis have been well-defined [78]. Interestingly, the protoplasmic shuttle streaming slows down or stop when the division occurs.

2. Plasmodium are sufficiently large [25]. The largest plasmodium grown covered a surface of 5.5 m^2 and weighted approximately 3 kilograms. As a microplasmodia, it can be grown in a liquid culture up to 100 litres. A plasmodium may be cut and separated, and both fragments will remain vital and continue growing. A fragment can become a functioning organism within minutes [79]. Two plasmodia will fuse with one another when they are in physical contact if the fusion type is identical [80].

3. Proliferation and differentiation are distinct, identifiable and controllable. Even with a complex life cycle of *P. polycephalum*, the control mechanisms of differentiation (spherulation and sporulation) are well known and can be controlled under laboratory conditions [27]. This switch between haploid and diploid states provides a significant advantage in producing and screening for specific mutants and the underlying mutations. [60].

Genetically, it was also previously documented that *P. polycephalum* showed an accelerated rate of evolution [61]. Although the genetic manipulation in plasmodia is difficult due to the nature of a plasmodium containing multiple nuclei per body, methods have been developed to knock down the expression of specific proteins [60]. Recently, the

genome of *P. polycephalum* was fully sequenced [60], opening a new window of genetic screening and targeted investigations. The genome of *P. polycephalum* showed higher molecular complexity compared to other organisms belonging to *Amoebozoa*. Moreover, a signal cascade system of receptor tyrosine kinases was also found in the genome of *P. polycephalum*, which was previously thought to be exclusive to multicellular animals.

In recent times, *P. polycephalum* has been utilized in biophysics and unconventional computing in pathfinding and control unit of a computer [60,81]. Some of the intriguing characteristics that allow a slime mould to perform these tasks are expanded below.

3.3.2 Networks and computations

The resurgence of *P. polycephalum* as an organism of interest is often attributed to the seminal paper of Nakagaki et al. in 2000 [16], where *P. polycephalum* was shown to find the shortest path through the maze. Since then, *P. polycephalum* was utilized in network optimization [82], and perform computational tasks [83,84].

Biological networks are interesting in that it is constructed without a central control [83]. One of the studies that utilized an optimized network structure of *P. polycephalum* simulated a railway network of Tokyo [34]. Using oat flakes to represent major cities and its tendency to avoid light to outline the coastline with illumination, they let *P. polycephalum* to build a network over a virtual map. Their hypothesis, although not explicitly stated, is similar to the OFT (Chapter 2). They assume that *P. polycephalum* have adapted through natural selection to balance three main aspects pertinent in building a transport network. These are:

1. A cost of production, represented by a total length of the veins
2. Efficiency of the network, which is the average minimum distance between nodes of a network
3. Robustness or fault tolerance of a network, which is defined as a probability of disconnection if a failure occurs in a random vein

These three aspects were compared between networks built by *P. polycephalum* and a man-made network.

Researchers first tested two methods of simulating a network formation. The first was to place *P. polycephalum* at the location where Tokyo would be, which is roughly located at the centre of the network, and let the organism grow and find food. The second method was to first grow *P. polycephalum* uniformly, and then apply food sources and light on top of already expanded plasmodium. Intriguingly, both methods produced a similar network, demonstrating that there is no directionality in the network organization. This is also expected, since *P. polycephalum* is a unicellular organism and do not have a centralized information processing unit. It is nonetheless impressive that the structure formation along with exploration of an unknown environment can result in a network that is equally efficient compared to a network built based on all the information

required to build an effective network. Then, they compared the *P. polycephalum* networks and a real network in terms of cost, efficiency, and robustness. Although the real network performed slightly better in robustness, *P. polycephalum* networks were similar in terms of cost and efficiency.

Then, a model was constructed to mimic the network of *P. polycephalum*, based on local flow reinforcement. They first utilized the Hagen-Poiseuille equation to describe the flux through a vein between two points. These two points are equivalent to two cities. During the simulation, one is randomly assigned as a source and one as a sink, so that the amount of fluid flowing is conserved. Based on previous observations that higher flow of protoplasm through a vein increases its thickness, they introduce a second equation where the thickness of the vein is influenced by the flux through the vein. Under the simulated conditions, the vein naturally constricts without flow, and higher flow results in feedback that increases the diameter.

Using the two parameters, I_0, which represents how much flow occurs between the two points, and γ, which controls the feedback strength, they simulated a network over the same map the *P. polycephalum* have constructed a network. By varying both parameters, the simulation could either produce a network with a minimal connection between the cities with low robustness, or a network with high efficiency and robustness, but a high cost. A specific parameter combination also resulted in a network that was very similar to the Tokyo railway network. The feedback parameter, although not discussed in detail in the paper, describes a degree interplay between the environment an the organism. It is an indirect measurement of the sensitivity of the organism during foraging on environmental factors such as quality of food.

Such findings can be further utilized and combined to provide a more holistic picture of foraging and exploratory behaviour. Schenz et al. observed *P. polycephalum* exploring a maze with two 90 degree turns, and how the growth front and veins are constructed as the organism progressed [85]. They found that during the straight corridor, the main vein was constructed in the middle of the path, but during turning, it cut the corner which resulted in center-in-center vein formation. They were able to write an algorithm that predicted the position of a vein based on the movement of the growing front of *P. polycephalum*. The algorithm was able to accurately predict the final vein formation. However, while this model showed that the formation of the vein and the movement of the growth front was linked, it was a phenomenological model and biological implications were unclear. Therefore, known processes of *P. polycephalum* migration was assessed and combined to give a more mechanistic model. Specifically, they described the migration behaviour as follows:

1. Leading edge or growth front formation via gel-sol transition. A chemical reaction to generate front movement has been previously established.

2. Protoplasm streaming generated by actomyosin contraction. Oscillating calcium concentration is thought to control the activity of actomyosin, which controls shuttle streaming.

3. Vein network formation. This was investigated with current reinforcement rule,

where more flows cause thicker and more persistent veins.

Then, the researchers added interaction terms between the three models so that all three separate processes, and the models that describe these processes, were linked. The resulting mechanism successfully simulated the center-in-center phenomenon seen in *P. polycephalum*. Also, if the interaction between the leading edge and the vein formation was turned off in the model, the vein construction hugged the wall much faster, rather than remaining in the centre of the corridor, showing that the interaction between different mechanisms was crucial in modelling the behaviour of the slime mould.

These networks do not only consider the shortest path problems, but also integrate other environmental factors, such as the risk of light exposure. *P. polycephalum* shows a negative phototaxis, as illumination causes reactive oxygen to form and therefore detrimental to survival. Nakagaki et al. tested whether these risks are being accounted for during the construction of the shortest path [86]. Researchers let *P. polycephalum* cover a rectangular arena completely and placed food sources in the opposite corner. The organism, without inhomogeneity of illumination, connected two corners with the shortest path. When parts of the arena were illuminated, *P. polycephalum* constructed a network so that refraction of path occurred at the boundary of the illumination. While the overall path length increased, the path through the illuminated arena was minimized. The length of the vein in the illuminated arena was also proportional to the intensity of the illumination, where stronger light induced a greater angle of refraction at the boundary.

Nakagaki et al. mathematically calculated this minimal path-finding by simulation of the current reinforcement model, where a flux through a vein positively influences the thickness of the vein. The sheet of plasmodium was represented as a fine mesh of networks, and each vein was either reinforced or vanished based on the flux between the two opposite corner. The effect of the risk of illumination was reflected as a parameter that modulated how fast a vein disappeared when they are not used. The simulation accurately depicted a typical behaviour of *P. polycephalum* vein formation in an inhomogeneous illumination. Even without centralized control of network construction, a slime mould was able to find a path that minimizes risk, and this behaviour can be described with local dynamics of vein formation.

The importance of *P. polycephalum* solving a maze [16] was that it was able to find the shortest path between two points. A model was constructed to describe this behaviour by Tero et al. in 2007, and mathematically proven to converge to shortest paths [33].

Numerous mathematical problems were attempted with *P. polycephalum*, utilizing this property of finding the shortest path. One such problem is the Tower of Hanoi, which is a well-known shortest-path problem [83]. Tower of Hanoi problem is stated as follows: N number of discs are stacked on top of each other in descending size, on one of three pegs. The problem is solved when the stack of discs are moved from one peg to another peg with the smallest number of moves. Only one disc can be moved at a time, only the top disc in a stack can be moved, and a bigger disc can't be placed on a smaller disc. Due to the sequential nature, all possible movements can be mapped on a 2-dimensional maze. Researchers applied *P. polycephalum* in this maze, and marked the

ends of the maze with food. *P. polycephalum* first covered the entire maze, made contact with both food sources and built the shortest path between the food sources within 24 hours. If the network was disturbed by the removal of a bridge, *P. polycephalum* network quickly adapted and built a shortest path in a new maze.

Travelling salesman problem (TSP) is also another type of optimization problem. Given N cities, one must find the shortest paths to visit each city only once and return to the starting city. Currently, only the exhaustive search method where all possible paths are compared with each other is the method that guarantees the discovery of the shortest path. The number of possible routes increases exponentially as a function of N, making the exhaustive search impractical in cases of large N. Researchers constructed a circular device where *P. polycephalum* was placed. On the plate, *P. polycephalum* attempted to maximize body size while minimizing the risk of illumination. They dubbed this process 'Amoeba-Based Computing' (ABC) [84]. By using a feedback algorithm to control illumination dynamics, *P. polycephalum* performed efficiently in finding short paths in the TSP problem. If two cells were introduced in the disc and remain separated with a barrier, the ABC could not find a solution. However, interestingly, if a single cell was divided by a barrier right before the computation, *P. polycephalum* still found a highly efficient solution to TSP. Authors concluded that the fragment from the same cell maintained a long-term memory to synchronize the search, even after cells were physically separated.

3.3.3 Foraging

When subjected to multiple ratios of protein to carbohydrates, *P. polycephalum* chose a ratio which gave them the highest growth rate. When the ideal ratio of nutrients was not provided as an option, *P. polycephalum* obtained the ideal ratio of nutrients by combining different food sources [31]. This is similar to an optimization problem known as the knapsack problem, where a value per mass must be maximized [87]. *P. polycephalum* integrated information about the nutrient ratio, and distributed its body to obtain a diet of the highest value to the organism, as represented by the fastest growth [31].

There is a growing number of studies that show an organism utilizes such rules to reach near optimum foraging behaviour. One such rule is an incremental departure mechanism, where the frequency of positive encounter increases the resident time on a patch. Previously, this set of rules were investigated in parasitoid wasps, with brains containing hundreds of neurons [88, 89]. These particular heuristics were also observed in bumblebees and humans [30, 90]. Latty and Beekman also observed the incremental departure rules in *P. polycephalum*, when they were subjected to multiple food sources with either high or low qualities [30]. Any encounter with food sources increased the subsequent exploitation time of the slime mould. The increase was stronger when the organism encountered a higher concentration of food. Therefore, this demonstrated that *P. polycephalum* can distinguish the quality of food, and this difference was also reflected in the decision-making process. Moreover, *P. polycephalum* demonstrated a memory capacity to recall the number of the previous encounter.

While these decision-making characteristics are interesting on their own, and the

widespread of these characteristics over wide taxa hints at a possibility of the universality of decision-making properties, the actual mechanism of the decision-making is still unknown. To delve into what type of mechanism is utilized in *P. polycephalum* to make decisions, multiple models were constructed to compare with the outcome of *P. polycephalum* on a two-armed bandit problem [35]. In this problem, an organism must compare two choices to determine which one has a higher reward. To choose the correct option, an organism must explore and evaluate both options. Humans are known to perform sub-optimally at this problem. Humans tend to change arms too frequently, expecting that the rewards rate change over time, and move away from higher rewards back to lower rewards option. Birds and fish, however, perform efficiently in this problem. Moreover, learning effects were shown to play a role in improving the test score when the same animal was tested multiple times.

This problem was ingeniously translated to *P. polycephalum* by creating a linear arena with discrete blocks. *P. polycephalum* is placed in the middle, and these discrete blocks can be replaced with food blocks. Sufficient biomass of *P. polycephalum* is transferred that it can cover the entirety of the linear arena. Therefore, a preferential movement towards one arm is a result of a choice, not influenced by a physical limitation. *P. polycephalum*, without training, always evaluated and chose the high-quality option, regardless of whether rewards were evenly or randomly distributed. The difficulty of choices was adjusted by decreasing the difference in reward rate between two arms. In more difficult challenges where two arms were similar in reward output, *P. polycephalum* still chose the correct arm, although the delay before a commitment was increased. The model that best described the behaviour of *P. polycephalum* was a 'relative success', in which a probability of choosing an arm is proportional to the previous rewards encountered on that arm. This is akin to an incremental patch departure rule, already demonstrated from the slime mould [30]. This strategy is computationally simple and can be utilized in a decentralized manner. Researchers also suggested that a possible mechanism is with a coupled-oscillator based sensorimotor system, and drew a parallel between this oscillation and firing rate of a neuron in a brain leading a decision-making process.

Based on optimal foraging, an organism chooses an option that maximizes its Darwinian fitness. This includes not only the energy maximization but also include other factors, such as balancing dietary requirements and predatory risk minimization. Moreover, based on its internal state, a foraging strategy may differ. For example, based on its hunger level, an organism may either choose to take more or less risk during foraging. These complex scenarios were presented for *P. polycephalum* [91]. In this study, starved and non-starved slime moulds were used in a foraging experiment where they were given a choice between high-risk but high reward option and a low-risk and low reward option. They utilized a 'behavioural titration', where the risks and rewards are adjusted until both options were equally chosen.

Both starved and non-starved *P. polycephalum* chose a higher quality option between two choices under no-risk conditions. However, when risks were applied to higher quality food by illumination while the lesser quality food was left in the dark, the relative concentration affected the behaviour of the slime mould. *P. polycephalum* chose the less

rewarding, but no risk option when the illuminated option was up to two times the concentration of the safe option. At three times the concentration, the slime mould was more likely to choose the risky but highly rewarding option, and when the ratio of concentration was more than five, virtually all *P. polycephalum* chose the risky option. Moreover, non-starved *P. polycephalum* was more likely to take risks under the concentration ratio below two. Although this experiment did not quantify the amount of risk, nor did the experiment attempted to vary or calibrate the amount of risk posed by the illumination, it was a clear indication that a trade-off was made in a unicellular organism to forego risk when the potential reward outweighed the possible cost.

Moreover, *P. polycephalum* was able to discriminate between its slime and slime from another species of slime mould [92]. When the slime mould was placed between two paths, *P. polycephalum* chose a path covered with slime from other species over a path with its own slime to reach food. Slime mould still preferred to forage on an unmarked path over a path covered with slime from other species. However, this avoidance of slime was not absolute and was compensatory upon the quality of the food. *P. polycephalum* generally chose a path without slime, even if the resulting food quality was lower than the ones in a slime. However, if the path of slime was sufficiently short, then the organism ignored its slime and chooses the higher quality food over an option without the slime. Therefore, *P. polycephalum* integrated both the attribute of the food quality, as well as the presence of slime to make a foraging decision.

P. polycephalum constantly produces and secretes a slime to protect itself from desiccation. This extracellular slime is composed of polyanionic glycoprotein [93] and is left behind as *P. polycephalum* moves. There have been several suggestions of the function of the slime, including protection and aid in nutrient intake [94]. However, Reid et al. [95] demonstrated that the slime may be used as external memory to aid in foraging. In an environment previously unknown to a forager, it would be beneficial to avoid sites that were already exploited or visited. One way to avoid re-visitation is to have a systematic search strategy, in which an organism moves in a specific way [92]. Another method is to use memory, by marking a place where a forager visited [96].

To test whether slime was used to aid in foraging, researchers built a Y-shaped maze with two arms, and at the end of the arm is placed with food. When one arm was coated with their own slime, *P. polycephalum* almost always moved to an arm without the slime. However, when both arms were covered with slime, *P. polycephalum* chose a random arm to forage, instead of remaining in place. Therefore, the avoidance behaviour was a choice from *P. polycephalum*, as the organism was capable of travelling over their own slime. *P. polycephalum* also utilized its slime to overcome a U-shaped trap over a chemical gradient. A common test for navigating robots, this trap requires an external spatial memory for successful completion [95]. Reid et al. successfully showed that *P. polycephalum* solved the U-shaped trap. Moreover, they demonstrated that the loss of this external memory, induced by covering the entire environment with slime, disabled the slime mould from overcoming the trap.

Part III

Results

Chapter 4

Alternative growth pattern of *P. polycephalum*

4.1 Introduction

The plasmodidum, a vegetative state of *P. polycephalum* extends, grows, and propagates as a network. There are no published reports of other growth patterns or structure formation, bar from the publications from the author and the working group of Prof. Dr. Döbereiner. A small number of works reported on spontaneous fragmentation upon rapid change of environmental conditions, specifically upon exposure to light or temperate change [97, 98]. However, this fragmentation results in very small fragments that contain only tens of nuclei, and therefore much smaller than microplasmodia.

Utilization of microplasmodia as a reproducible means of *P. polycephalum* also results in network formation, once the microplasmodia are transferred to a solid platform or when the shaking of the liquid culture is stopped. Generally, all active microplasmodia fuse and form one large component [75]. However, under specific conditions, microplasmodia undergo a transitional state where multiple fragments are formed. The morphology of these fragments is distinct from the network pattern, and exhibits directed motion with stable morphology (Figure 4.1).

In this section, a previously unobserved growth pattern of *P. polycephalum* is reported. This growth is referred to as 'satellite growth' to distinguish from the typical network growth. In satellite growth, motile fragments, named satellites, are formed that detach and move away from the patch. The new pattern occurs in the first 10 hours after inoculation, and all fragments produced eventually transforms into a network. Therefore, this growth is a transient state between microplasmodia and a macroplasmodium. Characteristics of this growth, as well as factors that influence the growth patterns, is described below.

This chapter is organized in the following order. First, the experimental procedures utilized during the doctoral studies are stated in detail. Then, a brief remark is given on how the satellite growth was first discovered, and alteration of the experimental parameters that inadvertently influenced the growth of *P. polycephalum*. The master's thesis

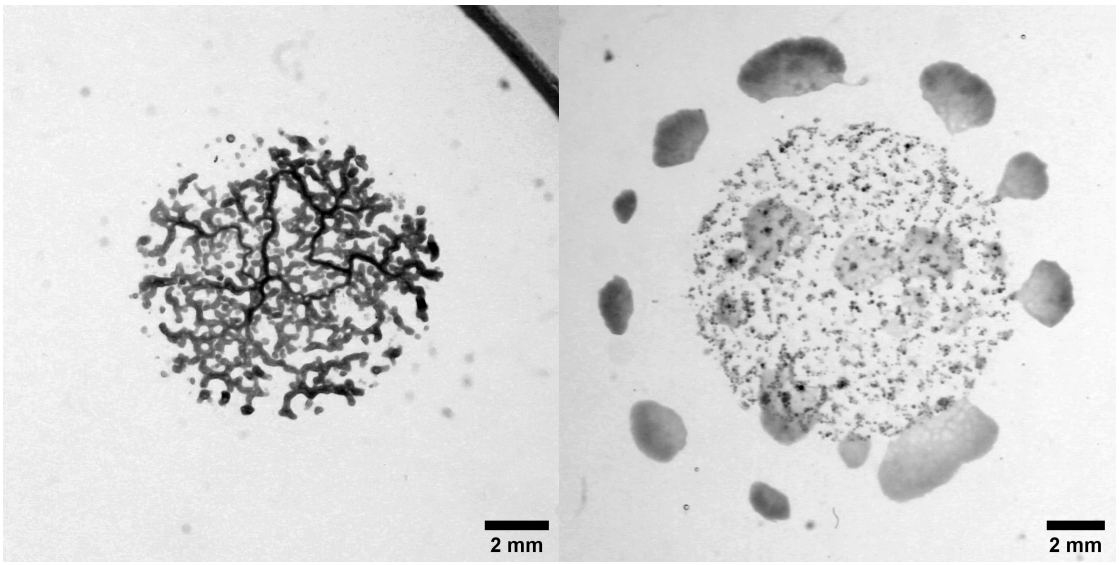

Figure 4.1: A snapshot of two different growths of *P. polycephalum* 9 hours after inoculation. Both growths are initiated from microplasmodia but based on different factors, they can grow either as a network (Left) or satellites (Right).

by the author is reviewed, to emphasize what has been investigated and discovered on satellite growth before the doctoral thesis. The central hypothesis of the thesis is then stated based on the data from the master's thesis, which considers the satellite growth to be an alternative growth strategy specifically designed to counter starvation.

The satellite growth is first qualitatively described, with snapshots of growth. Summed images are created from time-series experiments of satellite growth to better convey the dynamics of the growth. When satellite growths are observed, they follow a set of phases that can be visually identified. These are labelled and identified to remove ambiguity and to better describe and refer to different stages of the growth. Outcomes of experiments are shown to demonstrate the effects of environmental factors that can influence growth. Some of these observations are used as clues to establish models to describe satellite growth.

Then, the satellite growth was described quantitatively. First, how the age of the microplasmodia, counted from the inoculation of the liquid culture, influenced the growth when they were transferred to an agar plate was investigated. The growth of microplasmodia at different age was first compared visually at a macroscopic scale. Then the growths were simplified to areas covered, and the number of objects. The dynamics of these two parameters are compared between network and satellite growth.

The dynamics of the individual microplasmodium were then investigated at a microscopic scale. The diffusive properties, as well as the type of movement, were investigated by tracking the microplasmodium until fusion. Then, the trajectories of the microplasmodia were compared between satellite and non-satellite growth. The differences between the two growths, and how these differences influence the growth are discussed.

Finally, two main investigations on modelling the satellite growth are presented. The first is the modelling the displacement of the satellite, based on chemotaxis, from a publication by the author [23]. The second is the scaling of the satellite formation, which is based on a draft prepared by the author. The parameters obtained from the previous quantitative investigations are used to evaluate the model. Then, the implications of the model and the possible mechanisms that cause the satellite growth based on the assumptions of the models are stated, with references to the optimal foraging theory.

4.2 Experimental procedure

Culture maintenance

Physarum polycephalum (WT31 × LU898) was kindly provided by Prof. Wolfgang Marwan (Universität Magdeburg). *P. polycephalum* was maintained as microplasmodia in a liquid growth medium called Wachstumsmedium (WM) (Table 4.1). Cultures were grown at a constant temperature at 24°C and rotation with a rotation frequency of 180 rotations per minute. The shakers were placed in a dark room with minimal light exposure.

New cultures of microplasmodia were prepared by harvesting 2 mL of the previous culture aged between 3 - 4 days, discarding the supernatant and transferring the pellet to the 100 mL WM in a 500 mL Erlenmeyer flask. Microplasmodial age was measured from the time of this inoculation. Making a new microplasmodial culture from the previous microplasmodial culture counted as one passage. Microplasmodia were prepared from spherules of the original *P. polycephalum* once the passage number exceeded 30.

Experimental preparation

Microplasmodia were harvested by centrifuging a liquid culture at 331 g for 3 minutes. Generally, 2 or 5 mL of the culture was centrifuged based on age and visual estimation of microplasmodial density. Supernatants were removed as much as possible without losing a significant portion of the pellet. The pellet was then resuspended with a sterile medium. MilliQ filtered water, WM, or WM without glucose were used as a medium based on experimental purpose.

The volume of the pellet was estimated from the graduation of the centrifugation tube. Generally, an equal volume of the medium was added to the pellet. However, depending on the experimental need, as much as 8 times the volume of medium was added to the pellet to lower the concentration of the microplasmodia. The medium and the pellet were mixed thoroughly by pipetting up and down until no clumps were visible. Then, the resuspension was applied dropwise onto an agar plate, creating a circular patch of microplasmodia. A volume of 20 to 80 µm was used to create these patches. Agar plates were filled with semi-defined medium (SDM) with 1.7% agar (Table 4.3). In experiments specifically designed to induce satellites, glucose was withheld from the medium. The

density of the microplasmodia was not specifically controlled. Dilutions were used to provide a wide range of coverages to compare the effect of the density on the formation of satellites. Inoculated plates were dried for 15 minutes in a sterile bench. 9 or 3 cm diameter plates were used, depending on the imaging acquisition methods. Generally, multiple patches of microplasmodial inoculations were set on 9 cm plates, while 3 cm plates contained only one patch, and used exclusively for microscopic observations.

Table 4.1: Wachstumsmedium (WM) per 1 Litre

Ingredient	Amount
Bacto Trypton	10 g
Yeast Extract	1.5 g
D(+) Glucose monohydrate	11 g
Citric acid, water-free	3.54 g
Iron sulfate heptahydrate	0.084 g
Calcium chloride dihydrate	0.6 g
Potassium hydrogen phosphate	2 g
100x MMZ solution	10 mL
pH adjusted with 4N NaOH	4.6

Table 4.2: MMZ solution per 1 Litre

Ingredient	Amount
Magnesium sulfate heptadydrate	60 g
Manganese(II) chloride dihydrate	6 g
Zinc sulfate heptahydrate	3.4g

Table 4.3: 2x semi-defined medium for 1 Litre

Ingredient	Amount
D(+) Glucose monohydrate	20 g
Bacto Soyton	20 g
Citric acid, water free	7.08 g
Iron(II) chloride tetrahydrate	0.078 g
D(+) Biotin	0.01 g
Thiamin hydrochloride	0.08 g
Potassium hydrogen phsphate solution, 80 g/L	50 mL
Calcium chloride dihydrate solution, 41.2 g/L	50 mL
Magnesium sulfate heptahydrate solution, 24 g/L	50 mL
EDTA-disodium salt dihydrate solution, 9.2 g/L	50 mL
Zin sulfate heptahydrate solution, 136 g/L	0.5 mL

Image acquisition

Two different imaging apparatus were used to observe the growth of *P. polycephalum*. The first is a custom-built observation apparatus with a DSLR camera, termed 'Photobox'.

The relative humidity of the Photobox was kept at 88% by employing a supersaturated potassium chloride solution [99]. The temperature was kept at 24°C. The experiment was illuminated with a retro-fitted monitor, and the illumination did not affect the growth of *P. polycephalum*. Inoculated plates were observed for a minimum of 10 hours, and pictures were taken in either 0.5, 1 or 2 minutes interval. Image acquisition was done with a Canon EOS 50D with a Canon EF macro lens (50 mm, f/2.5) using the manufacturer-supplied software. As of November 2017, the camera was upgraded to Canon EOS 5DS R with the same lens, improving the resolution from approximately 14 µm/pixel to 12 µm/pixel. All images were exported as a jpeg format.

The second imaging system was the AxioZoom V.16 microscope from Zeiss with AxioCam mono 506 as a camera with Zen software supplied with the microscope. Using the Plan NeoFluar Z 1x/0.25 FWD 56 mm objective, the resolution at the lowest magnification was 6.49 µm/pixel. The microscope was then equipped with a custom-built incubation chamber with built-in humidity and temperature control from Okolab. The relative humidity was kept at 95% and the temperature was kept at 24°C. The agar plates for the microscope were filled higher to ensure that the microplasmodia can be properly focused. Inoculated plates were observed for a minimum of 10 hours, and pictures were taken in 15 seconds interval. All images were exported as either a tiff or jpeg format.

Image processing

All image processing and mathematical analyses were performed with MatLab (2013 and 2017b, The MathWorks, Inc.) and FIJI [100].

The time-series experiments from the Photobox were first converted to a greyscale 8-bit image by isolating the blue channel of the RGB composition, as the blue channel provided the highest contrast between the sample and the background. Then the pictures were cropped to contain only the growths of *P. polycephalum*. This was done based on the picture taken after 10 hours of observation as a reference, and the window that encloses all the growth was used to crop the rest of the images.

After cropping, images from both imaging systems were segmented with a custom script, which utilized a moving window to determine local threshold values as used in [75]. The segmented images were saved and served as a basis for all other analysis.

Physical parameters of growth

The segmentation simplified the image into backgrounds and objects. The objects identified from the segmentation represents the biomass of *P. polycephalum* (B). Using the segmented image, the number of objects, N and the area covered by these objects A_{total} were identified. It was assumed that all structures are of equal height and density, and therefore biomass is represented as an area, and the grey values were discarded.

From the segmented image at $t = 0$, a mask was established by a convex hull that contains all segmented objects (Figure 4.2). This mask was considered as the patch area

A_p. Area coverage, C was calculated by dividing A_{total} with A_p at $t = 0$.

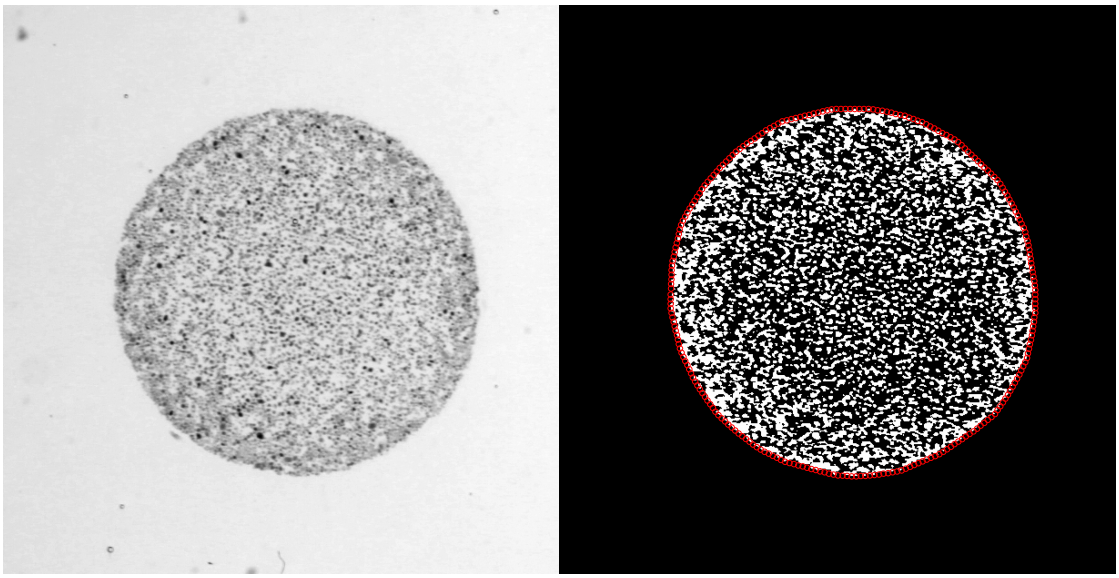

Figure 4.2: The raw image of the satellite experiment at $t = 0$ (Left), and the segmented image with a convex hull (Right). The raw image was converted into a black and white image, where the black represents the background, and the white represents areas covered by *P. polycephalum*. A convex hull (Red circles) was constructed to encompass all the white objects, which is defined as the patch area A_p.

The measurement of the satellite was performed with the segmented image at $t = 540$ minutes. This was when all the satellites briefly stop and referred to as the pause state. Different states and phases are defined in the later section in detail (Section 4.6.1). The satellite was identified as an object that is separated from A_p (Figure 4.3). The area of the satellite was designated as A_s, and it is approximated as an oval to calculate the aspect ratio R. R was defined as the ratio between the minor and major axis, b and a respectively. The distance travelled by the satellite, d was measured between the centroid of the satellite and the nearest border of the patch.

Akaike Information Criterion

To evaluate the goodness of fit, Akaike Information Criterion (AIC) and the Akaike Weight were used to score and compare different models. AIC is widely used for evaluating multiple models and determining a model that best fits the data, by measuring distances between the estimated and true distribution of the data [101–103]. AIC is calculated as:

$$AIC = Nln(RSS) + 2k \tag{4.1}$$

where N is the number of data points, RSS is the residual sum of squares, and k is

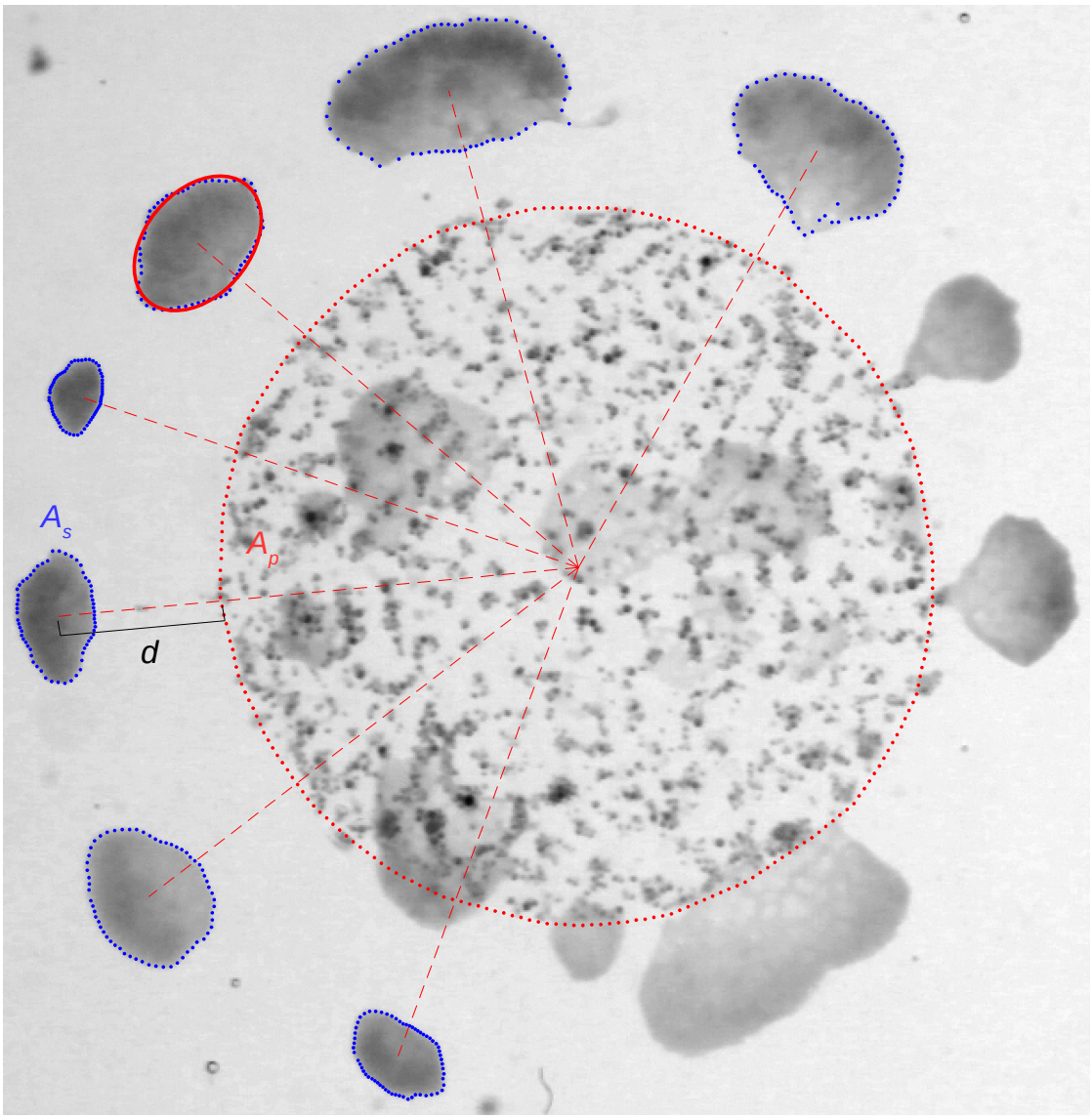

Figure 4.3: Identification and characterization of the satellite growth. The patch area A_p was calculated from the image at $t = 0$ (Figure 4.2), marked by the red dots. The mesoplasmodia were identified as satellites with size A_s (Blue outlines) when they are detached from the patch at $t = 540$ minutes. As long as some parts of the mesoplasmodia touch the patch, these were considered a connected component and not satellites. The distance d travelled by satellites was calculated by drawing a line between the centroid of the satellite and the patch and calculated between the intersect of the line and the circumference of A_p and the centroid of the satellite. The aspect ratio R was calculated by approximating the satellite into an oval shape (Solid red line).

the total number of model parameters. Lower AIC scores indicate a better fit. To quantify how much better a model is compared to another, the Akaike Weight is calculated:

$$w_i(AIC) = \frac{exp(-\frac{1}{2}\Delta_i(AIC))}{\sum_{j=1}^{J} exp(-\frac{1}{2}\Delta_j(AIC))} \tag{4.2}$$

where,

$$\Delta_i(AIC) = AIC_i - AIC_{\min}$$

J indicates the total number of models compared, and the index i indicates the model in question. The Akaike Weight of a model can be used to determine how good a given model is by computing the ratio between the Akaike Weights. In this case, the number indicates the likelihood that a given model is better than the other model. The Akaike Weight can be normalized with a total sum of the Akaike Weights. Then, the Akaike weight of each model represents the probability that it is the best model for the data [103].

4.3 History

The first systematic approach to reproduce the satellite growth was undertaken by Tanja Huxoll in 2012, based on previous observations from the workgroup that primarily focused on network growth. The conditions and images recorded by Tanja Huxoll was taken by the author, which then performed statistical analysis as a part of the master's thesis.

From April of 2014 and onwards, the shaker that contained the liquid microplasmodial culture was moved into an incubator to better control the incubation temperature. For the projects focused on the network growth of *P. polycephlaum*, a small fluctuation of the incubation temperature did not affect the growth outcome. However, satellite growth was much more sensitive to the incubation temperature. Also, moving the shaker inside an incubator had an added benefit of minimizing the light exposure. The effect of incubation temperature of liquid microplasmodia is discussed in the subsequent section (Section 4.4).

On February 2016, it was found that the calculations in the agar concentration of the agar contained an error. New agar plates were prepared with 1.7% agar percent, with fixed heights. Initially, the agar percentage was thought to be a non-factor in satellite growth. However, it was found later that the stiffness of the substrate indeed affects the satellite growth, but not necessarily the onset of the satellite formation. This effect is qualitatively described later (Figure 4.10), and the experiments were performed with the corrected agar conditions from this point on. Therefore, any satellite growths observed before February 2016 are not included in the quantitative analyses.

On January of 2018, 3 strains of *P. polycephalum* were gifted by Prof. Wolfgang Marwan. However, one of the strains was mislabelled WT33 $\times$ LU898 by the laboratory of Prof. Marwan, while it was, in fact, WT31 $\times$ LU898. Originally, the statistics were calculated separately, as they were thought to be different strains. However, after the

Table 4.4: Statistics on the satellite growth per glucose concentration in agar. Glucose refers to the concentration present in the agar plate.

Glucose (g/L)	Experiments	Patch	Satellite	Success (%)
0	12	54	13	24.1
5	7	19	1	5.3
10	6	21	0	0
15	8	27	0	0
20	6	22	0	0

mislabelling was identified, the statistics were combined and treated as the same.

Also on January of 2018, the author increased the rotation speed of the centrifuge from 1300 to 3000 rotations per minute (RPM), increasing the gravitational force from approximately 331 g to 1750 g. Here, g represents the acceleration due to earth's gravity, which is approximately 9.81 m/s^2. However, this lowered the probability of the satellite growth to occur, and the centrifugation speed was reverted to 1300 rotations per minute on October of 2018. The effect of the centrifugation speed on the growth of microplasmodia is not investigated in this work.

4.4 Previous work

As part of a master's thesis by the author, statistics were collected on the occurrence of the satellite growth, based on the age of microplasmodia and nutrient content on agar. Part of the data from the master's thesis, from April to September of 2014, was collated with data obtained during subsequent doctoral work to provide a clearer understanding of *P. polycephalum*'s foraging behaviour.

Before April of 2014, the incubation temperature of microplasmodia was not controlled. However, even from the uncontrolled data, it was evident that the satellite growth was only observed when glucose was not present in the agar plate (Table 4.4). Any experiment with glucose higher than 10 g/L did not produce any satellite growth, and only one satellite growth was observed from a glucose concentration of 5 g/L. Therefore, later experiments were prepared exclusively on agar plates without glucose to maximize the chance of inducing satellite growth.

Moreover, satellites were not observed from microplasmodia aged from 1 to 5 days, but only from 6 days and older (Figure 4.4, panel (a)) when the temperature of incubation was not fixed. When the incubation temperature was fixed at 23°C, the satellite growth was observed exclusively on day 6. When this temperature was lowered to 21°C, the age of microplasmodia that produces satellite growth shifted to day 7. Therefore, it was suspected that the state of microplasmodia determined the onset of the satellite growth, and this state was affected by the incubation temperature.

To better describe the growth of the microplasmodia and how it was affected by tem-

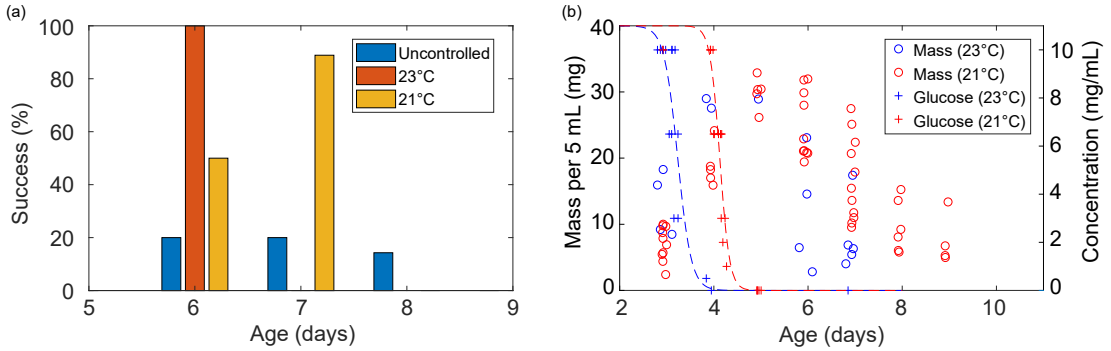

Figure 4.4: The effect of temperature on satellite growth. Satellite growth was observed only from microplasmodia older than day 5 (Panel (a)). In 23°C, the satellite growth exclusively occurred on day 6, while lowering the temperature shifted this to day 7. Moreover, controlled incubation temperature increased the success rate of satellite growth in general. The temperature affected the growth rate of microplasmodia and glucose consumption (Panel (b)). In 23°C, the peak biomass and the depletion of biomass occurred at day 4, whereas in 21°C this occurred on day 5. The dashed lines indicate the best fit of the logistic function on glucose concentration.

perature, the biomass in the liquid culture was measured at different times. Biomass was measured by taking 5 mL sample of the culture, which was then dried in an oven until the measured weight did not fluctuate within 24 hours. The peak mass reached during the growth of microplasmodia was similar in both temperatures. However, the peak was reached faster at the higher temperature by about a day (Figure 4.4, panel (b)). Unlike other prokaryotic growth curves, which resembles a logistic curve [104], biomasses of *P. polycephalum* microplasmodia decreased after reaching a peak [105].

The glucose content inside the culture was also monitored with glucose monitoring strips. Although the accuracy of the strips was lower than other methods of measuring the glucose concentration, it provided quick access to the glucose level without disrupting the incubation. A logistic function was used to obtain the time of depletion based on the data collected. This particular function was used, as prokaryotes in liquid cultures were approximated as a logistics function [104]. Therefore, it was expected that the consumption of nutrients would follow a similar trend. The glucose was depleted around the same time when the peak biomass was reached (Figure 4.4, panel (b)). Moreover, the depletion occurred rapidly within a day. The difference in time of glucose depletion was almost identical with the difference in the average age of a satellite growth in two different temperatures.

From the master's thesis, it has been therefore concluded that glucose is a strong inhibitor of satellite growth. Furthermore, the temperature affected satellite growth, as well as the growth and depletion of nutrients. Specifically, in higher temperatures, the growth of microplasmodia and the depletion of glucose occurred earlier. This was thought to influence the age of microplasmodia that produce satellite growth. Monitoring the glucose content showed that the microplasmodia are starved for about 3 days before the satellite growth occurs. After about 4 days after glucose depletion, microplasmodia turned into spherules and became dormant. Given the impact of glucose in agar in satel-

lite growth, this also supported the notion that a lack of a carbon source and starvation were important factors in inducing satellite growth.

What has not been done in the scope of the master's thesis is the quantitative and detailed analysis of the satellite growth and its related parameters. For example, the age of microplasmodia was described in a day interval. In the subsequent work, all ages were calculated by the minute to better quantify the minute effect between days. Moreover, terms are defined and established to better describe and compare satellite growth with each other, as well as against network growth.

4.5 Hypothesis

It remains a difficult task to reliably reproduce satellite growth. While the external conditions were narrowed down and could be well-controlled, the internal factor reflecting microplasmodial age appears to vary drastically, even with our best efforts. Even when microplasmodia were harvested at the same age based on the time when the cultures were inoculated, the harvested amount of pellets varied. Occasionally, network growth or no growth was observed instead of satellite growth even when all parameters were fulfilled, and there was no plausible explanation other than inherent stochasticity in a biological system. It was clear, however, that this growth occurred in a tight time window, and along with its distinct pattern suggested that this may be a specialized response.

Based on the master's thesis, the following facts are established on satellite growth.

1. The 'age' of the microplasmodia is an important factor in inducing the satellite growth The satellite growth was only observed when 'old' microplasmodia were used. Microplasmodia younger than 5 days old did not produce satellite growth, but only network growth (Figure 4.4, panel (a)). Moreover, microplasmodia did not show active growth when they were harvested later than the satellite-inducing age.

2. The lack of glucose is crucial in inducing satellite growth. The satellite growth was primarily observed when the agar plate did not contain any glucose (Table 4.4). Moreover, glucose was depleted in the liquid culture by the time microplasmodia produce satellite growth (Figure 4.4, panel (b)).

Therefore, satellite growth is induced in a stressful condition, where survival is in jeopardy. We hypothesize that this is an alternative growth strategy of *P. polycephalum* induced by prolonged starvation. This alternative growth is a foraging behaviour to look for nutrient sources, particularly glucose, that microplasmodia can readily use as an energy source. As they are placed in an environment that lacks glucose, and the information on the surrounding is limited, *P. polycephalum* performs a systematic search as they radially expand as satellites. This behaviour is an attempt to maximize the search area to maximize the probability of encountering a new nutrient source.

Moreover, all microplasmodia in the patch are genetically identical, as they are fragmented from one plasmodium. Therefore, it is advantageous to form multiple fragments

to increase the probability that one of these fragments may survive. Forming one component increases the risk that a failed search would result in the inactivation and possible death of the slime mould. The alternative growth strategy maximizes the chance of survival by not only maximizing the search but also forming multiple fragments.

This maximization concept is in parallel with the basis of the optimal foraging theory (Chapter 2). In the satellite growth, the chance of survival is maximized instead of net energy intake. The 'currency' maximized in the satellite growth is the search area, to maximize the encounter probability of new food sources.

4.6 Qualitative description of the satellite growth

In this section, the satellite growth is assessed and investigated visually. The primary goal of this section is to establish and define terms to describe the satellite growth, based on the publication by the author [23]. To do this, several snapshots of the satellite growth are shown, along with a summed image which shows the dynamics of the growth. These terms will be used throughout the thesis to describe and refer to the various aspects of the satellite growth.

The secondary objective of this section is to show the effect of various environmental factors on the growth of *P. polycephalum*. These effects were consistently reproduced, however not systematically investigated. Some of these effects are utilized in a later section to support assumptions in constructing the model to describe the satellite growth pattern.

4.6.1 Definition of temporal phases

In line with the terms macroplasmodia, which refers to a large plasmodium and microplasmodia, quasi-spherical microscopic fragments of plasmodium, we utilize 'mesoplasmodia' to refer to any intermediate stages of aggregation arising from the fusion of multiple, but not all, microplasmodia. The term 'satellite' was applied because the mesoplasmodia surrounded the circular patch in an orbit, which drew parallels to the satellites in space orbiting the earth. A satellite, a motile mesoplasmodium created from microplasmodia of *P. polycephalum*, is defined as a motile body that detaches from the patch of origin in a satellite growth. Hence, all satellites are by definition mesoplasmodia, but not all mesoplasmodia are satellites. A satellite growth is defined as follows, as described in [23].

Although the satellites were unique in size and numbers produced between experiments, the overall pattern satellites produced were all similar. Distinct phases could be identified even from qualitative observations. Therefore, a general description of satellite growth was established based on patterns on an SDM agar without glucose.

The phases of satellite growth are divided into pre-protrusion and post-protrusion phases, with three distinct states (Figure 4.5).

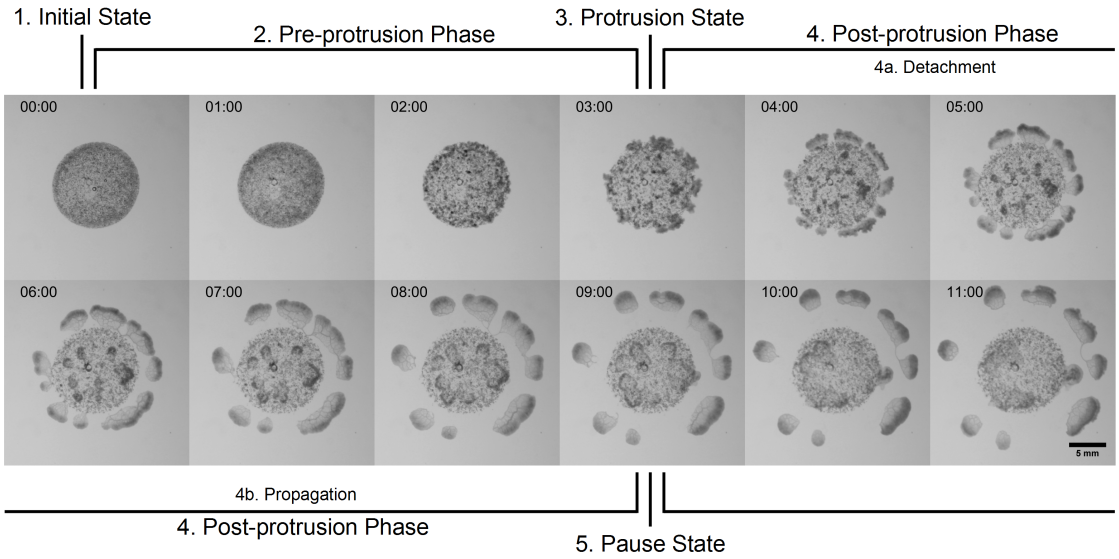

Figure 4.5: A temporal progression of the satellite growth, adapted from [23]. Snapshots of a typical satellite growth are displaced in an hourly interval. The initial movement of microplasmodia is evident between 0 to 1 hour. Protrusions are apparent at 3 hours, and by 4 hours it is well-developed. Satellites start detaching from the patch and maintain their shapes until 9 hours, where they stop. The shape of satellites fluctuates after the pause state, and they continue to move. States and phases are indicated accordingly. Time indicated as hh:mm.

1. Initial state (0 minute by definition)

   The experiment is initiated when microplasmodia are harvested from the liquid culture and inoculated on an agar plate.

2. Pre-protrusion phase

   The first phase lasts from the initial state until the first protrusion of the to-be satellite is observed. In this phase, two main events are observed: aggregation and fusion of microplasmodia.

   (a) Aggregation: After inoculation, microplasmodia move closer to one another to form clusters. The first set of aggregation appears to be driven by capillary forces when evaporation of residual resuspension liquid on the patch rapidly displaces microplasmodia, which occurs in the first hour of the experiment. Microplasmodia continue to move throughout the course of the experiment in a seemingly undirected fashion until they get close to other microplasmodia to aggregate.

   (b) Fusion: Observations show that not all microplasmodia participate in fusion events, even if microplasmodia appear to be in contact with another. Fused mesoplasmodia before protrusion do not appear similar to the mesoplasmodia after protrusion but are rather network-like. In higher concentration of microplasmodia, it is difficult to discern where and when these fusion events take place. The fusion phase starts after the first set of aggregations and ends when

the first protrusion is observed. Fusion continues to occur between fragments of *P. polycephalum*, even between mesoplasmodia after the protrusion state.

3. Protrusion state

   This is a state where a protrusion of satellites crosses the border of the patch. The first protrusion may be observed between 120 to 240 minutes. Generally, all satellites from the same patch protrude approximately at the same time.

4. Post-protrusion phase

   The second phase includes the propagation of satellites from the patch until they pause. This phase includes detachment and propagation of satellites.

   (a) Detachment: Once protrusion occurs, biomass is shuttled from inside the patch to the outside, forming an oval-shaped satellite. Depending on the size, the time of complete detachment from the patch varies. Occasionally, umbilical cord-like veins connect a mesoplasmodium to other mesoplasmodia or the patch. These veins may persist for a long time, even until the pause state.

   (b) Propagation: This is the phase where satellites move radially away from the patch after the detachment. Satellites maintain constant direction and shape, and these characteristics remain relatively stable until they pause. The speed of a satellite also appears to be constant, until it decelerates to a stop. Satellites, in close proximity, can interact with one another – two satellites may fuse to become one larger satellite, or be repelled by other satellites and change directions. It is currently unclear what dictates the type of interaction between satellites, or the length scale at which the interaction occurs.

5. Pause state

   All satellites, without exception, stop around 540 - 600 minutes after the initiation state. Even between experiments with different protrusion and detachment times, the pause times are similar. The body of satellites slightly condenses in size compared to the size during the propagation, and there are complex internal wave dynamics observed during this stationary phase.

After the pause state, the satellite growth pattern appears to diverge into three categories. In the first case, satellites transition into networks by forming holes within the body and constructing veins. Satellites can also continue to move, maintaining a characteristic satellite movement, but in a different direction. Lastly, satellites move, but their morphology and the direction of movement are continuously changing, resembling an amoeboid movement [106]. It is currently unknown which factors influence the outcome after the pause state. However, satellites originating from the same patch collectively exhibits only one of these patterns.

There are other motile mesoplasmodia arising from the patch that are not satellites. Notably, when the microplasmodia that typically lead to satellite growth are placed on water agar without any nutrients, smaller motile fragments are produced with different patterns than the satellites (Figure 4.8). This is different from network growth, and therefore likely another type of alternative growth. However, in this thesis, only the experiments that meet all the criteria specified above are classified as satellite growth pattern.

4.6.2 General outcome of the satellite growth

It is difficult to convey the dynamics of satellite growth in a static medium. The movements are hard to notice in a time series pictures, especially if the movement is relatively slow and the morphology of the moving object is stable. Therefore, to better visualize the progression of the satellite growth, all segmented images from a time series experiment are summed on top of each other to capture the dynamics of the growth in a single image (Figure 4.6, right). This image is referred to as a summed image. A summed image is a greyscale image, and the intensity at each pixel indicates the duration that the pixel is occupied by *P. polycephalum*. An intensity of 1, represented by white colour, indicates that the slime mould occupied that space for the entire duration of the experiment, while an intensity of 0, black, indicates that the slime mould has never visited that area. Summed images in this work are shown with enhanced contrast to better visualize the moving path of satellites.

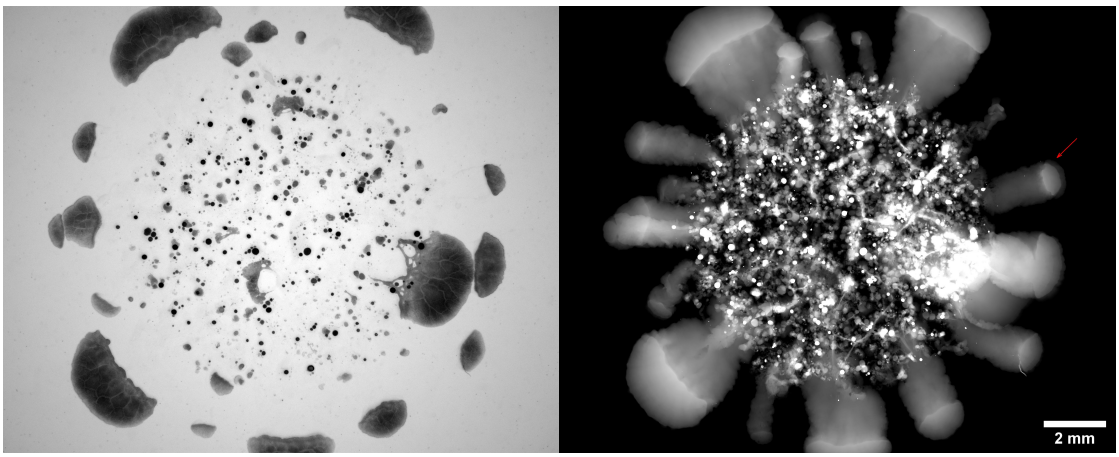

Figure 4.6: A typical outcome of a satellite growth at a pause state (Left) and a summed image (Right). Numerous crescent-shaped satellites surround the patch, but the movement is difficult to infer from a snapshot. With a summed image, it is clear which patch satellites took from the patch to the position at the pause state. In a summed image, no internal networks are visible inside the patch, and the paths behind the satellites are straight with relatively constant width. Some motile fragments deviate from the straight path and travel less distance compared to the majority of satellites. These are not counted as satellites. A satellite shows a forward movement after the pause state, and this is seen as a less illuminated area after the satellite shape. This is indicated with a red arrow.

Overall, the summed image shows a cloudy trace of the path of satellites from the

patch (Figure 4.6, right). The background is black, as the biomass never covered these areas. There are multiple small round structures in the patch. These are likely immobile microplasmodia that did not participate in the formation of satellites. Some of these can be also seen in the static picture at pause state as black dots. Not all microplasmodia participate in the fusion. There are some residual network structures within the patch, showing how the internal biomass was transferred to the border.

The path between the patch and the satellite is relatively straight, and its width is relatively constant. However, the paths emerge from the border of the patch and do not impede into the inside. This shows that satellite formation occurs near the border, but not inside the patch.

Although the path of a satellite is relatively straight, the boundaries of these paths are not straight but ruffled. This shows that the morphology, as well as the movement, exhibits some variation as the satellite progresses. The segment of the path immediately behind a satellite is illuminated with slightly higher intensity. This shows that the motility speed is approximately constant until it slows down, eventually coming to a stop in the pause state. It has already been established that all satellites make a pause around 9 hours (Figure 4.5). This is the reason the satellites are better illuminated than the path that it preceded. In some cases, a faint shadow is observed after a satellite. These are especially evident from satellites on the right side in the summed image (Red arrow). These satellites likely either expanded or exhibited further motility after the pause. The formation of satellites occurs with equal distribution along the border of the patch, indicating no directional preferences.

In figure 4.7, a different dynamic of satellite growth is observed. A network structure is visible inside the patch, which connects all the emerging satellites. Moreover, satellites have extended network structures trailing behind them. However, these network structures are not visible from a static image. Since these fine networks behind satellites appear neither blurred nor faint, they must be present for a considerable amount of time. It is indeed occasionally visible, that larger satellites have internal vein structures. These internal structures are therefore stable and fixed in a place, and do not shift in position during locomotion. Rather, they are continuously constructed and removed as satellites propagate. First, these internal veins were suspected to be the same as the external veins of a network. However, when these satellites were fixated and their internal structures were investigated with transmission electron microscopy, no structural differences were found within these mesoplasmodium that suggested presence of veins [107]. Therefore, these internal veins possess unique characteristics to allow a flow of protoplasm without solid structural support.

It is suspected that the residual network structure is the transition between the network and satellite growth. The author conjectures that these residual networks are more readily visible with younger microplasmodia, and older microplasmodia produces a satellite pattern devoid of these structures. It is also possible that higher coverages of microplasmodia are more likely to form a network structure, perhaps via the percolation mechanism as reported in [75]. However, satellite growth patterns occur within 10 hours

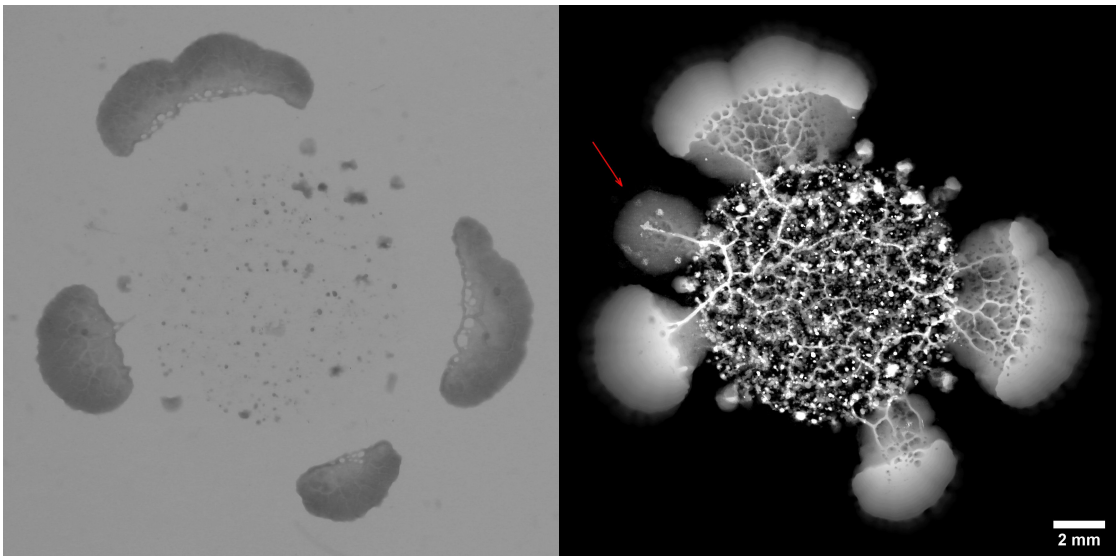

Figure 4.7: An outcome of a satellite growth at the pause state (Left) and the summed image (Right) with internal networks. Unlike in figure 4.6, satellites are larger, and most microplasmodia have disappeared from the patch, indicating that they have fused and formed satellites. Moreover, an extensive network structure is visible from the summed image that connects all satellites. The width of the path of the satellite is not constant, but increases as satellites come out of the patch. There appear to be five satellites from the summed image, but only four are remaining at the pause state. One of these satellites has formed and protruded, but its biomass has later been distributed to the other satellites (Red arrow).

after inoculation, while the percolation networks generally takes 24 hours or more [108].

4.6.3 Effect of environmental factors on satellite growth

Due to the inherently stochastic nature of the satellite growth, as well as the limited time window during which microplasmodia initiate this growth, efforts were focused on reproducing the satellite growth rather than on investigating parameters that affected the various characteristics of satellites. Efforts to vary external parameters usually led to either network growth or no growth at all and experimental conditions were quickly reverted. Therefore, while it was clear that satellites could be reproduced with some success under the conditions stated in the experimental procedure (Section 4.2), it was not clear how far these conditions could be altered until the satellite growth no longer occurred. In this section, the limited evidence of external parameters affecting the satellite growth is described. Each of these experiments was performed at least three times to confirm that the observations are not a one-time event.

The first obvious question that arises is the effect of nutrients other than glucose on the growth of *P. polycephalum*. It was clear that the absence of glucose is crucial, but how do other nutrients affect growth? To this end, no systematic studies were conducted to investigate these effects. However, several experiments were performed with agar that contained only water. In this environment, a different migratory pattern was observed.

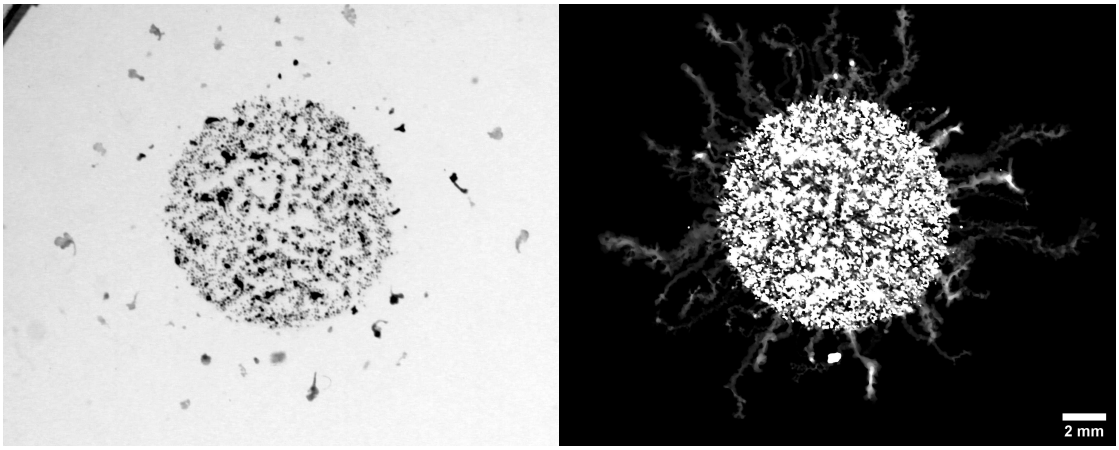

Figure 4.8: An outcome of growth at 9 hours (Left) and the summed image (Right) on a water agar without nutrients. Smaller motile fragments migrated away from the patch, while the majority of microplasmodia remained inside the patch. The trajectories, as seen in a summed image, were not straight and had many turns. However, all fragments still radially propagated away from the patch.

On a water agar with microplasmodia with a satellite-appropriate age, microplasmodia did not sufficiently fuse to form mesoplasmodia, but smaller fragments moved out of the patch (Figure 4.8). These movements resembled typical amoeboid movement, where both the direction of movement as well as the shape of the fragment was unstable and frequently altered [106]. Eventually, these fragments stopped and formed a dark, condensed body, which was assumed to be a dormant form referred to as spherules (Figure 3.1). The migratory nature, as well as detachment from the patch, was maintained, but the stability of the shape and the direction was lost. While these fragments emerged around the same time the satellite protrusion occurred, their movements could not be characterized as those observed in the satellite growth. Therefore, it was suspected that other nutrients affected the behaviour of *P. polycephalum* by allowing microplasmodia to fuse and provide more stability to the search pattern. Another interpretation was that since the water agar is a much harsher environment than the glucose-absent SDM agar, the migratory behaviour was reinforced while coordinated search efforts are minimized.

The effect of glucose was also further investigated by adding it directly to the inoculum. In these experiments, microplasmodia were resuspended with WM, which contained 11 g/L glucose, along with other nutrients. Then, an experiment was performed on an SDM agar without glucose. In this case, the addition of WM was not sufficient to suppress satellite formation, but the number of satellites formed was severely reduced (Figure 4.9). While microplasmodia resuspended with water produced numerous satellites, which were separated from the patch, only a few bodies of reduced size emerged from the patch resuspended with WM. Moreover, mesoplasmodia in the WM-resuspended patch were located in the centre, whereas in the water-resuspended patch the mesoplasmodia were located near the border. The reduced distance travelled by satellites in the presence of nutrient was consistent with the hypothesis that the satellite growth is a foraging pattern, as the presence of glucose in the patch reduced the need for an organism to move

away to find new food sources.

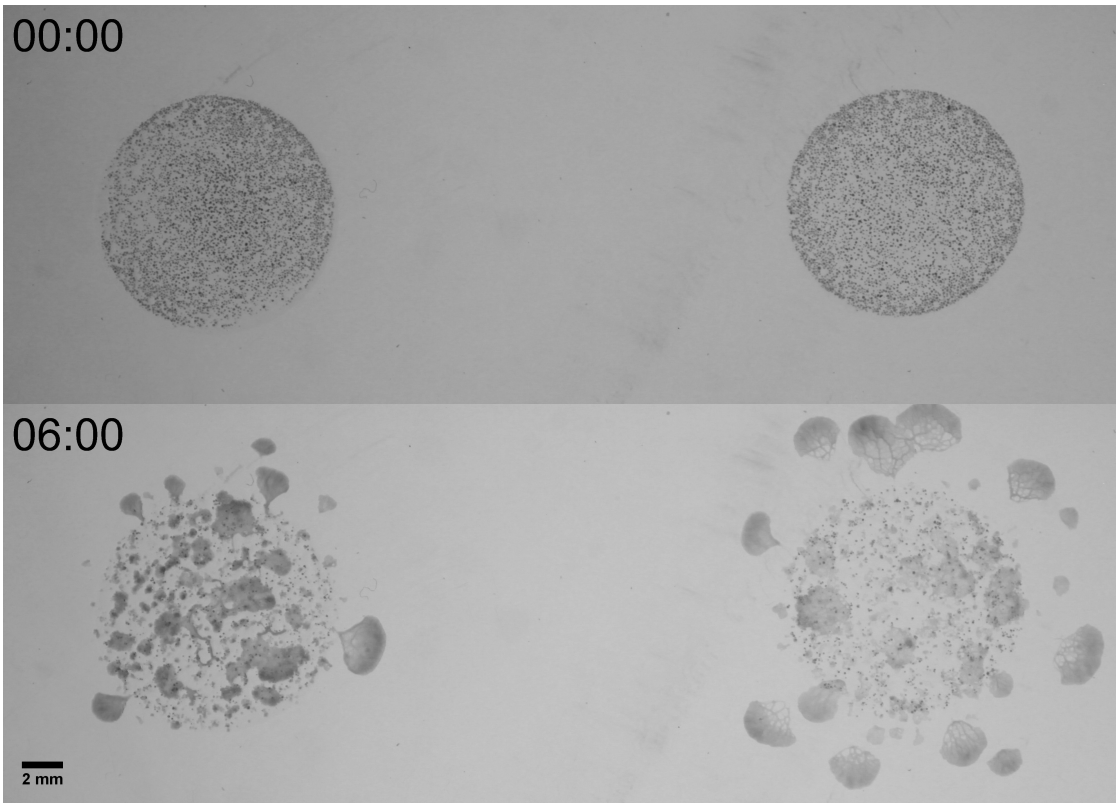

Figure 4.9: The effect of nutrients on satellite growth. Two patches of satellite experiment were prepared with microplasmodia from the same culture. Different media were used to resuspend and plate the microplasmodia. The left patch was resuspended with WM, while the right patch was mixed with sterile water. At $t = 0$, two patches were indistinguishable from one another. However, after 6 hours, a clear difference in the satellite formation was observed. The patch on the left produced only a small number of satellites, while many mesoplasmodia were still connected to the patch. The patch on the right showed a typical satellite growth, where numerous satellites formed and radially migrated away from the patch. Time is indicated in hh:mm.

The thickness, as well as the concentration of the agar, affected the satellite formation. The concentration of agar changes the stiffness of the resulting gel, with a higher concentration of agar creating a stiffer substrate. It was already known that the stiffness of the substrate had a significant effect on network topology [109]. The agar concentration did not hinder satellite formation but altered the shape of the satellite, as well as the resulting network formed thereafter. To investigate this subject, from the same microplasmodial culture, three experiments were prepared with different agar conditions (Figure 4.10), and snapshots were taken 10 hours later.

With an agar percent of 1.7%, a typical experimental condition, numerous satellites were formed. Having passed the pause state, these satellites formed many protrusions and have already exhibited signs of network transition (Middle). In 3.4% agar percent, satellites appeared much smoother (Right). Fewer satellites were formed, but the size of

these satellites was comparable to 1.7%. On 1.7% agar prepared with double thickness, a different satellite pattern emerged (Left). Many satellites were formed, but with a much smaller size than the two previous patterns. The distance travelled by these satellites were also smaller. The thickness of agar may affect diffusion, as chemicals can diffuse further in the vertical direction rather than horizontally. This supposition was further investigated in the later section, where diffusion of a signal molecule is discussed as a candidate to describe the distance travelled by satellites (Section 4.8).

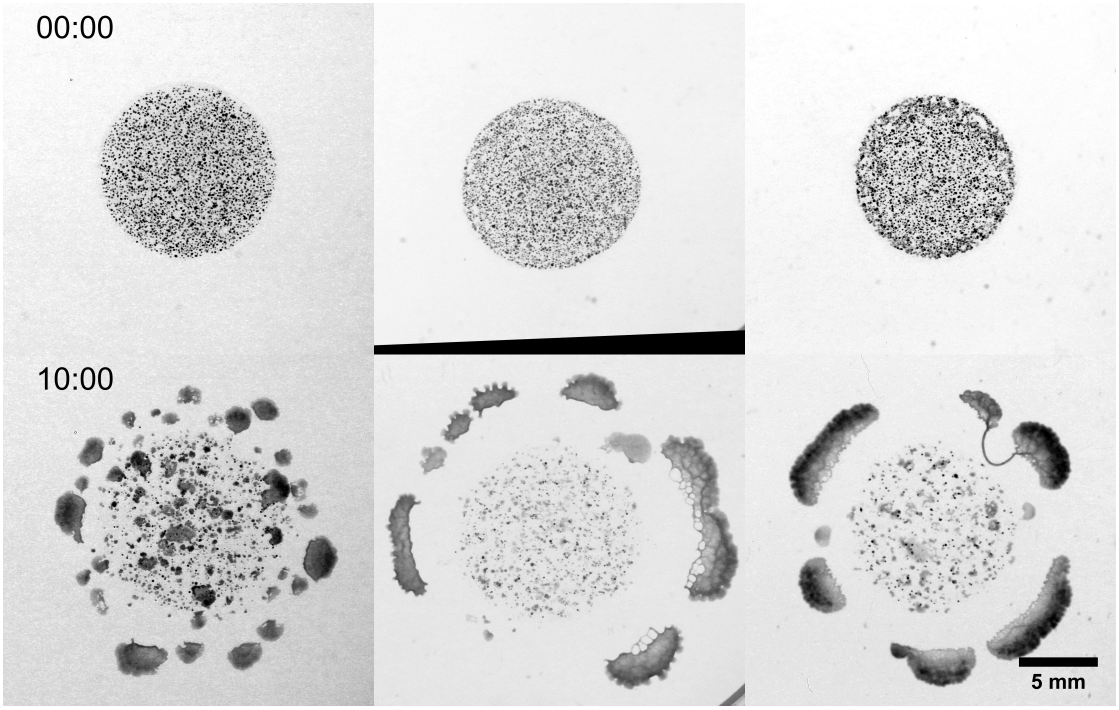

Figure 4.10: The effect of stiffness of the substrate on satellite growth. Three patches were prepared with the microplasmodia from the same culture, but each patch was prepared with different agar conditions. The left patch was placed on thick 1.7% agar, which is the softest condition and twice the thickness of the other agar. The right patch was placed on thin 3.4% agar, which is the hardest, and the middle patch was placed on a thin 1.7% agar. Initially, all three patches appeared similar. However, in soft conditions, numerous small satellites were formed, whereas stiffer substrates induced larger satellites. The time of observation is indicated as hh:mm.

Lastly, the effect of obstacles on the trajectories of satellites was investigated. It was suspected from early on that the supernatant from the microplasmodial culture played a role in the formation of satellites. Initially, an extracellular slime form *P. polycephalum* was proposed as a candidate for inducing the migratory behaviour, as it was known that *P. polycephalum* avoids its own slime [92]. Moreover, since microplasmodia were cultured for an extended period in the same liquid medium, a waste product or signal chemical could have been accumulated in the liquid culture that may cause the migratory behaviour.

Neither addition of the slime, nor the supernatant from a satellite-producing mi-

croplasmodial culture to younger microplasmodia affected their growth pattern. However, when the supernatant of its own culture was harvested and deposited near the patch, the trajectory of a satellite was altered (Figure 4.11)

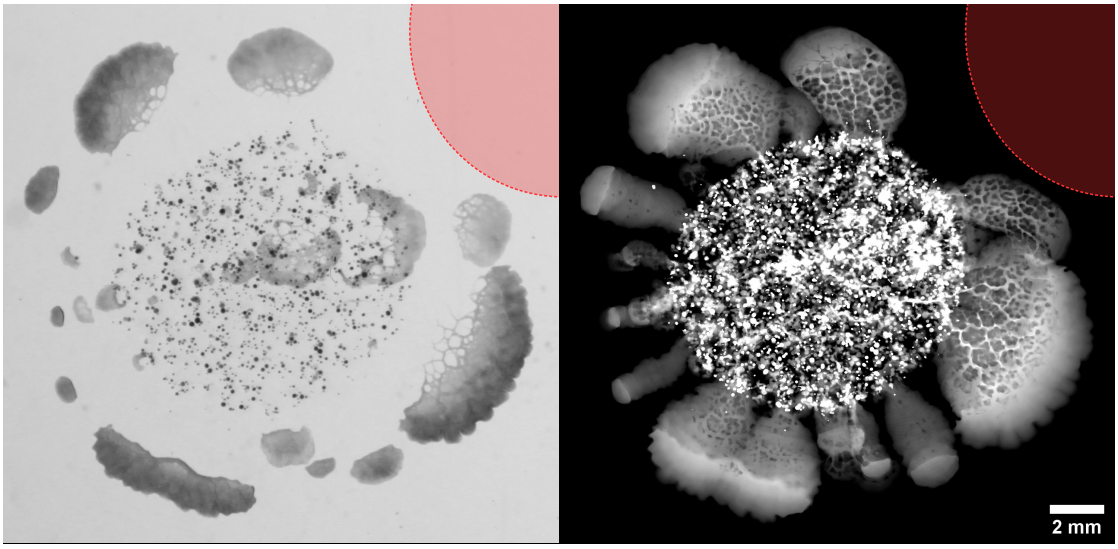

Figure 4.11: An outcome of satellite growth with a chemical barrier (Left) and the summed image (Right). During the preparation of the satellite experiment, the supernatant of the microplasmodia was harvested and placed on the agar (Red circle). From the snapshot at the pause state at 9 hours, it was evident that no satellites overlapped with the deposit. From the summed image, it was clear that satellites initially formed near this deposit, but changed their trajectory so that they avoided the deposit. The trajectories were altered well before making contact with the boundary of the deposit.

In the static image, it was not clear whether satellites simply did not form near the top right corner, or have formed but turned away from the deposit (Figure 4.11, left). This ambiguity was resolved in a summed image, where satellites formed ubiquitously along the border of the patch, but the top right satellites deviated from the usual radial expansion to a curved path, which never touched the deposit. This suggested a diffusive chemical that influences the motility of *P. polycephalum*. This was used as supporting evidence in section 4.8 to form a hypothesis of a signal molecule that dictated the motility of the satellites.

4.7 Quantitative description of the satellite growth

In this section, the satellite growth is analyzed quantitatively, based on segmented images of the time series experiments. The goal of this section is to observe and compare the dynamics of satellite growth and other growth types in a macroscopic and microscopic scale. To this end, the growth is simplified into the number of objects and the area covered. How these two variables change over time and how they differ between growths are noted, and interpreted based on the hypothesis that satellite growth is a foraging strategy.

Since satellites are larger than microplasmodia, microplasmodia must fuse with one another to create larger bodies. In satellite growth, this occurs within a limited time (Section 4.6.1). Therefore, the movement of microplasmodium is also investigated to see whether the difference in growth is the direct result of the altered behaviour of the individual fragments.

4.7.1 Statistical analyses on satellite growth

A total of 205 satellite experiments were fully recorded as a time series with a fixed incubation temperature from the photobox (Table 4.5). In some cases, multiple plates were produced from one experiment and kept in an incubator. These parallel experiments were used to screen for different environmental conditions and checked for consistencies. Although the results from these parallel plates were recorded, no time-series data was saved and therefore they were not included in the statistics. Each experiment contained between 3 to 9 patches of microplasmodia, mostly from the same batch of culture. Occasionally two different batches of microplasmodia were used, but only one of these cultures was of satellite-appropriate age. An experiment was considered a success when any of the patches from an agar plate produced a satellite growth. All satellite experiments were performed on SDM agar plates without any glucose, with microplasmodia aged around 6 days, based on previous results on the conditions that induce satellite growth. All experiments were performed with the same strain of *P. polycephalum* in the photobox.

Table 4.5: Satellite experiments recorded. Mean age refers to the age of the microplasmodia, calculated from the inoculation of the liquid culture. σ is the standard deviation of the age of microplasmodia that produced a satellite growth.

Period	Total	Satellite	Success (%)	Mean age (days)	σ
All	205	114	55.6	5.94	0.20
2014.04.01 - 2016.02.03	58	31	53.4	5.93	0.14
2016.02.04 - 2016.10.02	31	25	80.6	5.93	0.24
2016.10.03 - 2018.01.17	18	9	50.0	5.94	0.05
2018.01.18 - 2018.10.07	51	15	29.4	6.01	0.08
2018.10.08 - 2019.05.01	47	34	72.3	5.92	0.26

Even with the best effort to keep the conditions constant, the satellite growth was only observed about 56% of the time. The variations in microplasmodial culture may have affected the satellite growth since each batch was inoculated with different amount of microplasmodia with varying age. However, it was considered more likely that the satellite growth process was inherently stochastic, with factors influencing the growth that are currently unavailable for observation. Satellite growth was particularly rare during the period when the centrifugation was performed with higher speed (2018.10.18 - 2018.10.17, 29.4%). How the increase in the gravitational force affects microplasmodia was not investigated, although the overall vitality and the competence to grow seemed unaffected.

The two periods with the highest success rate of the satellite growth (2016.02.03 -

2016.10.02 and 2018.10.08 - 2019.05.01) were the periods where the experimental conditions were kept identical as described in the experimental procedure (Section 4.2). The mean age of microplasmodia that produced satellite growth was also relatively stable, although experiments mostly utilized 6 days old microplasmodia. The largest variance on the age of microplasmodia corresponded to the highest success of satellite growth. The change in experimental conditions may have narrowed the window during which the microplasmodia perform the satellite growth. The slightly elevated mean age for satellite formation was observed during the period of high centrifugation speed, although the difference was minimal and no further investigation was performed.

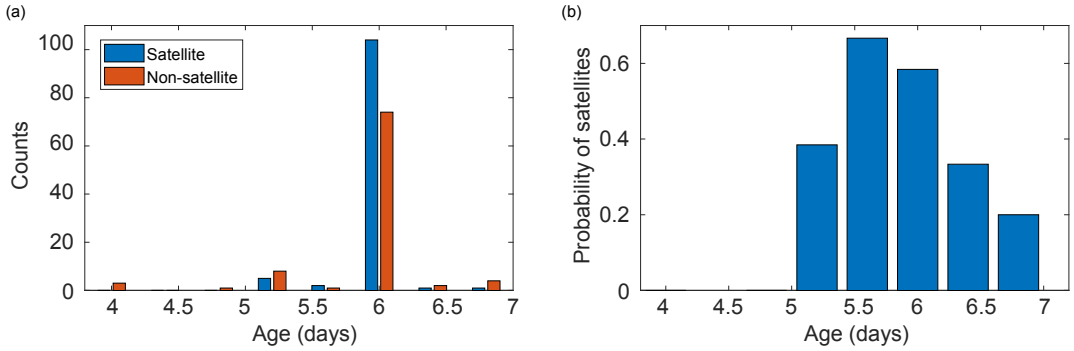

Figure 4.12: Onset of the satellite growth is influenced by the age of the microplasmodia. The total count of the satellite and non-satellite growths (Panel (a)) and the probability of the satellite growth (Panel (b)) are plotted based on the age of microplasmodia. Data were pooled into the 0.4-day interval from 3.8 days. Most experiments were performed with microplasmodia aged between 5.8 and 6.2 days, as the focus was to produce satellite growth. The probability of observing satellite growth (Panel (b)) was the highest around day 5.6, although the sample size was small. Younger and older microplasmodia around day 6 showed a lower rate of satellite growth, as expected.

To investigate further on the age dependence of the satellite onset, the data were pooled based on the age of microplasmodia (Figure 4.12). The satellite growth was observed from microplasmodia aged between 5 to 7 days old. The highest rate of satellite growth was observed around age 5.6, although not enough experiments were done with these microplasmodia to validate this claim. It is evident, however, that the satellites are not as likely to be observed with microplasmodia aged younger than 5 or older than 7.

4.7.2 Growth dynamics of *P. polycephalum* from selected examples

Qualitative comparison

The satellite growth, although precisely defined by their phases (Section 4.6.1), showed variations between growths. One obvious difference was the number and the size of satellites produced, which will be discussed extensively in the subsequent section (Section 4.9) Other than the differences that could be spotted with static visual cues, there were also changes in the dynamics of microplasmodial movement and expansion. To better describe the satellite growth, and also to determine how different parameters differ from network

formation to satellite formation to inactivity, growth of *P. polycephalum* was observed in detail from microplasmodia aged between day 5 to 7.

The figure 4.13 shows the general trend of growth from microplasmodia from different ages. Young microplasmodia, aged 5.4 days, formed a network structure with thick growth fronts (Row (a)). Protrusions were not readily visible at 3 hours after inoculation, and all components were connected with a vein that ran through the patch at 9 hours. There were some finger-like protrusions evident on the growth front as well. However, most of the biomass already vacated the patch, indicating that it already exhibits some migratory behaviour. In previous works by Fessel et al. [75], microplasmodia stayed on the inoculated spot for an extended period time longer than 9 hours. The migration was only observed after the establishment of a giant network component connecting the majority of the plasmodial mass. Microplasmodia used for these investigations were younger than 5 days, and agar contained various levels of glucose (Personal communication). Therefore, the presence of glucose and the age of microplasmodia affected the migratory behaviour and growth pattern of *P. polycephalum*.

Microplasmodia aged around 6 days produced satellites that detach from the patch of inoculation. Protrusions of the mesoplasmodia were visible at 3 hours mark (Figure 4.13, row (b-d)). In some cases, not all of the protrusions detached and formed a satellite (Row (b)), but remained attached to the patch. Some network structures or veins were observed within the patch that connected mesoplasmodia with each other. Occasionally, these structures persisted and form an umbilical-cord-like structure that connected the detached mesoplasmodia to the patch (Row (c)). However, in general, network-like properties were less pronounced as the satellites emerged. Fewer external veins were visible, and sheet-like structures dominated (Row (c, d)). Their growth fronts were also smoother than the growth fronts of a network.

As the microplasmodial age increased, mesoplasmodia detached faster to become satellites, and intermediate network structures were less pronounced (Figure 4.13, row (d)). Umbilical cord-like structures were no longer present. Also, there was the second onset of the mesoplasmodial protrusion, where a mesoplasmodium came behind already detached satellites (Row (d), red arrow). These were not considered satellites, although the distinction became difficult if they were completely detached from the patch at the pause state. These motile mesoplasmodia also hindered the accuracy of the analyses, as they generally exhibited greater velocity and caught up to the satellites, leading to a fusion between the two. Conscious efforts were made to exclude these secondary motile mesoplasmodia from analyses. There were several experiments where only the secondary motile mesoplasmodia were observed, without any satellites. In terms of adaptive strategies, these motile fragments are likely the same type of growth as the satellites. However, these secondary patterns were only noted and not treated as satellite growth.

Microplasmodia at day 7 were inactive, as they likely had undergone a spherulation process to assume a dormant form (Figure 4.13, row (e)). There was a small subset of microplasmodia that were still active and motile, but no collective movement was seen in the first 9 hours of experiments. Given sufficient time, these microplasmodia resuscitated

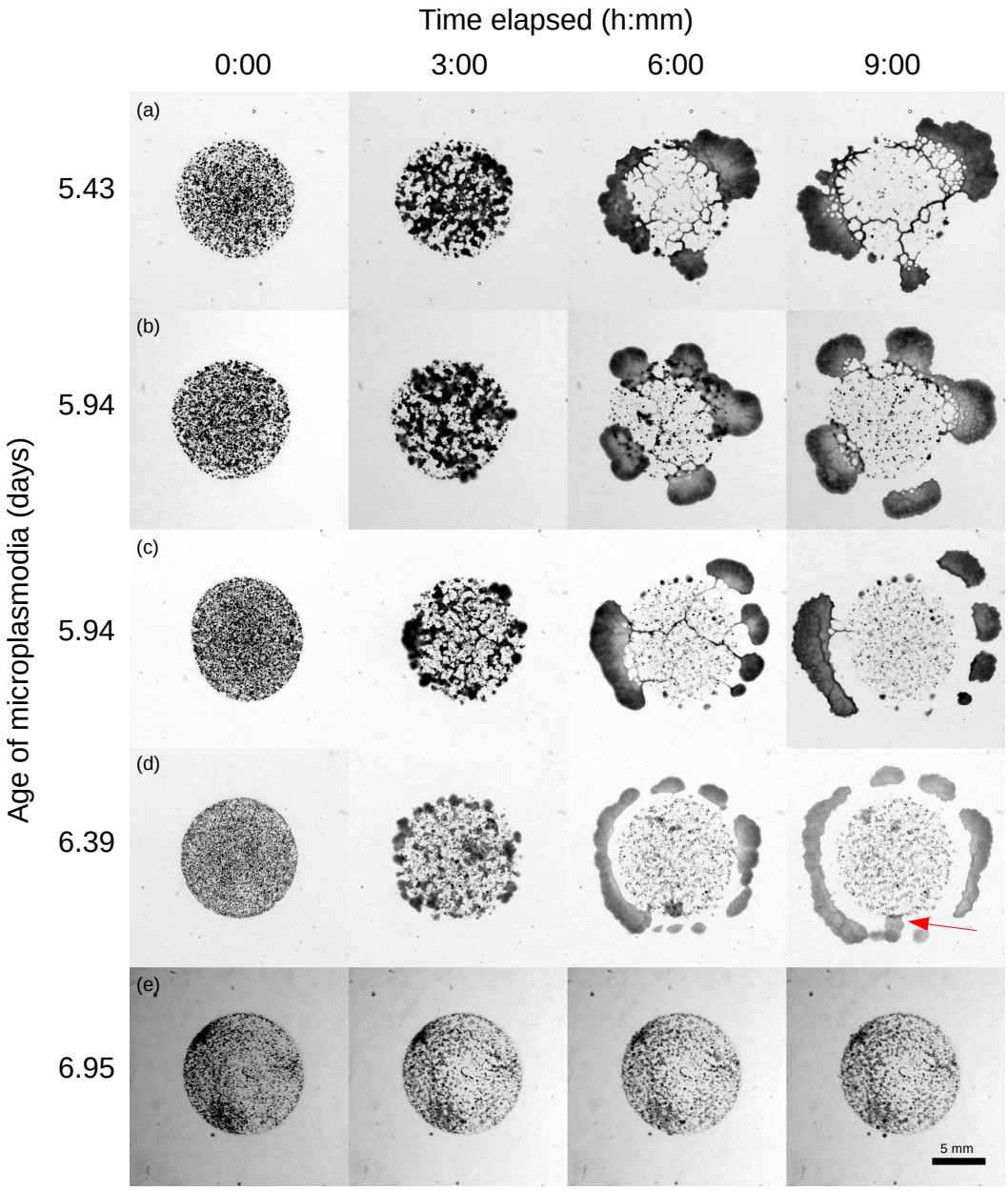

Figure 4.13: Different growths of *P. polycephalum* from microplasmodia aged between 5 and 7 days. 5 days old microplasmodia produced a network, although the tendency of migration away from the patch is already evident (Row (a)). The first growth pattern from microplasmodia aged 5.9 produced a mixture of satellite and network growths (Row (b)). In another experiment, microplasmodia of the same age were able to produce more satellites, although the umbilical cord-like attachment from the left satellite was still visible (Row (c)). As the microplasmodia aged, satellites tended to detach earlier (Row (d)). By day 7, microplasmodia remained inactive for the first 9 hours of observation (Row (e)). There were differences in microplasmodial shape, as the older microplasmodia tended to be smaller in size and rounder in shape. Moreover, as the age progressed, more microplasmodia remained inactive and do not participate in the fusion.

themselves and fuse. However, they built networks instead of forming satellites after the resuscitation. Therefore, satellite growth appears to have very strict prerequisites that need to be met before it commences.

Quantitative comparison

To quantitatively describe the differences in growth and foraging dynamics of these patterns, images from the time-series experiments were segmented, as described in section 4.2. The goal of the analyses of the segmented images was to identify parameters that are distinct between satellites, networks and non-satellites. The unique features of the satellite were the complete detachment from the patch, as well as the relatively constant morphology and size after detachment. Therefore, the number of objects, as well as the area occupied by these objects, were analyzed based on where they are located based on their initial positions. In the segmented images, the objects represented the fragments of *P. polycephalum* and the area represented the biomass. A mask was generated for this purpose, from the patch at $t = 0$, by computing a convex hull (Figure 4.2). Then, this mask was used in segmented images to identify whether an object has detached from the patch.

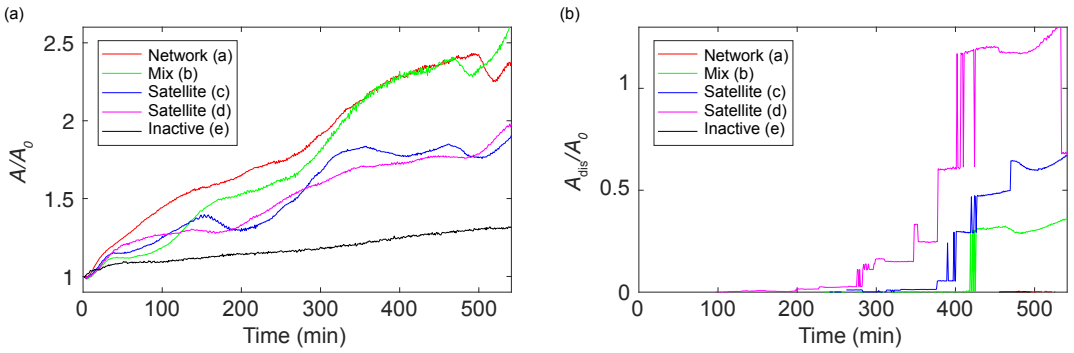

Figure 4.14: The dynamics of the occupied area growth is different between growth types. The total area (Panel (a)), and the area disconnected from the patch of inoculation (Panel (b)) are plotted over time. Both areas are scaled with the initial total area. The growths in figure 4.13 are shown in the graph, and the corresponding rows are indicated in the legend. In general, the total area increased over time in all growth types. The network growth (a) showed a faster increase compared to the satellite (c-d) and inactive growth (e). The mixed growth (b) initially showed similar dynamics with satellite growths, but after 300 minutes became almost identical with network growth. Inactive growth, as expected, did not show any significant patterns, although the overall area still slightly increased. In the plot of disconnected area (Panel (b)), only the satellite and mixed growths (b-d) were noticeable, as other growth types did not produce fragments that detached away from the patch. Step-like trajectories were apparent, indicating the moment when satellites separated from the patch. After this step, the plot was relatively flat and did not show significant increase, indicating that the satellites, once detached, did not expand significantly. This step also appeared to be synchronized between experiments. Frequent jumps after detachment indicate a segmentation error.

The total area occupied by *P. polycephalum* increased over time for all microplas-

modia (Figure 4.14, Panel (a)). A simple explanation is that the organism grew and increased its biomass. However, these microplasmodia were extensively starved, and the agar lacked a readily usable carbon source. Therefore, it was more likely, at least in part, that the increase in area was due to the rearrangement of biomass rather than the growth of biomass. The increase in area was the greatest when the growth involved network formation (Growth (a)). In satellite growth (Growths (c, d)), the area increased about twofold in 9 hours, while the network growth reached about 2.5 times the original area in the same interval. The growth mode where both satellite and network was observed (Figure 4.13, row (b)), has been found to be characterized by the dynamic similar to the satellite growth initially, but network-like later on. The increase in total area was not at a constant rate, and there appeared to be phases where the growth was faster.

Plotting the portion of area disconnected from the patch clearly distinguished the satellite growths from the non-satellite growths (Figure 4.14, panel (b)). Discrete jumps were visible only from growths that produced satellites (Growths (b-d)). Repeated jumps back and forth in rapid succession indicated an error resulting from inaccurate segmentation. There appeared to be a correlation between the time when jumps occurred between different experiments. This similarity is further investigated based on a larger set of data (Figure 4.16) (Section 4.7.3).

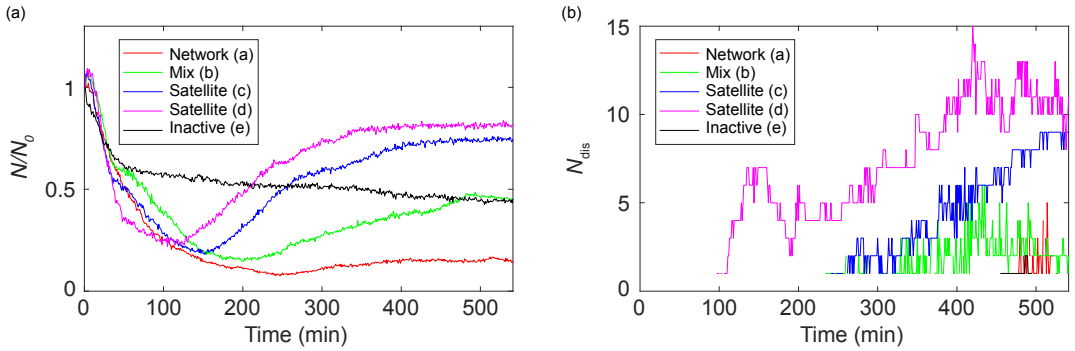

Figure 4.15: The dynamics of the number of objects is different between growth types. The total number of objects, scaled with the initial number of objects (Panel (a)), and the number of objects disconnected from the patch occupied by *P. polycephalum* (Panel (b)) are plotted over time. The growths in figure 4.13 are shown in the graph, and the corresponding rows are indicated in the legend. Initially, all growth types showed a rapid decrease in the number of total objects (Panel (a)). The inactive growth (e) was the first to escape the descent, and maintained a relatively stable number thereafter. The network growth (a) fell the longest and the lowest and maintained a stable number of objects after the fall. In mixed and satellite growths (b-d), recovery of the number of objects was evident after the initial decrease. This was likely caused by inactive particles that were hidden within the mesoplasmodia and revealed as the satellites migrated away. Only the growths with satellites produced disconnected objects, as expected (Panel (b)). Inactive and network growths were present only after 480 minutes, and its contributions were likely a segmentation error, as they do not possess a disconnected component. The satellite growth with older microplasmodia (d) showed early onset of disconnected objects, appearing at 100 minutes. However, the disconnected area only increases after 250 minutes (Figure 4.14, panel (b)), and therefore this early-onset was also likely an error. The other satellite and mixed growths appeared after 250 minutes.

The analyses on the number of objects give hints on how the fusion between fragments occurs (Figure 4.15, panel (a)). Since microplasmodia must fuse to form satellites as well as networks, it was expected that the fusion rates differ between different growths. However, after the segmentation, fusion and two microplasmodia in close proximity or contact could not be distinguished. Therefore, the decay shown in the figure may be over-represented. The decay rate is further investigated with a higher resolution in a later section (Section 4.7.4).

In all experiments, the number of objects decreased rapidly during the first hour. The initial rate of decrease was similar between all experiments. The inactive 7-day microplasmodia differed from the rest of the growths in the sense that the decrease was stopped after an hour, and the number of objects N/N_0 remained relatively stable (Figure 4.15, panel (a), growth (e)). In all other active growths, the N/N_0 decreased below 0.3 (Growths (a-d)). In the network growth, the objects did not recover and remain low (Growth (a)). The growths involving satellites showed a recovery in the number of objects (Growths (c, d)). It was suspected that this was caused by inactive microplasmodia remaining in the patch, as disconnected objects had evacuated the patch as satellites. When mesoplasmodia formed inside the patch, they tended to form on top or near these inactive microplasmodia. This essentially hid these objects, causing the number of objects to be underestimated. When mesoplasmodia and satellites migrated away from the patch, these inactive particles reappeared, causing an appearance of N/N_0 recovery. This recovery was the greatest in satellite growth with 6.4 days old microplasmodia (Growth (d)).

The number of disconnected objects over time did not indicate the time when satellites disconnected from the patch, likely due to faults in the segmentation (Figure 4.15, Panel (b)). The number of disconnected objects at the end was larger than the number of satellites, despite significant efforts in image processing. In both satellite growths, 4 satellites were found, but the segmentation identified 7 components (Growths (c, d)). Also, the number of disconnected objects were unstable, frequently jumping back and forth. Nevertheless, the number of disconnected objects clearly distinguishes between the satellites and other growths, as these non-satellite growths did not show significant activity in this measurement.

In summary, the growths of *P. polycephalum* at different ages of microplasmodia were visually distinct. These distinctions were captured by simplifying the growth as the area occupied by the slime mould, as well as the number of fragments of the slime mould. Large jumps were noticed, especially in the disconnected area and objects dynamics. From a small sample size, the jumps appeared to occur at the same time, but this coordination is expected to be averaged out when larger data is used to analyze the growth dynamics.

4.7.3 The mean growth dynamics of *P. polycephalum*

Quantitative description of the mean

To better compare the growth dynamics of the satellites to the non-satellite growth, the average dynamics of the entire data were plotted. To compare between experiments with varying coverage and patch size, both the area (A) and the number of objects (N) were normalized with the initial value. Experiments contained multiple patches, and each patch was considered as individual data. Patches were divided into three types:

1. Satellite growth, in which at least one satellite was observed from the patch.
2. Non-satellite growth, which was prepared at the same time as the patches with satellite growth, but no satellites were observed. The distinction was made so that in these experiments, there was clear evidence that microplasmodia were appropriate for satellite formation, but other factors were not met for supporting the satellite growth.
3. Other growth, which contained all other experiments. No satellites were observed in these experiments.

Also, 4 sets of experiments were imported from the dataset of Dr. Adrian Fessel, who generously provided percolating network growths. These experiments were performed with 3 days old microplasmodia on an SDM agar plate with 5 g/L of glucose. Therefore, the difference in dynamics could be attributed to either the presence of glucose and/or the age of the microplasmodia. Nonetheless, it provided a good point of reference to identify factors that are unique in satellite growth.

The three growth patterns except the network growth showed similar dynamics in the change in the area occupied by *P. polycephalum* (Figure 4.16, panel (a)). These three growth types were almost indistinguishable before 100 minutes, where A/A_0 increased as a saturating curve. It was intriguing that there was a rapid increase in the area in the beginning, which eventually slows down. Some of this may be the contribution of residual supernatant drying from the patch, and microplasmodia settling onto the agar plate. Moreover, microscopic observation suggests that the microplasmodia undergo structural rearrangement during this period (Figure 4.26), which may also contribute to an increase in area.

A/A_0 remained relatively stable from 100 to 200 minutes (Figure 4.16, panel (a)). During this time, microplasmodia actively moved and fused to form mesoplasmodia. The distinguishable feature arose around 200 minutes, where satellite growth (Blue line) increased faster than the other cases. The satellite growth showed another saturation-type growth, which plateaued around 480 minutes. This slowing down of area expansion was also seen in other growths, albeit very weakly. Qualitative observations showed that satellites generally maintained a stable morphology and did not appear to expand. The increase may be caused by inactive microplasmodia that did not participate in the fusion of satellites. These microplasmodia sometimes formed mesoplasmodia that migrate much later than the first satellites (Figure 4.13, red arrow). Also, the intensity in the grey-scale image of the satellite was much weaker than of the microplasmodia, suggesting that it

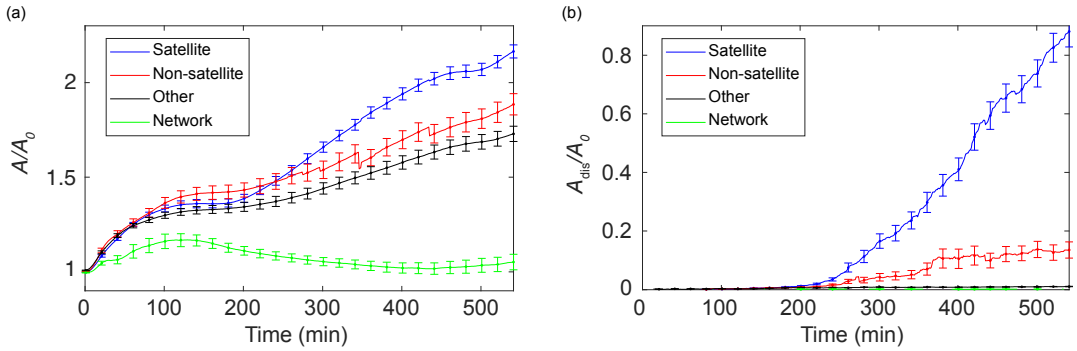

Figure 4.16: The dynamics of the mean area growth are different between growth types. The total area (Panel (a)), and the disconnected area from the patch occupied by *P. polycephalum* (Panel (b)) were plotted over time. The trajectories were pooled and averaged based on the type of growth. The descriptions of each category types are given in the section 4.7.3. Overall, all growths except the network showed an increase in the total area over time (Panel (a)). Interestingly, the network growth only showed a marginal increase in the first 100 minutes, and then fluctuated near the initial total area. Satellite growth showed the greatest increase. The trajectory showed two plateaus, one around 150 minutes and the other near 480 minutes. Only satellite growth showed a large increase in the disconnected area (Panel (b)). Non-satellite growth showed a small contribution after 450 minutes, which might represent the secondary motile mesoplasmodia. The increase in the disconnected area in the satellite growth appeared to be linear. The number of data points averaged is shown in table 4.6. Error bars indicate a standard error of the mean.

may be of a different height.

The network growth showed distinct dynamics compared to the other three growths. A/A_0 did not appear to increase at all before 540 minutes (Green line). There was a slight increase in A/A_0 in the first 100 minutes, similar to the other growths. However, the increase was much weaker, and it reverted to the same area as the initial condition. Since an increase in area was only observed in growths with adverse conditions, this suggested that the area expansion may be an adaptive strategy against starvation.

The disconnected area normalized with the initial total area A_{dis}/A_0 from the patch showed clearly that the satellite growths produced fragments that separate from the patch of origin (Figure 4.16, panel (b)). There was a slight jump in the non-satellite growth around 450 minutes (Red line). This may be the contribution of motile mesoplasmodia seen in figure 4.13 (Red arrow), although the data were not extensively investigated for this phenomenon. Unlike from the plots shown in figure 4.14, panel (b), there were no distinct jumps, as these would likely have been averaged out. The increase was relatively steady and linear, showing that there was no defined time for satellites to completely break away from the patch. It was however not clear whether this is because satellites continued to separate from the patch even at the later stages of the experiment, or whether the area of satellites themselves increased over time.

While the A/A_0 analysis showed that the satellite growth increase in its area the fastest, the object dynamics suggested that its components may also move the fastest

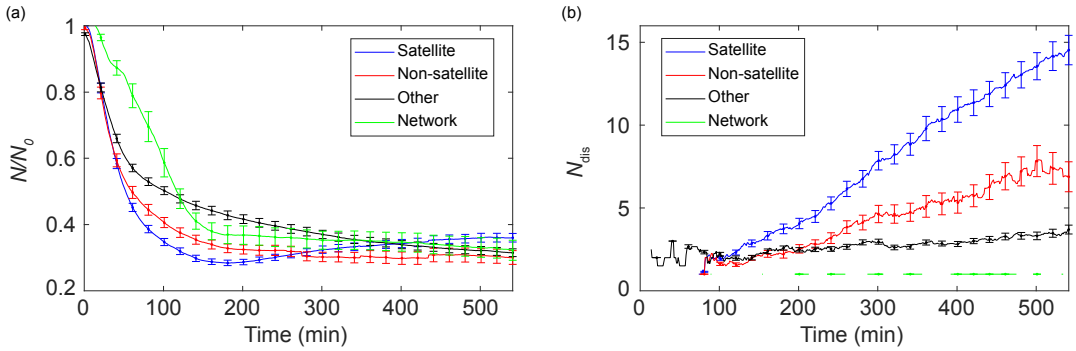

Figure 4.17: The dynamics of the mean number of objects are different between growth types. The total number of objects (Panel (a)) and the disconnected objects from the patch (Panel (b)) were plotted over time. All three growth types except network showed a rapid decrease in N/N_0 in the first hour (Panel (a)). The rate of decrease was the greatest in the satellite growth, whereas the time during which the number of objects decreases is the shortest. The decrease was similar to an exponential decay. The satellite showed a recovery in N/N_0 after the initial decrease. This was likely the contribution of inactive components remaining in the patch. As expected, the satellite growth showed the largest positive increase in the number of disconnected objects (Panel (b)). The rise of the N_{dis} coincided with the moment when the A_{dis}/A_0 increases (Figure 4.16, panel (a)). Non-satellite growth showed a small increase after 400 minutes, also corresponding to the jump in A_{dis}/A_0. The non-zero disconnected objects in other growths were likely the contribution of errors of segmentation and defining the patch boundaries. Error bars indicate the standard error of the mean.

(Figure 4.17, panel (a)). The decrease in the number of objects is attributed to the fusion of microplasmodia. Since microplasmodia are initially separated, they must move to find adjacent microplasmodia to fuse. Therefore, a faster rate of decay indicates the faster motility of microplasmodia. In the object dynamics, all three growths except the network growth were nearly identical in the beginning, starting with a rapid decrease (Blue, red and black lines). However, the three growths were distinguishable after 1 hour, where the three graphs separated from one another with varying rate of decrease.

In other growth, the objects decreased more slowly (Black line), while a much steeper rate of decay was observed in satellites and non-satellites (Blue and red lines, respectively). Satellite growth was distinct from the other two growths due to the fastest rate of decay, and also due to a local minimum within the experimental time. The minimum of N/N_0 for satellite growth was reached around 180 minutes, and then the object number recovered and gradually increased until the end of the experiment. This was likely due to the inactive components hidden within the mesoplasmodia, which is recovered from segmentation when satellites move away from these particles.

The network growth showed a distinct behaviour in that the initial decrease did not resemble an exponential decay, but rather a bell-curve (Green line). However, the transition point from a steady decrease to a stable line was similar to the satellite growth around 150 minutes.

The disconnected number of objects showed a similar pattern with the disconnected

area (Figure 4.17, panel (b)). Since the satellite growth in both panel (a) and (b) showed a steady increase, the increase in area was in part due to the continuous appearance of new disconnected objects. The non-zero values seen at the beginning were likely due to segmentation errors.

Since it was hypothesized that the satellite growth can be characterized as a search pattern, the area *P. polycephalum* explored was also measured. This search area counted all the area it has been at up to some time point, while the total area only counts the area an organism currently covered. It is assumed that the patch area is already surveyed, and therefore it was counted as a part of the search area, even though *P. polycephalum* may not have covered all the initial area. Therefore the search area at pause state equals the area illuminated by the summed image. The search area was also normalized with their respective patch size A_p instead of the total area at $t = 0$, because of the scaling of the satellites is based on the size of the patch, as will be explored in a later section (Section 4.9).

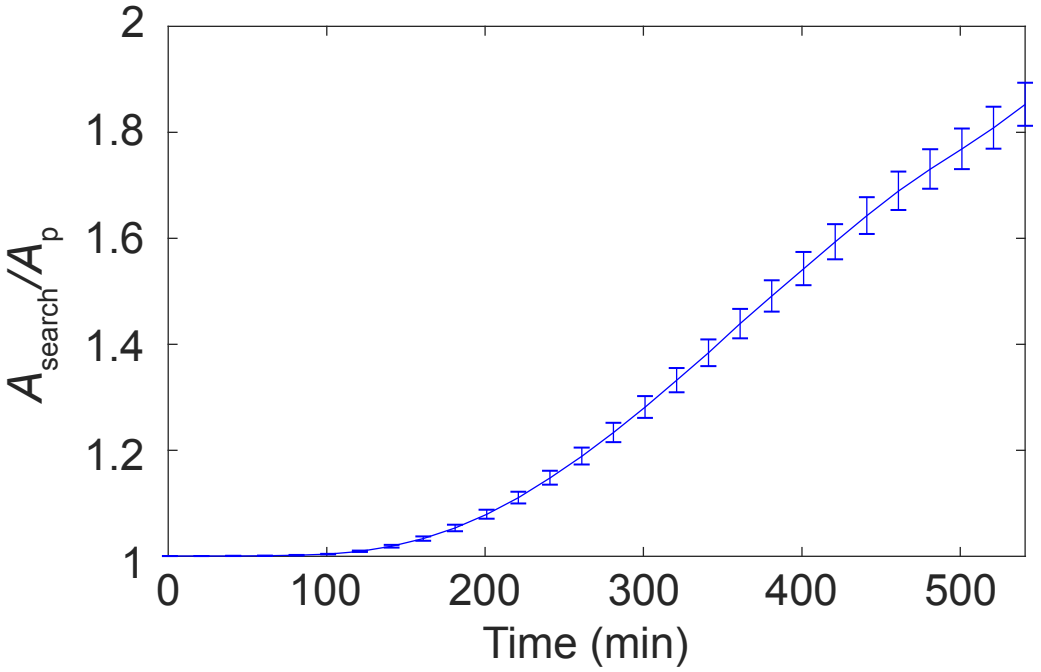

Figure 4.18: The area searched in a satellite growth, normalized by the patch size of origin. The increase is noticeable after 100 minutes, likely the appearance of first protrusions. The curve appears to weakly resemble a logistics function, with exponential growth at the beginning and asymptotic rise at the end, although the asymptote is not yet visible in the plot. Error bars represent the standard error of the mean.

The searched area began its increase after 100 minutes (Figure 4.18), which was earlier than the time at which first disconnected objects emerged, indicated by A_{dis} (Figure 4.16, panel (b)), and slightly slower than the N_{dis} (Figure 4.17, panel (b)). Since the definition of A_{search} assumed that A_p was already searched, the increase occurred only

when a protrusion outside of the initial patch occurred. Therefore, it was clear why the increase in searched area preceded the A_{dis}, as protrusions must occur before satellites could form. The earlier occurrence of N_{dis} before A_{search} further suggested that there may be a segmentation error, and protrusions may have been mistakenly counted as fragmented components. It was difficult to assess, whether this increase in A_{search} was mainly due to the propagations of A_{dis} or growth of A_{tot}.

To summarize, the satellite growth could be clearly distinguished from other growth patterns of *P. polycephalum* from dynamics of the area and number of objects. The satellite growth showed the largest increase in the total area and the fastest decay rate in the total number of objects. How these characteristics contribute to change the growth pattern is unclear. However, a faster decay rate would help microplasmodia to achieve faster fusion to create mesoplasmodia, which may aid in creating satellites.

As expected, the satellite growth was the only growth that showed noticeable dynamics in disconnected area and objects. Non-satellite showed some dynamics in these plots, due to the secondary motile mesoplasmodia appearing from the patch. These were not considered a satellite growth and therefore no further studies were performed. It is unclear, however, how much these motile mesoplasmodia contributes to the dynamics of the satellite growth, as some satellite growth exhibit both satellites and the secondary motile mesoplasmodia.

The dynamics of the first derivatives

To better compare the dynamics of the satellite growth in the area, the number of objects and search, the first derivatives of these plots were calculated with a Savitzky-Golay filter. Savitzky-Golay method utilizes a convolution method to calculate the value of the given point with predetermined weighted integers and a normalization factor based on the order of derivation, and a sampling window [110]. This is equivalent to the least-squares method, where the difference squared between the expected and observed values are minimized. The first derivative represents the slope and therefore a rate of change. It was of interest whether these growths had defined phases that could be defined with different growth speeds, or any distinguishing characteristics that could help further to investigate these patterns.

Between the first derivatives of A_{tot}/A_0 and A_{search}/A_p, it was immediately clear that both possessed a local minimum near 480 minutes (Figure 4.19). This was interesting because A_{tot} and A_{search} were not directly related, as the search area increased only when previously unexplored areas were visited. Moreover, since satellites were separated and detached from the patch, their locomotion speed was initially expected to be the only factor influencing the search area, rather than the total growth rate. The growth of the total area, therefore, was thought not to influence the rate of search. The minimum at 480 minutes was expected, although somewhat early, in A_{search}/A_p, as the pause state occurred around this time, and all movements of satellites temporarily ceased at this point (Figure 4.5).

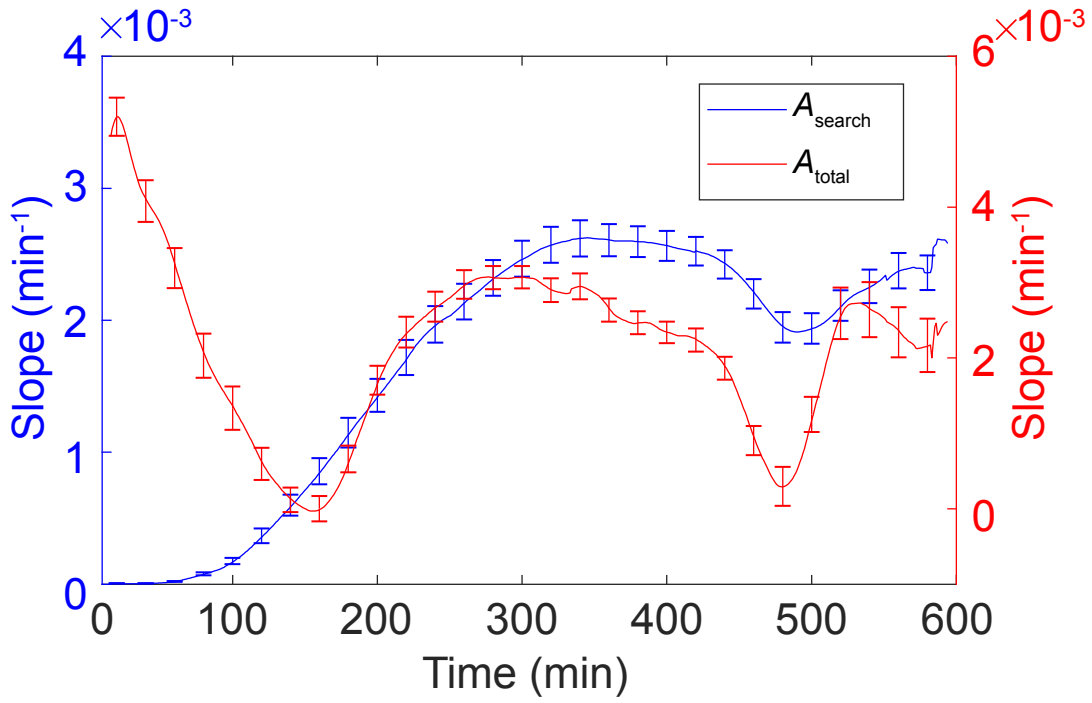

Figure 4.19: The first derivative estimate of the total area (A_{tot}/A_0) and searched area (A_{search}/A_p) over time. The slopes were calculated in 30-minute interval for each experiment separately, then the mean and the standard error of the mean were calculated and plotted. The left y-axis represents the A_{search}, and the right y-axis represents the A_{total}. Both plots exhibited a local minimum at around 480 minutes. A_{tot}/A_0 showed an additional local minimum at around 150 minutes. The error bars indicate the standard error of the mean.

From this graph, however, the pause state and the growth dynamics of the area appeared to be related. It was noted that the oscillation temporarily slows down during mitosis [78], and the time elapsed from the beginning of the experiment to the pause state was approximately in line with the interval of cell division. Coordinated behaviour of fragmented satellites suggested that their behaviours were somehow synchronized, and mechanisms involved in their cell cycle was considered to be one of the methods that an organism could align their behaviours with one another. A further biochemical investigation is required to reveal and confirm the state of cell division at various stages of satellite growth.

The first local minimum around 150 minutes in A_{tot}/A_0 was in line with the time when the first protrusion occurred. During this time, the biomass was redistributed rather than expanded, from inside of the patch towards the outside. Rapid transportation and displacement of biomass may have resulted in decreased expansion. Therefore, during the protrusion state, the growth of area temporarily slowed down due to the satellite formation.

The dynamics of A_{tot}/A_0 matched the two states defined in the satellite growth (Figure 4.5). Whether these growth dynamics dictate the phase, or whether the phase of the

satellite growth alters the area growth remains to be further investigated.

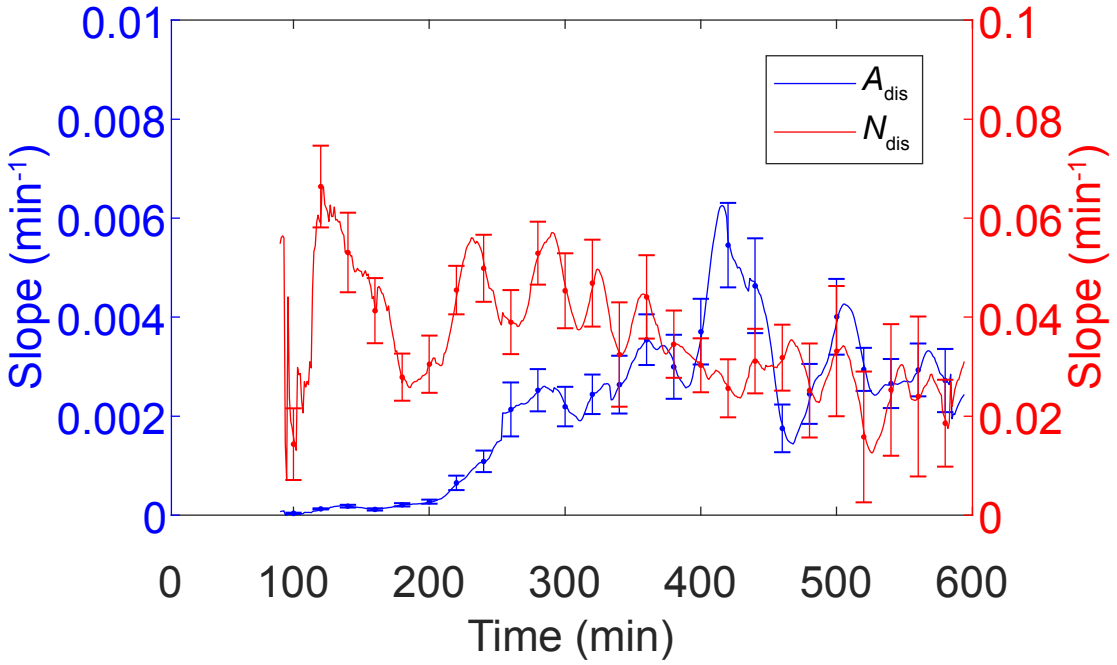

Figure 4.20: The first derivative estimate of the disconnected area (A_{dis}/A_0) and number of disconnected objects (N_{dis}) are plotted over time. The slopes were calculated for each experiment separately, then the mean and the standard error of the mean were determined and plotted. The two plots were dissimilar, and no obvious patterns were recognized. The error bars indicate the standard error of the mean.

The derivatives of A_{dis} and N_{dis} did not share any similarities (Figure 4.20). There appeared to be no correlation between the A_{dis} and N_{dis}, which came as a surprise, as these two parameters directly represented the unique characteristic of satellite growth. Moreover, their respective derivatives were composed of multiple peaks, without clear patterns or local extrema. However, several qualitative observations showed that satellites decrease their area as they reach the pause state, and therefore a local minimum should also appear in A_{dis}. A valley near 480 minutes of A_{dis} may represent this minimum.

One possible explanation of the deviation was that the secondary motile mesoplasmodia, as well as other disconnected components, may have appeared after 300 minutes, hindering a proper analysis. However, phases were evident in A_{tot} (Figure 4.16), and therefore made it difficult to reconcile this deviation. Another explanation was the segmentation error, as satellites during propagation were very translucent and appear to be thinner than the rest of the forms, such as networks and microplasmodia. While these errors were compensated in A_{search} because of cumulative calculation of the area, missing biomass would directly impact the analyses on A_{dis}.

At this point, it was clear that the local minimum at 480 minutes is shared be-

Table 4.6: Parameters from the fit based on equation 4.3, and their standard errors from different growths.

Experiment type	n Total	N_0	τ (min)	b
Satellite	142	0.836 ± 0.007	40.5 ± 0.6	0.285 ± 0.002
Non-satellite	81	0.744 ± 0.010	43.6 ± 0.9	0.316 ± 0.003
Other	136	0.600 ± 0.007	50.7 ± 0.9	0.408 ± 0.002
Network	13	0.914 ± 0.023	114.7 ± 15.6	0.203 ± 0.007

tween A_{tot} and A_{search}, and possibly A_{dis}, and this time corresponded to the pause state. Locomotion of satellites was therefore related to the change in the total area of *P. polycephalum*. This suggested a possibility of a shared mechanism of controlling the area and locomotive properties, where rearrangement of microfilaments and cortical layers may be required.

In summary, the first derivative of the area and object dynamics revealed and matched the phases and states previously defined with qualitative observations. The protrusion phase could be identified from the first derivative of the total area, while the pause state was visible from the total area, total search area, as well as disconnected area. This revealed that satellite growth is correlated with the change in the total area of *P. polycephalum*, which was previously not expected.

4.7.4 Modelling the object dynamics as an exponential decay

Since microplasmodia must collide with one another to fuse, it seemed appropriate to use a phenomenological model of exponential decay, as the rate of decrease depended on the number of objects present. Therefore, the initial decrease in the number of objects was used to obtain parameters for the exponential decay function, which is

$$N(t) = N_0 e^{-\lambda t} + b. \tag{4.3}$$

While the number of the objects was already normalized, there was a delay in decay in the first 30 minutes of the experiment, before the decay occurred. Therefore, N_0 was also treated as a free variable to represent the delay before the decay occurred. Moreover, unlike a true exponential decay, there was a nonzero asymptote in these experiments. A percolating network would eventually reach an object number of 1, however, the time dependence of the percolation has not been investigated. A satellite growth where all microplasmodia participate in fusion would decay to the total number of satellites. However, the number of satellites has a scaling relationship with the density of microplasmodia, which will be discussed later (Section 4.9). Therefore, an offset b represented progress in percolation for network growth, and for other growths represented inactive microplasmodia that are left out from fusion. The rate of decay, λ, in this case, was a measurement of the likelihood of fusion between microplasmodia. Then, the mean lifetime of microplasmodia, τ, was calculated as $\tau = 1/\lambda$

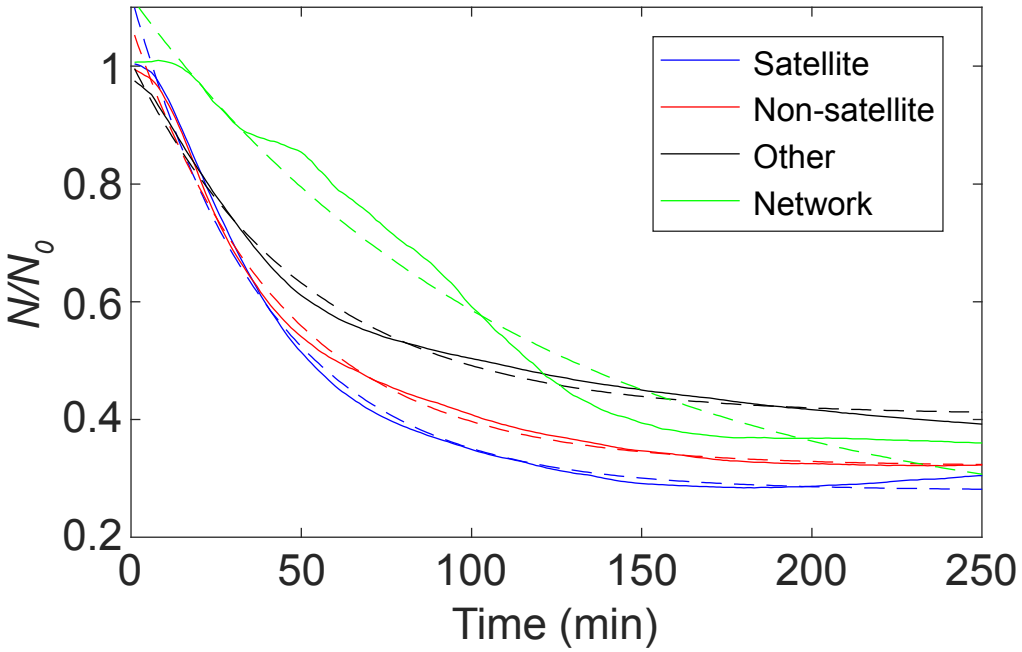

Figure 4.21: First 250 minutes of the dynamics of the number of objects and exponential fits. The solid line indicates an average from experimental data, and the dashed line is the exponential decay fit. All growth types except the network growth agreed well with the exponential decay fit. The parameters for the fit are given in table 4.6

Due to the offset b, N_0 appeared to vary widely (Table 4.6). However $b + N_0$ for all growths were close to unity, with the largest value of about 1.1 were observed . The network growth did not fit well with the description of exponential decay (Figure 4.21, green line). However, network growth also did not have a smooth curve due to the small number of samples. All other growths showed a good agreement with exponential decay fit. τ was the smallest in the satellite growths, which indicated that the microplasmodia in a satellite growth were likely to fuse more rapidly than in the other growths. This may be significant since the satellite growth was temporally coordinated, and protrusion occurred about the same time across experiments (Section 4.6.1). Therefore, satellites must form within a fixed time. Higher fusion rates may allow microplasmodia to aggregate faster and form satellites, while a diminished rate of fusion fails to produce these mesoplasmodia within the time limit. The 'other' growth type had the largest b, likely from contributions of inactive growths, such as one seen from 7 days microplasmodia in figure 4.13, row (e).

To further investigate whether the decay rate of the object depends on the age of microplasmodia, the experiments were pooled based on age, instead of the growth type. Decay rates were calculated individually by minimizing the squared difference between the fit and the data. Then, these data were represented as a boxplot (Figure 4.22).

The decay rate λ increased as the age of microplasmodia used in the experiment

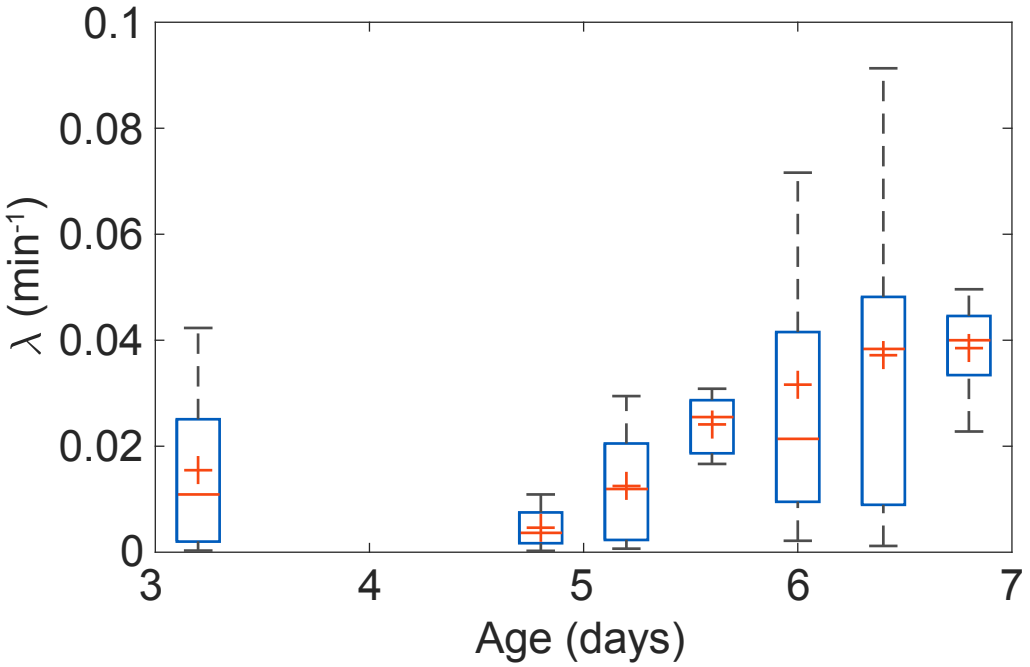

Figure 4.22: The decay rate λ based on age of the microplasmodia. The data at age 3 represent specimens grown in the presence of glucose, while all the other data were obtained on agar without glucose. There was a clear increase in the decay rate from day 5 to day 7 microplasmodia. The red cross represents the mean, while the blue box bounds 25^{th} and 75^{th} percentile of the data. The extended error bars indicate two standard deviations from the mean.

increased (Figure 4.22). This may be an indication of increased motility in older microplasmodia. The rate sharply increased when microplasmodia pass the 5 days mark, and appeared to reach an asymptote after 6 days. Interestingly, the decay rate at day 3 was comparable to that of a day 5, while the microplasmodia just before day 5 showed a much smaller decay rate. Since the glucose was depleted around day 4 (Figure 4.4, panel (b)), microplasmodia may first attempt to slow their metabolism to minimize the energy expenditure, resulting in reduced movement. After day 5, a starvation response of microplasmodia is activated, which results in an increased motility, leading to a larger fusion probability.

As seen in figure 4.12, no satellites were observed before day 5, and the occurrence of satellites jumped just before day 6. This was in line with the decay rate, which showed a jump between day 5 and day 6. The mean lifetime of microplasmodia, τ, will be used in a later section to estimate the time scale of fusion between microplasmodia (Section 4.9).

In summary, the decrease in the number of objects was successfully modelled using an exponential decay function. The decay rate parameter λ showed that the microplasmodia in a satellite growth exhibit the greater rate of fusion. Moreover, λ was dependent on the age of microplasmodia, rapidly increasing from day 5, and reaching a plateau on day 6.

This corresponds to the probability of satellite growth based on age, which only occurred after the age of day 5. Therefore, the motility of microplasmodia plays an important role in inducing satellite growth.

4.7.5 Observation of the satellite growth at microscopic scale

Comparing different equipments

The microscopic observation of the satellite growth posed a unique challenge in scaling lengths. Microplasmodia themselves are on the order of 100 microns, while at the end, the satellite pattern may range from millimeters up to centimeters. While the DSLR camera was suitable for capturing the entire growths at large scales, tradeoffs were made with regard to the spatial and temporal resolution. In contrast, the microscope, due to the narrow field of view, could not capture the entirety of the satellite growths. Moreover, since one cannot predict before from which portion of the circumference of the patch satellites may emerge, selecting a location to observe was improbable. To alleviate these issues, a new type of microscope was utilized, which could capture both the macroscopic overview of the migration as well as the microscopic detail of oscillation.

To translate the experiment from the photobox (Section 4.2) to the microscope posed additional challenges. First, an incubation chamber was custom-made to provide temperature and humidity control that could be mounted on the microscope. However, the experiment slowly went out of focus during the observation, due to the evaporation of water from agar plates. Then, the humidity in the microscope incubator was raised from 88% to 95% to combat an issue of narrow depth of field, which led to thinning of the agar layer causing problems in prolonged experiments that were not present in the photobox. Also, the thickness of the agar was increased to reduce the distance between the microplasmodia and the lens, to meet the narrow working distance of the objective. It had been reported that the softness of the agar affects the behaviour of *P. polycephalum* [109], and the morphology of satellites were also affected by the substrate stiffness (Figure 4.10).

While the changed conditions were successful in inducing the satellite growth under the microscope, there were some differences in the growth pattern readily visible. To better compare these differences, the growth dynamics from the two observation system were compared.

The dynamics of the occupied area from two equipment were distinct, where microscope data showed a smaller increase in the total area (Figure 4.23, panel (a)). Moreover, the non-satellite growth showed a greater increase than the satellite growth in the microscope, which was not the case in the photobox (Dashed lines). The reason behind this difference was unclear, although the mean was taken from a relatively small sample size from the microscope (N = 12 and 11 for satellites and non-satellites, respectively). Therefore, more data is required to determine whether a systematic effect occurs in the microscope observation. The disconnected area, however, showed a remarkable consistency between the equipment (Figure 4.23, panel (b)). In both satellite and non-satellite growth, the dynamics of the disconnected area were almost identical. The onset of the

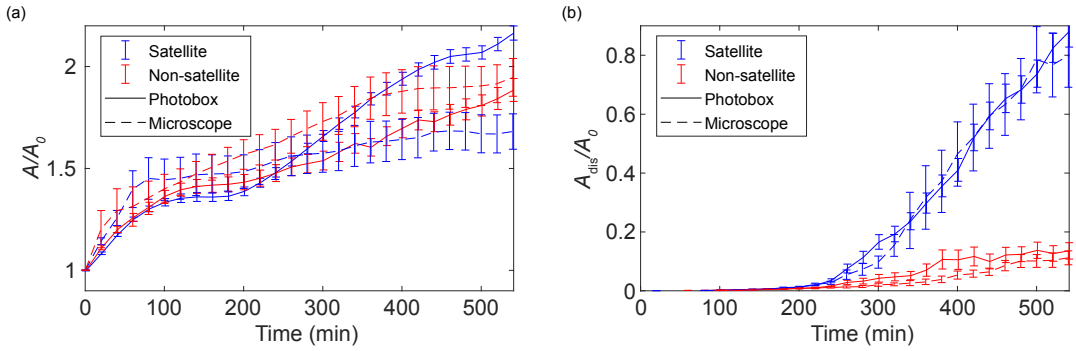

Figure 4.23: Area dynamics of satellite and non-satellite growth from the photobox and the microscope. Solid lines indicate data from the photobox and dashed lines from the microscope. In general, experiments from the microscope showed a smaller increase in total area (Panel (a)). Moreover, in the microscope, non-satellite growth showed a greater area than the satellites, which was not the case in the photobox. The disconnected area showed a remarkable similarity between the equipment, showing that the separation was the hallmark characteristics of the satellite growth (Panel (b)). Error bars indicate the standard error of the mean.

increase was also very similar between the equipments, demonstrating that the fragmentation of mesoplasmodia from the patch was the characteristic feature of satellite growth.

One of the issues of the experimental analyses was that during the segmentation process, it could not distinguish between two microplasmodia in contact, and two microplasmodia during fusion. In DSLR photos, most microplasmodia in contact could not be distinguished after segmentation. The recovery of objects in satellite experiments after 120 minutes were attributed to the imprecision of this segmentation (Figure 4.17, panel (a)). With the microscope data, the recovery of the number of the object was much smaller and occurred much later (Figure 4.24, panel (a), dashed line). However, the initial decay of the object number was nearly identical between the equipments, showing that the photobox was capable of capturing the initial dynamics of the microplasmodial movement and fusion. The non-satellite growth in the microscope showed a much slower decay and was distinct from the non-satellite data obtained from photobox. All non-satellite data from microscope were acquired with a centrifugation speed of 3000 RPM, which may also have affected the behaviour, although the satellites from these experimental conditions did not exhibit any noticeable differences.

The disconnected number of objects was much higher in the microscope data (Figure 4.24, panel (b)). There were more disconnected components in the microscope than the photobox, indicating that a larger number of satellites were formed in the microscope. However, the general increase in the number of disconnected objects also suggested the possible contribution from the noise during segmentation being counted as disconnected objects. The non-satellite growth from microscope showed a similar number of disconnected components to a satellite growth from the photobox. The increase in resolution might have caused a better distinction of objects near the border, causing overestimation of disconnected objects.

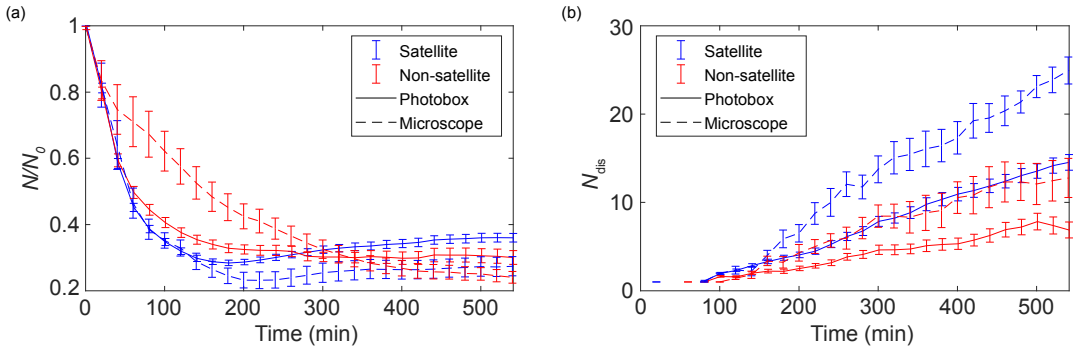

Figure 4.24: Number of objects dynamics of satellite and non-satellite growth from photobox and microscope. Solid lines indicate data from photobox and dashed lines from the microscope. The decay of total objects from the satellite growth was consistent between the equipments, especially in the first 120 minutes (Panel (a)). Deviations occurred thereafter, where the photobox showed object recovery, while the microscope did not. Non-satellite growth showed a slower decay under the microscope (Panel (b)). Microscope data showed a higher number of disconnected components on average, in both satellite and non-satellite experiments. Error bars indicate the standard error of the mean.

In summary, there were some noticeable differences in the dynamics of growth between microscope and photobox observations. The deviations were the largest in the total area and the disconnected object dynamics. However, the disconnected area, as well as the total object dynamics showed remarkable consistency between the equipment. Therefore, it was concluded that in analyzing the motility of the microplasmodia, there were no significant differences between the two equipment, as the total object dynamics were nearly identical at the beginning of satellite growth.

The differences observed could be contributed to the difference in environmental conditions, such as the thickness of the agar or the humidity. However, since the satellite growth showed robustness against these parameters, no further optimization of parameters was performed. The deviations of the non-satellite growth were not explored.

4.7.6 Diffusive properties of microplasmodia

Introduction

Experiments performed under the microscope had two distinct advantages over the experiments on photobox: higher spatial and temporal resolution. This allowed detailed investigation on the movement of individual microplasmodia. It was of special interest how the microplasmodia interact in first 3 hours after of inoculation, as satellites were formed during this period. Moreover, the N/N_0 showed the greatest rate of decay in satellite growth, suggesting that microplasmodia may either move faster or fuse with one another more readily. Since the dynamics of the number of objects were consistent between the two equipment (Figure 4.24, panel (a)), the motility of individual microplasmodia were commenced under the microscope. Even with the greater resolution under the microscope, the detection of individual microplasmodia posed a challenge for two

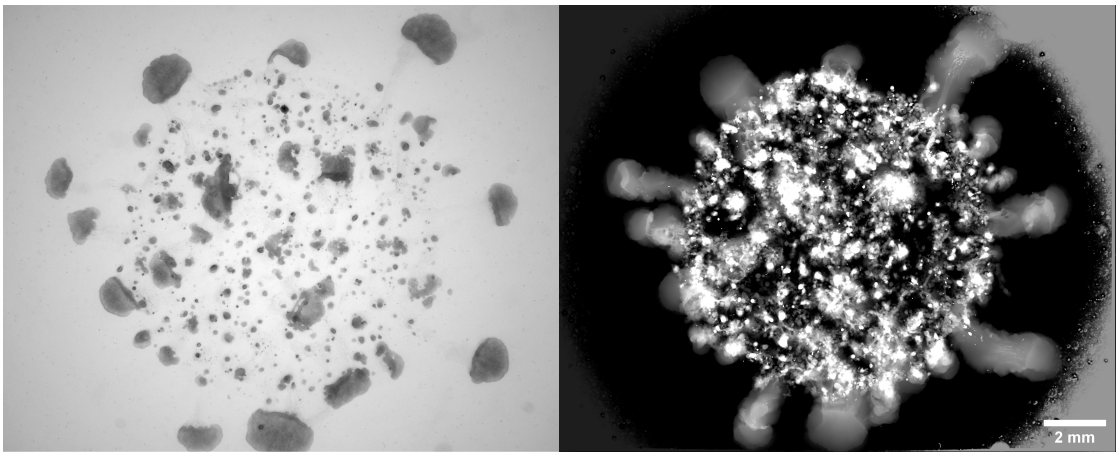

Figure 4.25: A static image after 9 hours (Left) and the summed image (Right) of a satellite-like mesoplasmodia formation from a paper towel dried patch. From a static view, it appeared to be a normal satellite growth. However, the summed image showed that the paths behind by the mesoplasmodia were different from satellites. Many paths were bent, path boundaries were uneven and the illumination on the path was weak. This showed that the morphologies of the motile mesoplasmodia were not stable and constantly shifted. Moreover, there was no strong illumination of the final shape at the end of the path, suggesting that the temporal correlation that defines satellite growth was violated.

reasons.

1. Microplasmodia exhibited directed radial movement towards the edge of the patch. This was likely caused by drying of the residual liquid during patch preparation. Not only did this affect the motility of the microplasmodia, it also tended to aggregate microplasmodia, making the distinction between individuals more difficult.

2. It was easier to prepare experiments with relatively high coverage, as preparing low coverages occasionally resulted in the coverage being too low, preventing satellite formation. It was impossible beforehand to know whether satellites would form, and the clear indication of protrusion occurred only after 3 hours. Since the dynamics before this protrusion were of interest, only a small number of experiments could be attempted per day, limiting the output.

To circumvent the problem stated in 1, the patches were dabbed with a paper towel during preparation to expedite the drying process. This was the original protocol employed by Tanja Huxoll during early investigations of satellite formation. However, this resulted in an unexpected pattern, where motile mesoplasmodia that resembled satellites were formed, but the uniform direction and stable morphology of satellites were lost (Figure 4.25). This, along with the altered trajectory of satellites with supernatant deposit (Figure 4.11), suggested that the residual liquid contained a signal molecule that gave a sense of direction for satellites. This possibility is further investigated in a later section (Section 4.8).

Furthermore, improved resolution revealed that microplasmodia underwent a morphological change in the first hour. During the directed movement in the first 30 minutes,

microplasmodia maintained their shape. However, after 30 minutes, presumably when microplasmodia are settled on the agar surface, many of the microplasmodia appeared to leak their protoplasm and thus increased their area (Figure 4.26). Moreover, the leaked protoplasm appeared to be more fusion-prone, mixing with other protoplasms. This may correspond to the increase in the total area A/A_0 in the first 100 minutes (Figure 4.16), and further supported the idea that the increase in area does not reflect growth.

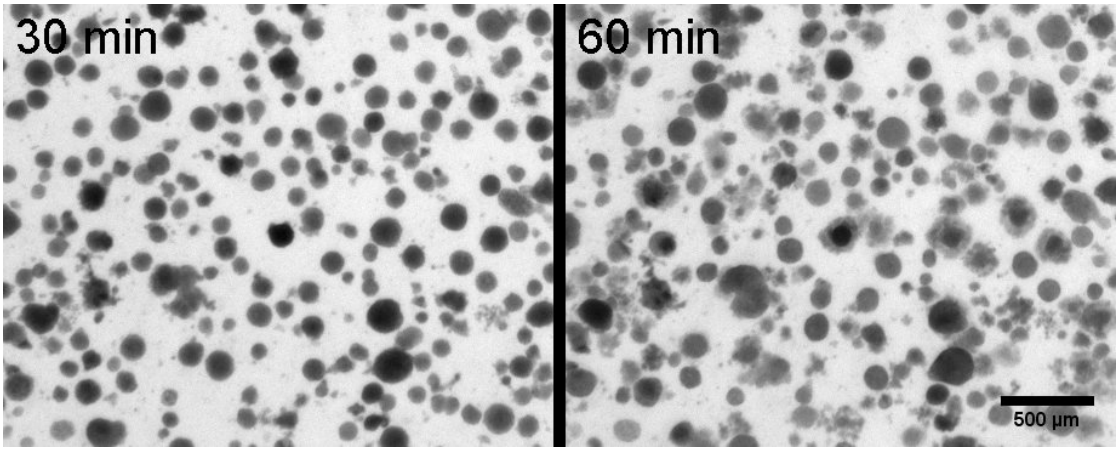

Figure 4.26: Static images of a satellite experiment at 30 and 60 minutes after inoculation. At 30 minutes, microplasmodia were relatively circular with sharp borders. After 60 minutes, the solid cores of microplasmodia were surrounded with less intense material, presumably the protoplasm leaked from the microplasmodia.

To better understand the dynamics of microplasmodia and how the fusion occurs to form precursor satellites, movements of microplasmodia were tracked. Data from microscope were used exclusively, to increase sensitivity in detecting their movements. The tracking was performed on each microplasmodium in a patch until a drastic change in area of the microplasmodia was detected. This indicated that the tracked microplasmodium has fused or made contact with another microplasmodium, and the tracking was stopped at that point. Then, the tracking data was used to calculate diffusive properties, as well as the distribution of step length and angles. The diffusion coefficient D of microplasmodia was calculated based on the mean squared displacement, to see what type of diffusivity was applicable. The step lengths of the microplasmodia were measured and their distribution was analysed, to assess whether the distribution followed Lévy of Gaussian statistics (Section 2.1.2).

Methods

In total, 21 experiments were recorded employing the AxioZoom V.16, with the lowest zoom with 15 second interval for 10 hours. Of these, 9 of the experiments produced satellites. However, all of these experiments exhibited active movement of microplasmodia, with microplasmodia aged around 6 days. All microscopic data were segmented as described in section 4.2.

After segmentation, the tracking of microplasmodia was performed with a custom script in Matlab. The tracking was done as follows:

1. The segmented image at $t = 0$ was used to identify all microplasmodia within the patch area A_p. The centroid and the area of the microplasmodia were recorded. These microplasmodia were indexed and tracked for 4 hours.

2. A microplasmodium was followed by loading the next frame, and applying the previous frame image to identify the overlap. Most of the time, this overlap correctly identified the same microplasmodium. When ambiguities arose, i.e. two elements were identified in an overlap, the object with larger overlap was considered the correct microplasmodium to follow. When there were no objects in the overlap, this increased the missing count by one. When the missing count increased to 5, the tracking was terminated.

3. All images were processed with a size filter to eliminate large components as well as noise.

A typical result of tracking is shown in figure 4.27. Red lines indicate tracked paths, attached to white particles, representing microplasmodia. Some of these lines lead to a larger aggregate, which indicates that the tracked microplasmodium moved and fused with other microplasmodia to form mesoplasmodium. Each red line indicates one trajectory.

After the tracking, the data were further filtered, so that the data with less than an hour of consecutive points from the beginning were discarded. Therefore, centroid data from each microplasmodia had different length of data points, with total tracking times ranging between one to four hours. The resulting centroid positions were used to calculate two aspects of the movement property. In total, there were 936 and 6060 usable tracking data obtained from satellite and non-satellite growth, respectively.

In order to determine diffusive properties of the microplasmodia, the mean squared displacement (MSD) was calculated from the centroid data. This was performed by taking the difference between x and y coordinates from all time points from the initial position separately, squaring the differences and summing them up.

The diffusion coefficients for were calculated from Einstein's relation [53]:

$$< (\Delta r)^2 >=< r(t+\tau)^2 > - < r(t)^2 >= 2nD\tau \tag{4.4}$$

where $< (\Delta r)^2 >$ is the MSD of the particle in a time interval τ, and n is the dimension in which the diffusion process takes place, i.e., for microplasmodia diffusing on an agar layer, $n = 2$. Therefore, D was measured by taking a first derivative of the MSD, using a Savitzky-Golay filter [110]. The slope was determined in a 5-minutes window.

The figure 4.28 shows a typical scenario of tracking a single microplasmodium in a patch. The microplasmodium started from the top right position, and as indicated by

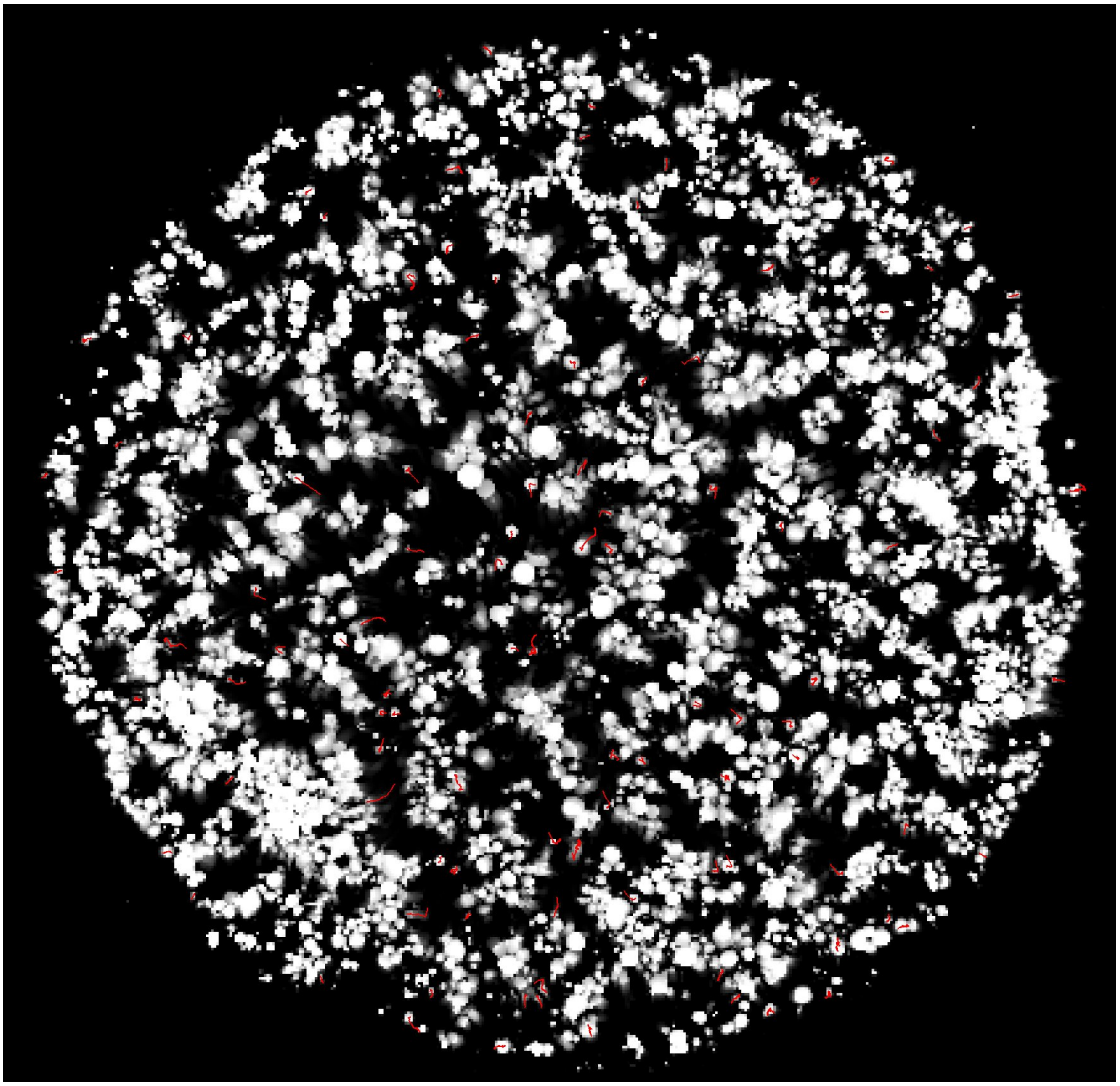

Figure 4.27: A summed image of a satellite growth in first two hours, and red trajectories indicating the tracked paths of the microplasmodia. Large components were not tracked, as determination of the centroid position were difficult to assess and validate. Tracking was terminated if the microplasmodia came in contact with a larger component.

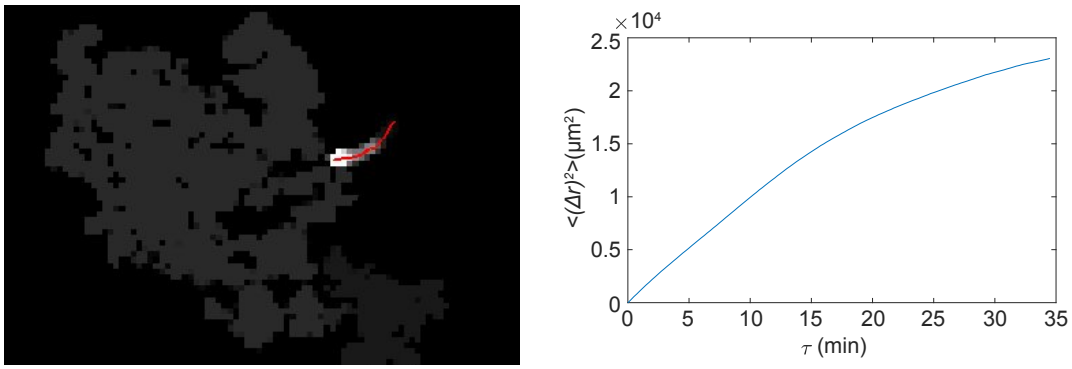

Figure 4.28: A summed image of a single microplasmodium until fusion (Left) and its corresponding MSD (Right). The red line in the picture shows the movement of the centroid of the microplasmodium being tracked. Two large bodies, with weaker intensities on the left and the bottom are the mesoplasmodia that the microplasmodium fused into. Tracking was performed for approx. 70 minutes, and therefore half of the acquisition time was set as the maximum τ. The MSD showed two distinct phases, where it is linear up to 15 minutes, and then slows down as an asymptote.

the red line, moved towards the mesoplasmodium and fused. The length of the tracking was 70 minutes, and therefore half of this length was set as the maximum time interval τ. The MSD exhibited an asymptotic behaviour, with a linear increase for up to approximately 15 minutes. The asymptote in larger τ suggested that the microplasmodium slowed down before fusing, suggesting a possible repulsive force between microplasmodia.

The step and the angle was measured between successive centroid positions for each microplasmodium. The angle of the step was measured using $\tan\theta = \frac{\Delta y}{\Delta x}$, where x and y represent the Cartesian coordinate of the centroid position. Then, the turning angle was calculated as the difference between the angle of the previous non-zero step length and the angle of the current step. Unlike the MSD, where the difference was calculated between the centroid at different τ, the steps lengths were calculated from centroids at a fixed interval.

If successive steps had turning angles within the tolerance value, these two steps were merged. Due to a high spatial and temporal resolution, the angles measured were discretized into cardinal directions and diagonal directions between the cardinal directions. Therefore, the tolerance angle was set to 30 degrees, to leave out all the cardinal and diagonal steps, and merge small deviations in trajectories. Once the steps were merged, the new angle of the step was calculated from the initial and final centroid position of the merged step.

The step count was the highest in one pixel length, which was the lowest unit length (Figure 4.29, panel (a)). Therefore, this suggested oversampling, where the data acquisition rate was faster than the typical step length of the microplasmodia. Therefore, later data were processed with 2.5 minutes interval, instead of 15 second interval used in figure 4.29. The angle distribution showed that the two dominant angles were 0 and 180 degrees (Figure 4.29, panel (b)). In fact, the microplasmodium was most likely to

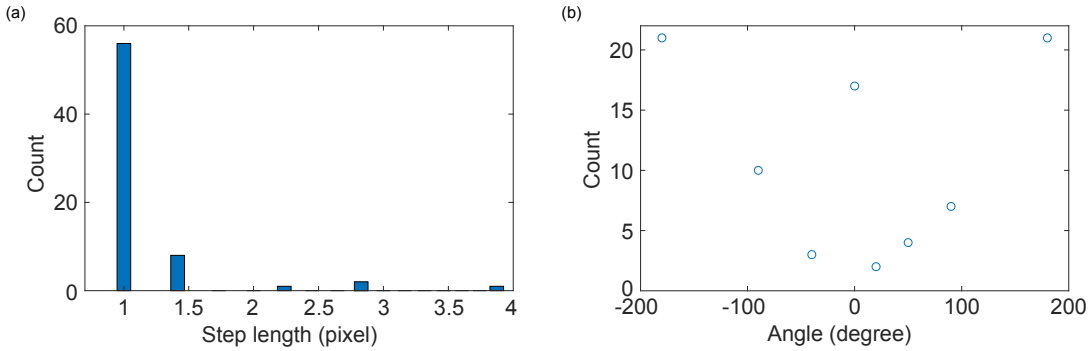

Figure 4.29: The step length and the turning angle distribution in the trajectory of a single microplasmodium, with a sampling rate of 15 seconds. The step distribution (Panel (a)) was dominated by steps of single pixel length, which suggested oversampling. Longer steps were progressively less likely. The angle distribution (Panel (b)) showed that the microplasmodia either kept the direction of movement (0 degrees), or completely turned to opposite direction (180 degrees). A right turn (-90 degree) was slightly favoured, matching the trajectory of the microplasmodia. Counts at -180 and 180 degrees are mirrored for representation.

take a step in an opposite direction, which did not reflect the trajectory seen in figure 4.28. This suggested that the oscillation of a microplasmodium may have affected this distribution. There is a slight favour towards -90 degree, which represents the right turn, which matched the curved path of the microplasmodium.

Diffusion of microplasmodia

P. polycephalum has in inherent oscillation behaviour, with period between 45 seconds to 2 minutes depending on environmental and internal conditions. This oscillation was also evident in the step and angle distribution, as the framerate of the acquisition was 15 seconds (Figure 4.29). This was alleviated by sampling the trajectory every 2.5 minutes for step and angle distributions. Since many trajectories were combined for MSD analysis, any residual effect of oscillation was expected to be averaged out in the diffusion analysis. Data were divided into two categories, namely satellite and non-satellite experiments, and diffusion patterns and step distributions were compared between the two.

The MSD plot of satellite growth was smooth and follows an asymptotic rise until the 60 minutes (Figure 4.30, panel (a)). After 60 minutes, the plot fluctuated with a large standard deviation. This was caused by the evaluation routine, which set the minimum interval to be at least 60 minutes. After 60 minutes, fusion of a microplasmodium caused the tracking to be terminated, gradually reducing the number of data at a given time. Therefore, the averaged MSD after 60 minutes were more prone to deviations and fluctuations. Non-satellites did not show a drastic fluctuation after 60 minutes, as much more data points were collected for this case. The MSD from the satellite growth clearly showed a larger increase than the non-satellite growth, especially in the first 30 minutes. However, they were at about the same MSD at 60 minutes.

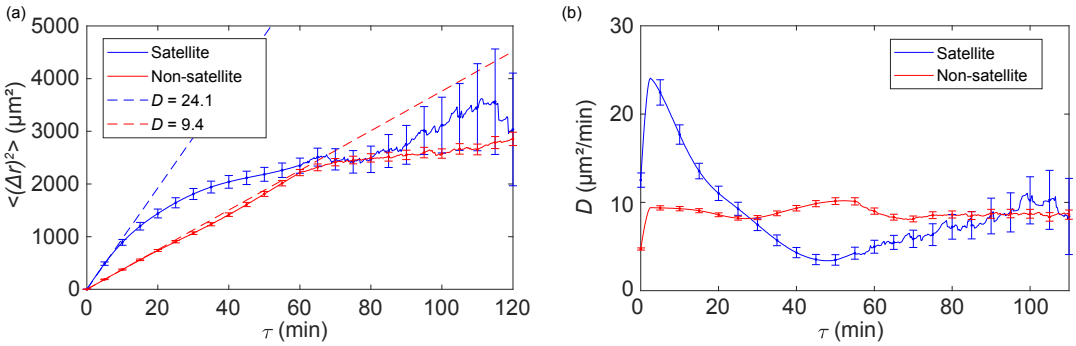

Figure 4.30: The mean squared displacement (MSD) (Panel (a)) and the corresponding diffusion coefficient D (Panel (b)) from satellite and non-satellite growth patterns in the first two hours of the growth, employing the time interval τ. The blue and red lines indicate the data from satellites and non-satellites, respectively. There appeared to be two phases of MSD on both satellite and non-satellite growth, divided at around 60 minutes (Panel (a)). Satellite growths showed a saturating increase in MSD until 60 minutes, then showed an irregular increase. Non-satellite growth had two linear phases with different slope. The diffusion coefficient estimated from MSD reflected this two phases (Panel (b)). Satellite growth had a steadily decreasing D, reflecting the saturating growth. Non-satellite growth had relatively constant D. The error bars indicate standard error of the mean, with the number of data points for satellites and non-satellites are 936 and 6060, respectively.

The diffusion coefficient, estimated as a slope of the MSD plot, reflected this trend (Figure 4.30, panel (b)). At the largest difference, microplasmodia in the satellite case diffused twice as fast as the microplasmodia in non-satellite growths. However, the differences vanished after 30 minutes, and briefly, microplasmodia from non-satellites exhibit faster diffusion. From the MSD analysis, it was concluded that the diffusion coefficient of the satellite growth was 24.1 μm^2/min, and the non-satellite growth was 9.4 μm^2/min. The typical interval τ where this free diffusion was valid is much shorter in the satellite growth ($<$ 10 min) than the non-satellite growth (approx. 60 min).

Limiting scenarios of free diffusion

The asymptotic increase of the MSD in satellite growth until 60 minutes resembled the MSD from an individual tracking (Figure 4.28). In a free diffusion scenario where a particle randomly moves, MSD should demonstrate a linear relationship with the time, as established from Einstein's relation (Equation 4.4). Therefore, the nonlinear behaviour suggested that there were other effects at play that limit the motility of the microplasmodia.

From the start of the evaluation, the particle tracking was performed until the microplasmodia ran into another particle. However, since the minimum data length was set to 60 minutes, after 60 minutes some trajectories disappeared due to fusion. In other words, only microplasmodia that did not fuse in the first 60 minutes were tracked. To see whether any physical explanation existed on this saturation of MSD, one possible, idealized distribution of microplasmodia is depicted in figure 4.31.

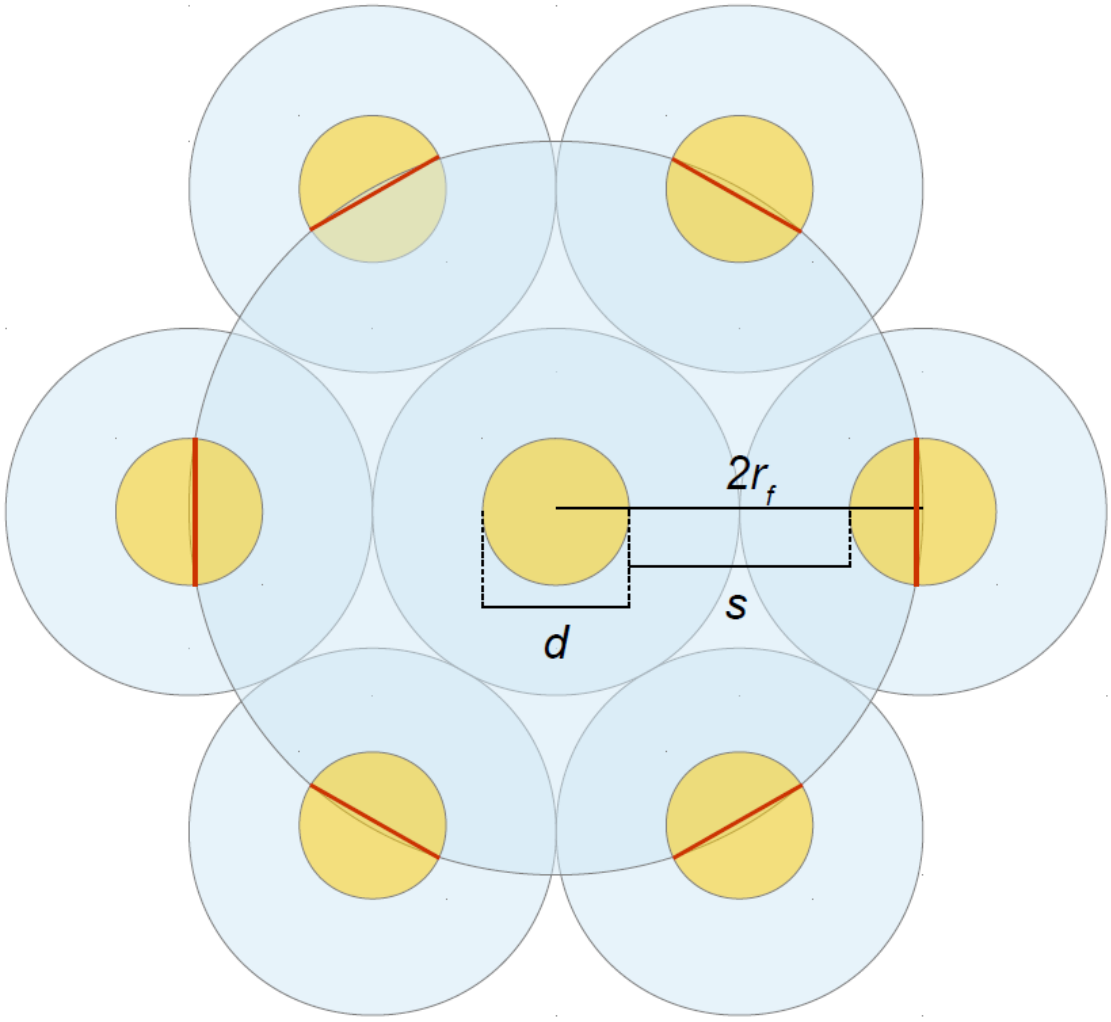

Figure 4.31: Diagram of an ideal distribution of microplasmodia and related parameters. In this idealization, all microplasmodia (Yellow dots) are perfect circles that are distributed homogeneously on a hexagonal grid so that the distances between all neighbouring microplasmodia are equal. Then, the free space around each microplasmodium can be approximated (Blue circles) with a radius of r_f, which is half the distance between the centroids of two neighbouring microplasmodia. The nearest distance between the microplasmodia is depicted as s, and this s must be crossed for two microplasmodia to fuse.

We assume an ideal scenario of homogeneous distribution of microplasmodia of identical shape and size. In detail, microplasmodia are assumed to be perfect, identical disks with a diameter d. Then, these microplasmodia can be fitted to a hexagonal grid, where one microplasmodium is surrounded with 6 neighbouring microplasmodia, all with the same distance from each other. Then, the physical distance s must be crossed by microplasmodia to touch another. This distance can be expressed as $s = 2r_f - d$, where $2r_f$ is the distance between the centroids of neighbouring microplasmodia. It is also assumed that the contact will always lead to the fusion As the segmentation cannot differentiate between fusion and microplasmodia in contact, this assumption sufficiently describes the

tracking observation.

Since the trajectory was removed once a microplasmodium fused, the remaining trajectories may be bounded within the neighbouring microplasmodia. On average, a microplasmodium has to migrate a distance s to contact a random neighbour. Hence, this distance is selected for scaling all relevant lengths.

The s of an experiment was calculated in the following way. In all experiments, the number of microplasmodia can be expressed as a density in a given area. This density is referred to as a coverage C and expressed as:

$$C = \frac{N_{\text{micro}} \times \pi(\frac{d}{2})^2}{A_p} \tag{4.5}$$

where N_{micro} is the number of microplasmodia inoculated in an experiment, d the diameter of the microplasmodia, and A_p the area of the patch where N_{micro} are located. Since it is assumed that the microplasmodia are homogeneously distributed, the distances from the microplasmodia to the closest boundaries must be the same. Since s can be expressed as the distance between the two centres of neighbouring microplasmodia, minus the diameter of a microplasmodium:

$$\begin{aligned} s &= 2(r_f - \tfrac{d}{2}) \\ &= \sqrt{\tfrac{4A_p}{\pi N}} - d \end{aligned}$$

Utilizing the definition of the coverage above (Equation 4.5), s can be written as a function of C:

$$s = d(\frac{1}{\sqrt{C}} - 1) \tag{4.6}$$

Therefore, the distance between microplasmodia is a function of their own size and coverage. Notably, even in constant coverage, the diameter affects the average distance. As expected, C is inversely correlated with s. Therefore, the coverage and the average size of the microplasmodia were measured from the segmented images at $t = 0$. A_p was calculated based on the method shown in figure 4.3 and an average size of the microplasmodia was calculated based on the number of objects and the segmented area within A_p. d was calculated based on the assumption that microplasmodia are perfect circles. Since different experiments had different C and d, the average distance s of each experiment was calculated and trajectories from the respective experiments were normalized accordingly. The displacement from the initial position was normalized with s, and the squared displacement over τ was normalized with s^2.

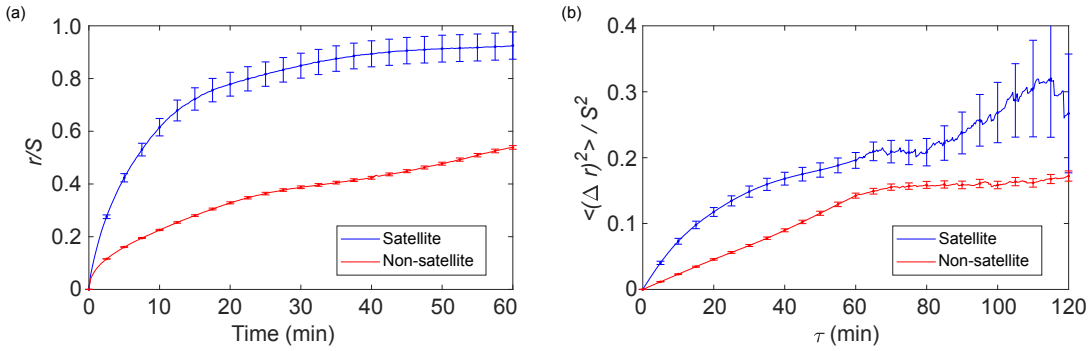

Figure 4.32: The normalized displacement (Panel (a)) and MSD (Panel (b)) based on the average distance between microplasmodia. The trajectories of the satellites were clearly saturating, and the asymptote appeared to be 1, as suspected. The trajectories of the non-satellites grew less quickly and did not show any significant effect of reaching the asymptote in the time frame of observation. The normalized MSD showed that the satellite growth reached an asymptote around 0.2. Interestingly, the MSD of non-satellite also appeared to halt its increase near 0.18. The error bars indicate standard error of the mean, and the numbers of data points for satellites and non-satellites are 936 and 6060, respectively.

The averaged trajectories of satellites and non-satellites were distinct from one another (Figure 4.32, panel (a)). First, microplasmodia from satellite growth showed much larger mobility than the non-satellite counterparts. The satellite trajectory was bounded by the distance between the microplasmodia s. This was expected, as the tracking selected trajectories that did not fuse in the first hour. It is unclear whether the asymptotic behaviour is caused by a close-range repulsion between microplasmodia, or simply by a sampling error from selecting only non-fused microplasmodia. From previous observations, two microplasmodia in a liquid remained in close proximity for a while before fusion, which may be represented here as the repulsion. It was also possible that the slime layer of the microplasmodia reduced their motility. The typical length scale of s was between 100 - 200 µm. Therefore, microplasmodia appears to move freely in the range of approximately 50 µm, and the diffusion assessment within this length scale is valid.

In contrast, trajectories from the non-satellite growths did not show strong asymptotic behaviour. In the first 60 minutes, these microplasmodia crossed about half of the distance of s. There appeared to be a plateau near 35 minutes, although the trajectory showed a general linear increase. Therefore, this decreased motility may cause a lack of fusion, and therefore lead to the failure to form satellites.

Scaling the MSD over τ did not alter the plot in a significant way (Figure 4.32, panel (b)). Both displacements showed an asymptotic effect near 0.2. Two distinct phases were also evident from both normalized MSD plots. In satellite growth, the normalized MSD showed a similar pattern as the averaged trajectories (Figure 4.32, panel (a)). After 60 minutes, an irregular pattern broke the apparent asymptotic behaviour and the MSD increased further.

However, the normalized MSD of non-satellite growth was bounded even after 60 minutes, showing only a marginal increase between 60 to 120 minute interval. This may suggest a repulsion or trapping effect between microplasmodia on a longer times scale.

As already suspected from the decay analysis of the number of objects N/N_0, where it was shown that the satellite growth had the shortest mean time of survival and therefore the fastest rate of decay (Table 4.6), the diffusion was also faster in the satellite growth. Therefore, the difference in the motility of the microplasmodia is one of the factors that determine the growth type of *P. polycephalum*.

The main assumption behind scaling the MSD with the typical distance between microplasmodia s was that the number of microplasmodia N was sufficiently large so that the coverage does not change in the first hour. However, it was immediately clear that the significant portion of microplasmodia fused with one another and left large gaps in the patch after 4 hours when satellites were assembled and start to migrate away from the patch. This effectively lowers the coverage and increases s. Therefore, this asymptotic behaviour was also expected to last a relatively short time before remaining microplasmodia diffused freely again. This was also partially evident from figure 4.30 in panel (a), where the trajectory of MSD from the satellites broke the apparent asymptote and rose after 60 minutes. While the asymptote breaking was not investigated in detail due to the large fluctuation and smaller number of samples, this pattern likely holds with more acquisition points. On the other hand, the MSD of the non-satellites appeared to be bounded even after 60 minutes (Figure 4.32, panel (b)). Further investigation is required to determine whether there is a close-range repulsive effect between microplasmodia or other physical effects that appears to trap microplasmodia specifically in non-satellite conditions.

It was expected that even with relatively few experiments, a sufficient number of data points could be acquired since there are hundreds of microplasmodia present in each patch. However, with stringent restrictions in an attempt to only record unbroken trajectories of non-fused microplasmodia resulted in smaller than expected sample size. Moreover, the age of the microplasmodia was not varied significantly, as the initial goal of the experiment was to produce satellites. Any experiments, even with desired external parameters, that did not produce satellites were collected and served as a control. Therefore, a systematic approach to measuring these diffusive parameters is needed to observe how the motility of the microplasmodia changes as a function of their age.

The coverage of these experiments was intentionally kept around 0.2, to improve satellite production while enabling better tracking of microplasmodia. It was not feasible to track microplasmodia successfully in higher coverages with the current experimental procedure, as the distances between them became too small. In lower coverages, the effects of the interaction between the microplasmodia may be lost, but better tracking data may be obtained. Future work should focus on tracking a few or even single microplasmodium at an improved temporal and spatial resolution for longer periods, to first establish the typical motility parameters of uninfluenced microplasmodium. Then the collective dynamics of the microplasmodia can be better assessed and understood.

Step length and directional angle distribution

The motility of a particle can also be described with respect to step lengths and its turning angles. The distribution of the step length can reveal whether the particle performs a random walk, or a Lévy walk (Section 2.1.2). This, in turn, reveals the type of diffusivity of the particle. Since the MSD analysis demonstrated that there was a clear difference in motility between the satellite and non-satellite growth, it was of interest whether the step length distribution of microplasmodia was also altered in the satellite growth. *P. polycephalum* exhibited a Lévy walk during exploration as a macroplasmodium, and experiments were performed to determine whether this trait was also shared in microplasmodia [52].

From the centroid tracking, steps and the angles of the steps were measured. A step was defined as a consecutive nonzero displacement between the sampling times with a turning angle of the movement within a tolerance value. When two consecutive displacements occurred with an angle within the tolerance, the two displacements were merged, and the angle of direction was recalculated from the initial and end positions of the merged step.

It was found that a sampling rate of 15 seconds, which equalled the acquisition speed did not yield any useful information, as the vast majority of the steps were of the unit length (Figure 4.29). Increasing the sampling rate consolidated many small steps into longer steps, at a cost of reduced resolution and a smaller number of steps. Therefore the sampling rate of 2.5 minutes was adopted, as it was longer than the typical oscillation period of the microplasmodia, yet still yielded a sufficient number of steps for analysis.

The figure 4.33 showed that there was no significant difference in the step length and angle distribution of the satellite and non-satellite growth. Therefore, it was suspected that in satellite formation, only the rate of movement was altered, and not the nature of this movement. However, the unit length steps still dominated, in both satellite and non-satellite growth. The angle distribution was also relatively even between the cardinal directions, except the 0 degrees. It was suspected that during the merging of steps within the tolerance angle, many merged steps assumed nonzero turning angles. Lower probabilities of the diagonal angles were also attributed to the lower probabilities of the step length 2 and above, as the unit step length can only assume cardinal directions.

In order to determine whether the step distribution resembled Lévy or Gaussian statistics, the parameters for each corresponding function were estimated using the least square method. However, with visualization, it was difficult to assess which model describes the data better (Figure 4.33). Therefore, the Akaike information criterion is used to compare the two models (Section 4.2). The Lévy function is given in equation 2.1, and the following Gaussian distribution was used:

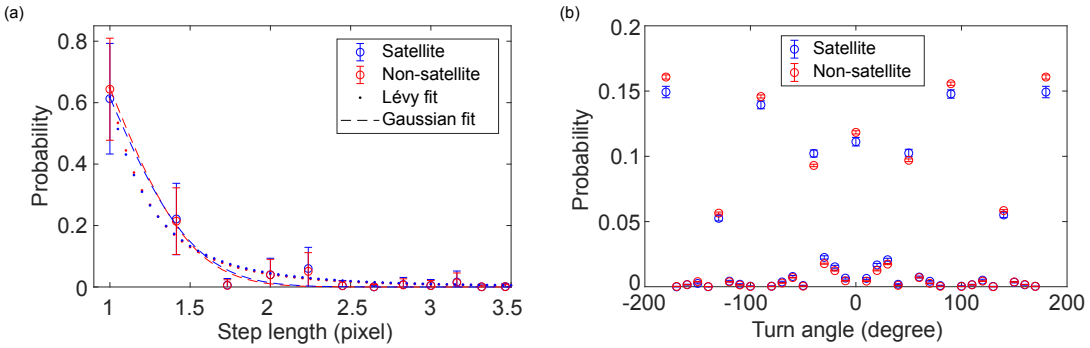

Figure 4.33: Step lengths (Panel (a)) and turning angles distribution (Panel (b)) of microplasmodia in first four hours of observation were measured with an angle tolerance of ±30 degrees, with 2.5 minutes as a sampling rate. Both satellite and non-satellite growth showed virtually identical distributions in both step lengths and the turning angle. The step length of 1 pixel dominated the distribution, with a rapid decay in probability for longer steps. Angle probabilities were similar between the cardinal directions. Between the diagonal movements, a smaller turning angle (±45 degrees) was favoured over the large degree (±135 degrees) of turns. The step distribution data were used to estimate Gaussian and Lévy parameters, by minimizing the squared difference. Counts at -180 and 180 degrees are mirrored for representation. The error bars represent the standard deviation. The parameters for the Gaussian and Lévy distribution are described in table 4.7.

Table 4.7: Parameters from the fit based on equation 4.3, and the standard errors from different growths. The Akaike weight represents the probability of the model to be the best fitting.

Data used	Parameter	From fit	Error	Akaike Weight
Satellite	σ	1.95	0.06	1
Satellite	Lévy	3.80	0.13	0
Non-satellite	σ	2.10	0.06	1
Non-satellite	Lévy	3.97	0.13	0

$$G(l_j) = \exp \frac{(l_j - m)^2}{2\sigma^2} \tag{4.7}$$

where the probability of the step length l_j is defined by the Gaussian function $G(l_j)$ with standard deviation of σ and the mean m.

Using AIC to evaluate both functions, Gaussian distribution clearly outscored the Lévy function in describing the distribution, both in satellite and non-satellite distributions (Table 4.7). Moreover, the Lévy parameter obtained was larger than 3, which indicated convergence into the Gaussian distribution [8]. Therefore, it was concluded that no Lévy properties were present in the motility of microplasmodia.

Unlike MSD analysis, the step length and angle distributions did not yield concrete results. The sampling rate, as well as an insufficient number of data, are likely the culprit. In order to better represent the motility of the microplasmodia into these distributions,

longer tracking data is required to enable longer sampling rates. The Lévy parameter obtained suggests that with sufficient acquisition, the distribution should converge to a Gaussian distribution, and therefore microplasmodia did not perform a Lévy walk. The angle distribution would improve with the help of longer sampling rates, as the dominant step length increases beyond the unit length, which allows more turning angles. Nonetheless, while it was not clear what type of movement microplasmodia utilized, it was clear that there was no significant difference in the type of movement between the satellite and non-satellite growth.

4.8 Modelling the displacement of satellite based on chemotaxis

The following section is based on a publication by the author [23]. The main difference between the publication and the thesis is that the pause state of the satellite was set at 10 hours for the publication.

Initial observation

Since the satellite growth has not been previously reported, there was no information on what possible mechanisms may drive the motility of the satellites. It was suspected that a satellite was a fragmented growth front, as the formation as well as the general morphology resembled the large sheet-like structure at the boundary of a *P. polycephalum* network. However, these growth fronts were supported by veins that shuttled the protoplasm through the entire body for expansion, while satellites were self-propelled with no obvious morphological shift during movement. Therefore, easily measurable parameters were first analyzed to see whether there were correlations between other physical characteristics to infer the type of mechanism that the fragment utilized for its motility.

First, the distance travelled by satellites d were analyzed and plotted against their own size A_s (Figure 4.34, and see Figure 4.3 for how these are defined). We were interested to see if and how the satellite size impacted the efficiency of the movement. The plot showed a large deviation below the size of 20 mm^2, and data points were focused on the left side and became sparse as the size of the satellite grew. This was caused by the tendency that satellite size and the number of satellites produced were inversely correlated. Satellites were either produced as many small satellites, or as large satellites but small in number. This scaling relationship is further explored in the subsequent section (Section 4.9).

The d rapidly rose initially, and slowly decreased and appeared to converge as the variance decreased as A_s increased. It was not clear whether larger satellites has a smaller deviation in d due to the small sample size. The largest d was recorded with relatively small satellites (A_s around 5 mm^2), which was about twice as long as the distance travelled by the largest satellite (11 versus 5 mm). However, no simple correlation between d and A_s existed.

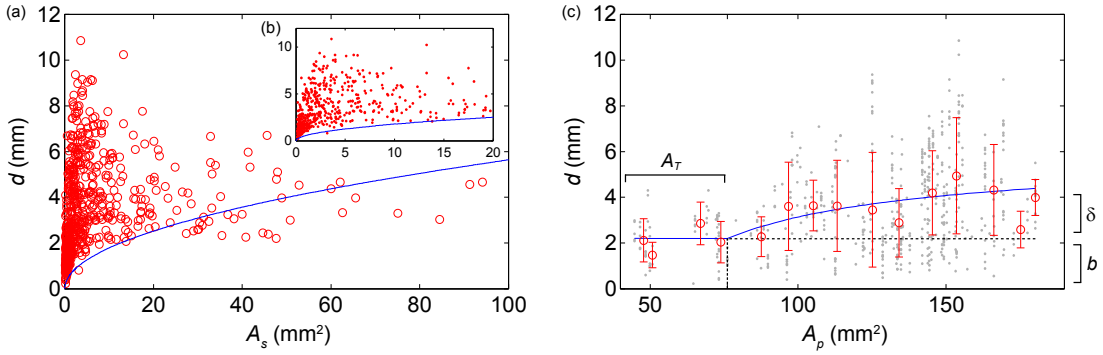

Figure 4.34: Distances travelled by satellites plotted against their own size (Panel (a)). The blue line shows the geometrical restriction assuming a perfectly circular satellite. Scatter plot of the data (Panel (a)). The maximal displacements showed a sharp increase, and gradually decreased as satellite size increased. Large satellites fell under the blue line, indicating their morphologies are restricted. Zoom-in of the plot on small satellites (Panel (b)). The geometrical restriction limits the distance travelled by small satellites, up to 20 mm^2. The distance travelled by satellites plotted against the patch area (Panel (c)). The distance remained relatively constant until about 80 mm^2 and then increased as the patch area became larger. Data points are represented by grey dots. The moving average of the distance travelled is indicated with red circles, with one standard deviation as the error bar. The blue line showed the fit of the experimental data using equation 4.8. Parameter values are given in table 4.8. The positions of A_T and b are indicated with dotted lines.

What was seen, however, was that there were minimal bounds the satellites travelled distances, which resembled a square root function (Figure 4.34, panel (b)). This was especially evident in smaller satellites. Since by definition satellites must be separated from the patch, and d was measured from the centroid of the satellite to the nearest border of the patch (Figure 4.3), this represents a geometrical restriction. The blue line in the figure 4.34, panel (a) is the radius of the corresponding A_s, assuming a perfect circle. In the low A_s region, this line represented the minimal boundary. This did not mean that small satellites were circular, as no information on their morphology is represented in the plot. However, larger A_s sometimes crossed below this boundary. Satellites located below this line cannot be ideal circles, as their radii would be greater than the distance they travelled, and therefore still attached to the patch. Therefore, satellites were more elongated and oval as their size increased, which was in line with the qualitative observation.

To further investigate whether the shape of the satellite was influenced by their own size, the aspect ratio of the satellites was plotted against their own size (Figure 4.35). The aspect ratio was defined as a ratio between the minor and major axis, measured by approximating the satellite as an oval (Figure 4.3). The general trend showed that the aspect ratio tended to decrease as the area of the satellite increased, as expected from the figure 4.34. However, the exact relationship between the aspect ratio and satellite size was difficult to assess. This problem was further compounded by a large variance of data in smaller satellites (Figure 4.35, panel (b)).

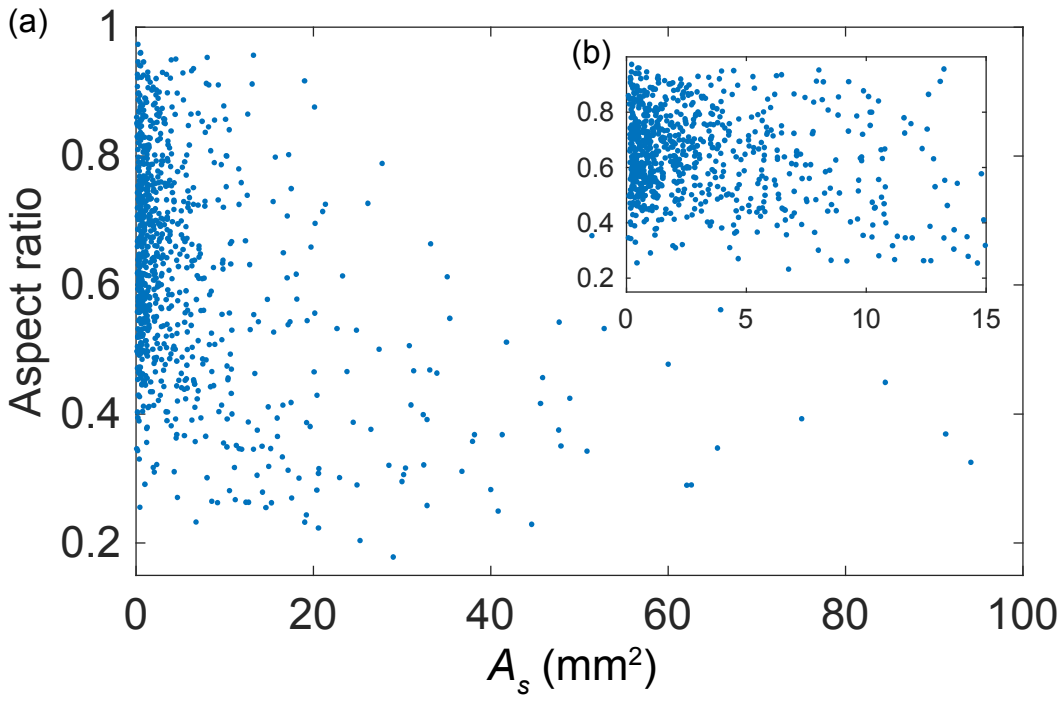

Figure 4.35: A scatterplot of the satellite size A_s and their respective aspect ratio. There was a general decrease in the aspect ratio as the satellite size increased. Small satellites showed a large variation of aspect ratio (Panel (b)), and did not exhibit any obvious trends.

Fitting and evaluating the fit

d was plotted against the patch area (Figure 4.34, panel (c)). The radial expansion of satellites suggested that the behaviour was controlled globally rather than locally, thus the factor that determines how far they travel may also be related to the patch. The plot showed a large variation across the patch area A_p. However, an asymptotic increase in d was recognized, especially from the moving average. Also, in low A_p, d appeared to be constant and independent of the size of the patch. To describe this trend, a piecewise function was devised:

$$d = \begin{cases} b & \text{if } A_p \leq A_T \\ b + \delta(A_p) & \text{if } A_p > A_T \end{cases} \tag{4.8}$$

Satellites from patches smaller than A_T travel a fixed distance b. Satellites from patches larger than A_T travel an additional distance of δ, which increases as the patch area increases:

$$\delta(A_p) = \frac{M \times \Delta A/K}{1 + \Delta A/K} \tag{4.9}$$

where $\Delta A = A_p - A_T$.

Table 4.8: Parameters from the fit based on equation 4.8, standard deviation and error ($N = 582$).

Type	M (mm)	K (mm^2)	A_T (mm^2)	b (mm)
Parameters	3.62	68.8	76.1	2.21
Standard deviation	1.90	81.1	13.5	0.23
Standard error	0.07	3.3	0.6	0.01

The experimental data were then fitted using this function with the least square method. Specifically, the residual square difference between the empirical data and the function was minimized, with all four parameters unbounded.

Due to large N, the errors of the parameters were small despite the large deviations (Table 4.8). The fit (Blue line) mostly lies within one standard deviation of the moving average (Red error bars) (Figure 4.34, panel (c)).

Due to the large variance from the data, it was difficult at first glance to determine how good our model fits the experimental data. Therefore, the Akaike Information Criterion (AIC) and the Akaike Weight were used to score and compare different models (Section 4.2).

To show that the model proposed was appropriate, we compared our model (*threshold*) with two other models: a simple linear model (*linear*), and a same saturating model as equation 4.9, but without A_T (*saturating*). The new models were also fitted with the same procedure as before. All three models were especially similar to one another in patch areas greater than 100 mm^2. The strongest difference was the jump caused by the threshold model at A_T (Figure 4.36).

Table 4.9: The Akaike weights of three models compared for different ranges of data. The weight represents the probability that it is the best fitting model. The fit parameters were derived using the data from the entire range.

Range	n	Linear	Saturation	Threshold
$<$80 mm^2	73	0.27	0.09	0.64
$<$100 mm^2	125	0.28	0.18	0.54
$<$120 mm^2	193	0.16	0.27	0.57
$<$140 mm^2	316	0.64	0.30	0.06
All	582	0.38	0.44	0.18

When AIC scores were calculated for three models with the experimental data, the differences were small. Since all three models show similar trajectories, especially in large patch areas where data points are concentrated, it masked the difference in data points in smaller patch areas. Based on the Akaike weights calculated based on this score, however, the threshold model outperformed the other two models up to 120 mm^2. When the models were scored with data from patch areas below 80 mm^2, where models deviate from each other, the threshold model clearly outperformed the other two models (Table 4.9). Based on the Akaike Weight analysis under 80 mm^2, which is where A_T lies,

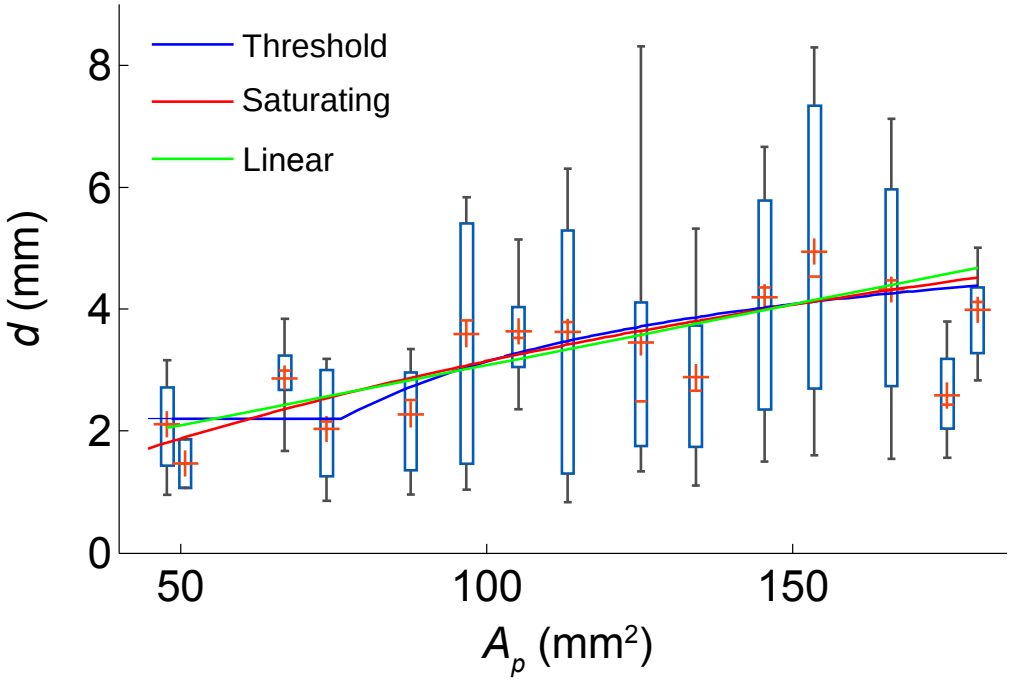

Figure 4.36: Three models considered to describe the distance travelled by satellites. The data is represented as a boxplot. The blue boxes indicate 25 to 75% percentile, and the extended lines indicate 9 - 91% percentile, with plus signs as the mean and the red line as a median. All three models were very similar when patch areas are greater than 100 mm^2, and the differences were most visible in smaller patch areas.

our threshold model was at least 2.3 times more likely to be the better model than the others considered, and 64% likely to be the best model in describing the data (Table 4.9).

Modelling based on diffusion

The satellite growth was visually striking in that all satellites from one patch seemed to travel approximately the same distance away from their origin, emerged and stopped at about the same time, all without a centralized system to control. We considered what type of mechanism would allow satellites to behave in a coordinated manner. First, we considered an internal clock that synchronizes when microplasmodia were placed on a solid surface. It is known that they undergo mitosis in 9 - 11 hours in synchrony [78], which is approximately the time after inoculation when satellites pause. However, the internal clock would not provide a sense of direction, therefore it would not explain the radial expansion of the satellites.

A quorum-sensing-like mechanism was also considered, where the behaviours were coordinated based on the concentration threshold of a signal molecule [24]. Microplasmodia may produce and excrete signals to communicate with other microplasmodia and coordinate behaviours. Moreover, *P. polycephalum* demonstrates extensive chemotactic

behaviour towards several known signal molecules, such as cyclic adenosine monophosphate (cAMP). This signal could be released along with slime, as the slime production drastically increases after 4 days. This is also about the same time when glucose was depleted in liquid culture (Figure 4.4, panel (b)), making it plausible that a chemical is released to signal starvation. Since we consider the satellite growth to be a response to lack of nutrients, the signal molecule would be produced by *P. polycephalum* when no longer detecting food. Slime itself may be a repellent that propels satellites away, as it is already demonstrated that this slime trace is used for external memory to increase in foraging efficiency by reducing re-visitation [92, 95].

Since experiments were performed on day 6, *P. polycephalum* has 3 days to produce the signal in response to starvation in the liquid culture after glucose was depleted (Figure 4.4, panel (b)), compared to 10 hours or less on an agar plate. Therefore, we assumed the production of the signal molecule on agar insignificant and all the signal molecules were transferred from the culture. We also assume that the signal molecule is stable for at least 10 hours, and the agar surface is large enough to be considered infinite on our length scale. To note, that preparation of microplasmodia includes aspiration of all supernatant, with resuspension of sterile water. It is suspected that pellets or the liquid surrounding the microplasmodia contain enough signalling molecules to induce satellite growth.

There are two pieces of evidence that support that a signal molecule is present in the spent medium of microplasmodia. When the supernatant of the microplasmodia was placed near the patch, emerging satellites avoided spots where supernatants were placed (Figure 4.11). These satellites clearly turned before making physical contact with the boundary of the spot, proving that there is a diffusive chemical that can impact the motility of *P. polycephalum*.

Secondly, when patches were quickly dried with paper towels, the emerging satellites lost their constant direction and stable morphology (Figure 4.25). Since the satellites formed, any disturbances caused by the drying did not impact the initial dynamics of microplasmodia. Therefore, the quick removal of the suspended medium also removed, to some extent, the signal molecule that plays an important role in satellite motility.

Therefore, a model was considered where a bioactive molecule is accumulated in the liquid culture and transferred to an agar plate. This bioactive molecule causes satellites to move out of the patch, via a chemorepellent effect. This hypothesized molecule will be referred to as a 'signal molecule'. In this scenario, the radial expansion of satellites is explained based on centralized localization of the signalling molecule in the patch. Moreover, if we assume that these signalling molecules freely diffuse through agar, the signals would continuously affect the satellites even after they are detached from the patch. It is also known that the diffusive properties in an agar layer are approximately the same as in water [111].

Based on AIC, the threshold model proved to be the best model to describe the relationship between A_p and d (Table 4.9). Then, an explanation is required as to why the

signal molecule only affects satellites when the A_p is above a certain size. To explain this behaviour, a threshold phenomenon is introduced. In many biological systems, there is a lower bound of detectable concentration. This is referred to as a threshold concentration, and have been demonstrated in *P. polycephalum* [112]. Therefore, it is plausible that in smaller patches, the diffusion front has a concentration of signal molecule that is below this threshold value. Only above A_T, the diffusion causes sufficient transfer of signal molecules so that this threshold concentration is reached to affect satellites, effectively 'pushing' the satellite farther away.

Therefore, We define C_T as the minimum detectable concentration of a signal molecule. Mathematically, C_T is expressed as:

$$C_T = \begin{cases} C(A_T, b) & \text{if } A_p \leq A_T \\ C(A_p, b + \delta(A_p)) & \text{if } A_p > A_T \end{cases} \tag{4.10}$$

The concentration of a signal molecule (C) at position b, of the patch with a threshold area (A_T), is the threshold concentration of the signal molecule. If the patch is smaller than A_T, the C at b is lower than C_T and does not affect satellites since it is below the detection limit. We also assume that the satellite 'sits' on this diffusion front, and the C_T is found where satellites are located in cases where $A_p > A_T$.

Simulating diffusion

To demonstrate this theory, diffusion was simulated with various size of A_p. The conditions described above are analogous to a diffusion problem with an instantaneous release of the compound on a defined area. This can then be solved using a Gaussian kernel and a patch function, $p(x', y')$, that describes a circular patch with a radius r [113]. The length scale σ was set as $\sqrt{4Dt}$, where D is the diffusion coefficient and t is the time, to represent the mean distance travelled by a signal molecule by a free two-dimensional diffusion:

$$\begin{aligned} C(x, y, t) \quad &= \int_{-\infty}^{\infty} \int_{-\infty}^{\infty} \frac{p(x', y')}{\pi\sigma^2} \\ &\exp\left(-\frac{(x-x')^2 + (y-y')^2}{\sigma^2}\right) dx' dy' \end{aligned} \tag{4.11}$$

where,

$$p(x', y') = \begin{cases} C_0 & \text{if } x'^2 + y'^2 \leq r^2 \\ 0 & \text{otherwise} \end{cases} \tag{4.12}$$

At $t = 0$. the patch is filled with a signal molecule with an initial concentration of C_0. We assume C_0 is the same in the model in all the patches, and the satellites stop at 10 hours after inoculation. Therefore, we were interested in the distribution of the signalling molecule after 10 hours of diffusion. The function of signal distribution can

then be expressed as a convolution of the Gaussian kernel and the patch function [114],

$$C(x, y) = (p * g)(x, y) \tag{4.13}$$

where g is the Gaussian kernel. Then the convolution can be solved numerically.

Two methods to solve this convolution were considered. The first method is the finite difference method, in which differential equations are approximated with difference equations. In order for this to be valid, the difference between each time step of the Gaussian evolution needs to be small. This process is computationally intensive, as the diffusion is simulated for each interval up to the desired time. The second method is to perform Gaussian convolution using an image filter. Due to the widespread utilization of Gaussian filter to blur images, this process and functionality are optimized in many programs, including python and Matlab. The test simulations were compared between the two methods, which gave almost identical results (Figure 4.37, panel (a)). Therefore, the Gaussian filter was used as the main method of calculating the diffusion length.

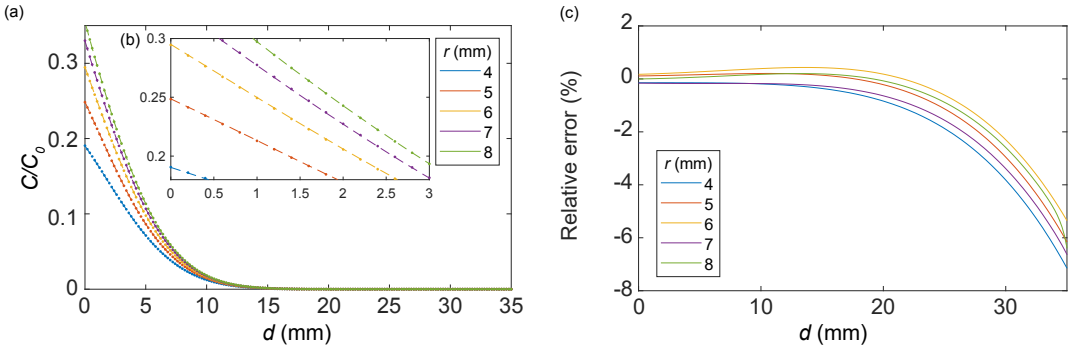

Figure 4.37: Diffusion simulation of a signal molecule with the finite difference method (FDM) and Gaussian convolution with a diffusion coefficient of 4×10^{-4} mm^2/s after 10 hours. 5 different circular patch sizes were simulated, with their radii r given in the legend. It is represented as a cross-section through the diameter of the patch, with the null point being the border of the patch by definition of d (Panel (a)). The dashed lines represent Gaussian convolution, and the dotted lines represent the FDM. Both were very similar, even when zoomed in (Panel (b)). The relative difference was calculated by taking the difference between Gaussian convolution and FDM and normalized with Gaussian convolution. The relative error remained within 1% range (Panel (c)). Larger errors occurred near the end, where boundary effects took place. For FDM, a length scale of 0.2 mm with an interval of 5 seconds was used. For Gaussian convolution, the length scale of 0.05 mm was used. Both were simulated on a 90 × 90 mm square grid.

Since both, the patch and the Gaussian distribution, are radially symmetrical, the result is represented as a cross-section through the diameter of the patch, with the null point being the border of the patch by definition of d. Then, the diffusion was simulated with different sizes of the patch, to see how the diffusion front was affected.

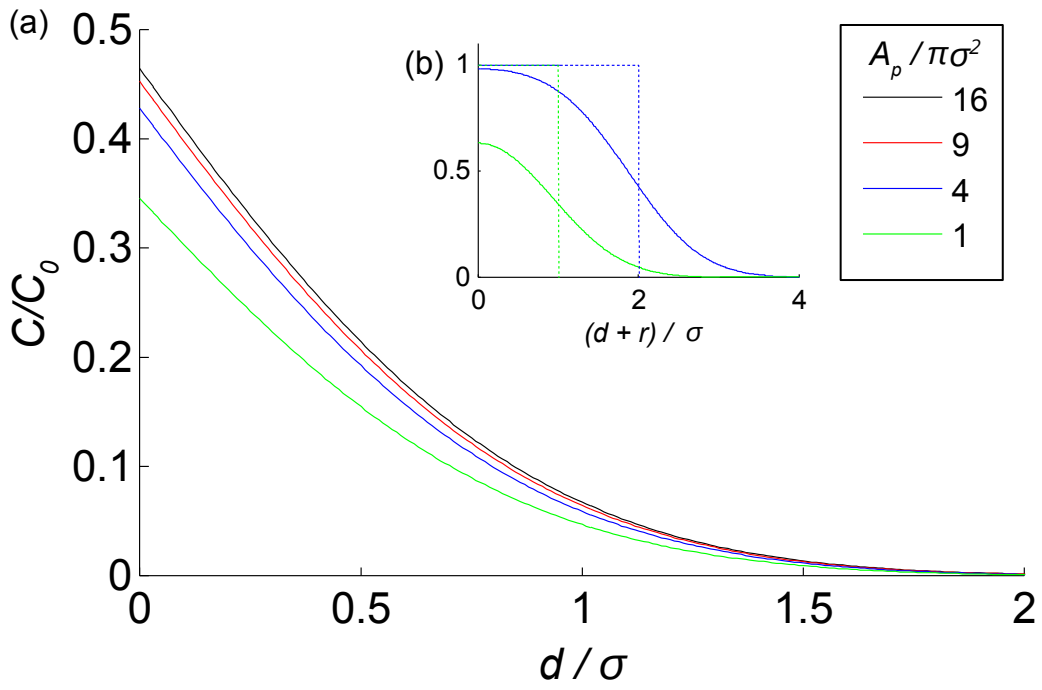

Figure 4.38: Concentration distribution of the signal molecule after 10 hours. Patches with greater A_p had larger C/C_0 in general (Panel (a)). The concentration rapidly decayed to 0 around $2d/\sigma$, regardless of A_p. The comparison of initial and final distribution of the signal molecule (Panel (b)). The x-axis was shifted so that the zero represented the centroid of the patch. The initial distribution was indicated with the dotted lines and showed that the patch size affected the shape of the final distribution curve. A_p is indicated in the legend and is normalized with $\pi\sigma^2$, and the corresponding distribution is represented with the same colour. σ equals $\sqrt{4Dt}$

The graph clearly shows that the larger patches have a larger concentration of diffusion fronts (Figure 4.38). At a fixed distance from the patch border, the larger A_p had higher concentrations diffused than the smaller patches A_p. Therefore, this proved that the A_p can influence the d with the diffusion of a signal molecule from the patch (Equation 4.10).

What is also evident is that the concentrations degrade to zero near 2 d/σ, regardless of the patch size. This indicates the presence of the asymptote described in equation 4.9. Moreover, a petri dish with a radius of 45 mm was used to produce agar plates. Assuming that 2 d/σ equals 20 mm, which is well within the boundaries of the agar plate, the diffusion coefficient comes out to be about 7 $\times 10^{-4}$ mm^2/s. In other words, as long as the diffusion coefficient is below the above value, the numerical solution is valid.

Fitting experimental data

Based on equation 4.10 and the parameter values from the fit, C_T can be calculated. However, the value of C_T is dependent on the diffusion coefficient D, and the actual

value of C_T of the system is unknown. Therefore, we focused on equation 4.9, and sought a diffusion coefficient that was consistent with parameters from the fit.

To do this, numerical solutions of diffusion with a particular diffusion coefficient over a range of A_p were generated. Then, C_T of this diffusion was calculated with A_T and b from the fit (Table 4.8), which in turn was used to calculate $\delta(A)$ with equation 4.9 (Figure 4.39 (a)). δ shows greater increase in larger diffusion coefficients as expected, since D dictates how fast the signal molecule diffuses.

Then, the sum of squared differences (χ^2) were calculated for all Ds against $\delta(A)$ of the fit (Figure 4.39 (b)). The minimum of the χ^2 was found by fitting a polynomial of the second degree to the result, which was given by $D = 5.98\ \times 10^{-4}$ mm^2/s. The χ^2_{min} was remarkably close to zero. This D lies between glucose ($6.0\ \times 10^{-4}$ mm^2/s) and cyclic AMP ($4.4\ \times 10^{-4}$ mm^2/s), and is similar to small amino acids [111,115].

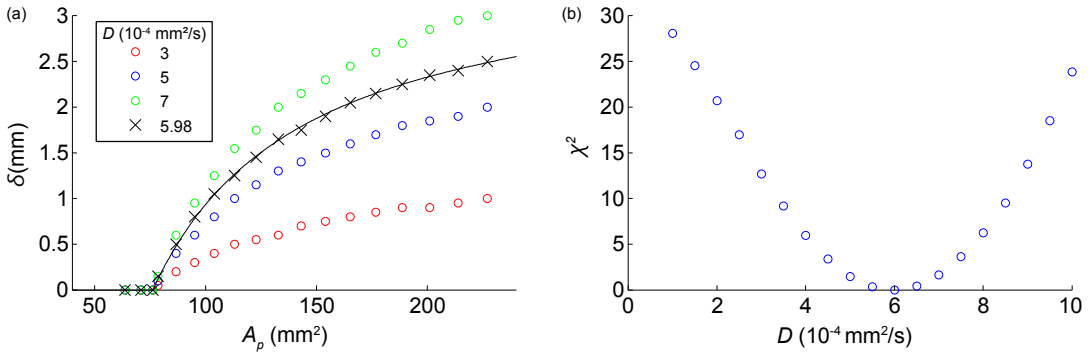

Figure 4.39: A diffusion coefficient that is consistent with the parameters in table 4.8 was sought. δ of the three different diffusion coefficients, as well as the experimental fit, are plotted (Panel (a)). The diffusion coefficients are shown in legends, with a unit of $\times 10^{-4}$ mm^2/s, with corresponding values represented with the coloured dots. The black line is from the experimental fit. Lower diffusion coefficients resulted in smaller δ. D with minimum χ^2 was calculated from figure 4.39 (Panel (b)) and subsequently plotted with black x markers, which showed remarkable agreement with the experimental fit. The sums of the difference squared between the fit and D are plotted (Panel (b)). As expected from the plot from panel (a), the minimum lies between 5 and 7.

4.9 Scaling of the satellite growth

The following section is based on a prepared draft by the author.

Initial observation

Although the satellite growth showed a remarkable temporal correlation in its behaviour (Figure 4.5), the shape, as well as the number of satellites produced, showed a large variation. In extreme cases, one circular satellite emerged similar to a ring, expanding as it migrated away from the patch. In most cases, however, many satellites formed

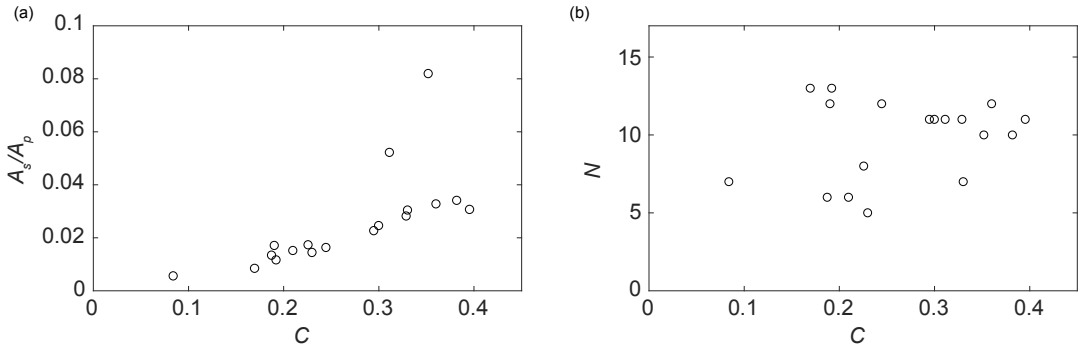

Figure 4.40: Satellite sizes A_s (Panel (a)) and the number of satellites N (Panel (b)) produced per initial coverage of microplasmodia C. There appeared to be a positive correlation between C and A_s, but no obvious patterns were recognized in N

with similar shape and size. It was first noted that the coverage, i.e. the density of microplasmodia at the initial state, was correlated with the size of emerging satellites. This was intuitive, as more biomass would be required to form larger satellites. However, it appeared that when smaller satellites emerged, they were numerous, whereas larger satellites tended to be few in number. Therefore, we first compared the number of satellites emerged, as well as their size, to the coverage of the corresponding patch.

To better compare the different sizes of satellites from different patch sizes A_p, the satellite size A_s was normalized with A_p of origin (See figure 4.3 for definitions). It was evident that A_s/A_p increased as the coverage increases (Figure 4.40, panel (a)). However, it was not initially clear if there was a correlation between the coverage and the number of satellites produced (Figure 4.40, panel (b)).

There were two extreme cases of the satellite growth observed. At one end, when insufficient biomass was present, no satellites were formed, presumably due to the lack of biomass to form mesoplasmodia. At the other end, when the patch was oversaturated with microplasmodia, one giant ring-like satellite was formed (Figure 4.41). These ring-like satellites were excluded from the analysis based on two reasons. First, the biomass and the coverage of the patch could not be accurately determined. Based on a simulation of random sequential adsorption, where circular discs were placed in a fixed area until no further placement was possible without overlap, the maximum coverage attainable without overlap was 0.547 [116]. Since this simulation was performed to avoid the overlap if possible, in an actual experiment the overlap was likely to occur much earlier. Therefore, large values of coverages were avoided during the analysis. Second, it was assumed during the construction of the model and will be explained later, that the major axis of the satellites enclosed the patch circumference as a boundary condition. Since at least three major axes were required to enclose the circular patch with a closed polygon, the minimum number of satellites from the scaling was 3. Therefore only the experiments with more than 3 satellites were used.

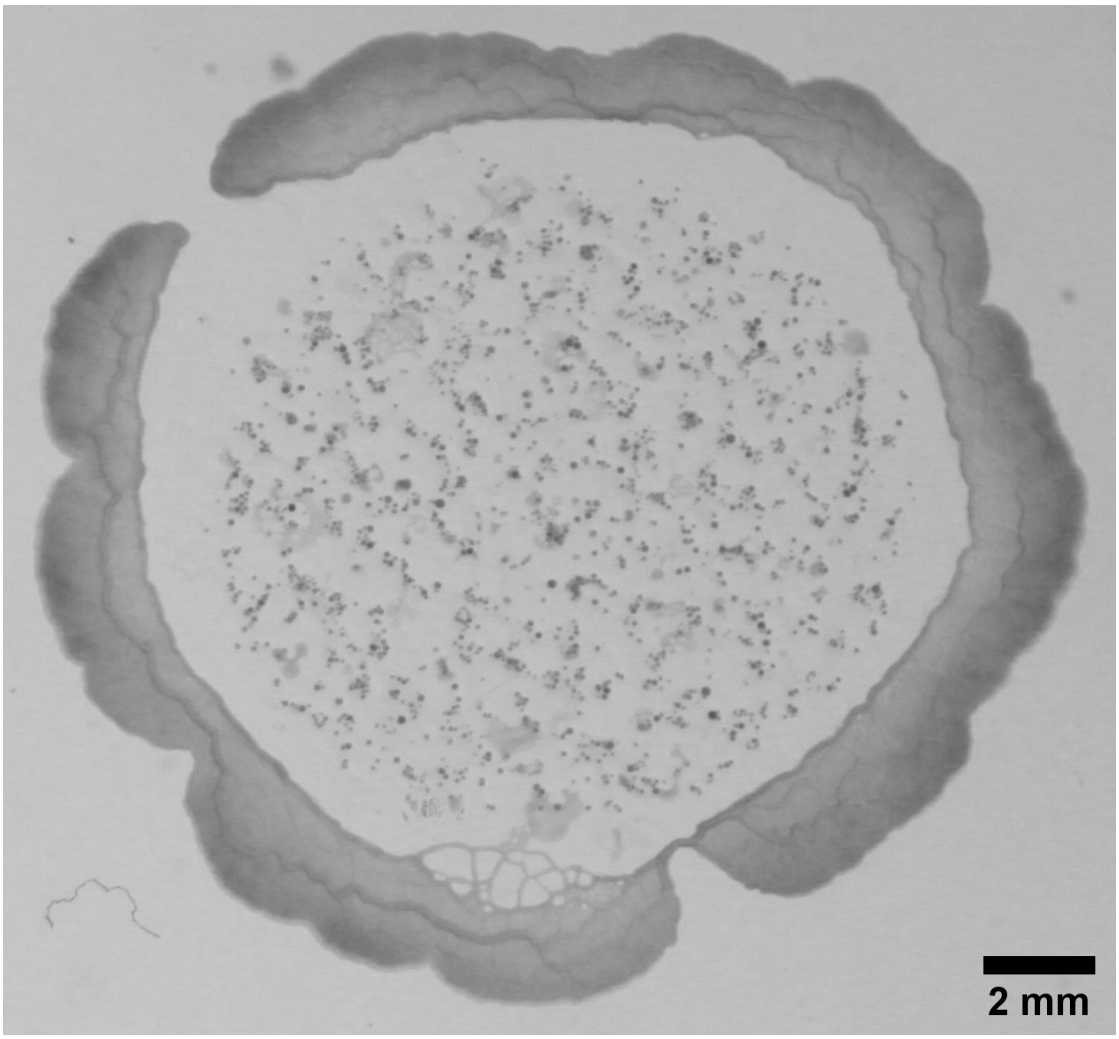

Figure 4.41: A ring satellite. Unlike other satellite patterns where satellites resembled a half-circle or oval, this satellite had a ring-like morphology. While excluded from the analysis due to the limitations imposed by the boundary conditions, there were several cases in extremely high coverages, one satellite was formed that expanded as it moved outward, reaching the theoretical maximum search area. Creases or indents along the moving front of the ring were observed, suggesting that it consisted of multiple satellites fused together.

Modelling based on the maximization principles

In the hypothesis of satellite growth, it was stated that satellite growth was an alternative growth strategy designed to counter prolonged starvation in a harsh environment (Section 4.5). To counter starvation is to forage for food, and prolonged starvation as an immediate lack of carbon sources would force an organism to act quickly. Therefore, it made sense that satellites migrated away from the patch, as the patch did not contain any nutrients, and crowded with other microplasmodia that resources would have to be shared with. Fragmentation, or rather the avoidance of forming an extended body, also increases the chance that one of the fragments would survive and pass on their genes [97]. Further, the fragments should maximize the search area, to maximize their foraging ef-

forts, and thus the survival of the batch.

To test whether satellites indeed maximized the search area, we made several assumptions on its behaviour to define mesoplasmodial dynamics based on observations and experimental conditions. The first assumption is that the biomass of *P. polyecphalum*. (B). remains constant throughout the duration of satellite growth. It was observed that satellites, during propagation, maintained their size and shape until the pause state [23]. It was also plausible, that during starvation *P. polyecphalum* prioritized exploration rather than growth. It was evident from previous observations, however, that the area covered by microplasmodia increased as time progressed (Figure 4.16). The scaling equations were derived based on the constant biomass, but the implication of the increased area is also later discussed.

The second assumption is that the height of *P. polyecphalum*, regardless of its state, is approximately the same and therefore the biomass can be represented as an area instead of volume. Some observations suggested that the height of microplasmodia varied, such as an apparent microplasmodial explosion observed during the first hour of satellite growth (Figure 4.26). Moreover, the intensities of the satellite in the greyscale image appeared less intense than that of microplasmodia. However, it was assumed that the variation was not significant and on the whole, the approximation remained valid.

Then, the satellite growth pattern was simplified into geometric shapes, as seen in figure 4.42. At $t = 0$, all microplasmodia, and therefore all biomass is placed in a circular patch with an area of A_p. In the end, N oval-shaped satellites, with an average size A_s and aspect ratio R surround the patch. The biomass B can be represented as a portion of A_p occupied by the microplasmodia called coverage, C. We assume that microplasmodia are homogeneously distributed within the patch, and all available biomass is transferred equally to satellites with identical sizes and shapes:

$$B = A_p \times C = N \times A_s \tag{4.14}$$

Since satellites did not change their size or direction of movement, understanding the initial formation of satellites was a crucial step in determining their search efficiency. If satellites are to maximize the search area, then their axis tangent to the patch border should be as large as possible, to maximize the search path width. If their shape and size remain constant, a crowding occurs at the initial release of satellites from the border to prevent overlapping (Figure 4.42, panel (b)). Therefore, A_s and N are restricted based on A_p. Based on the previous assumption that all satellites are identical, we express the major axis a of a satellite with respect to the patch radius r_p as

$$a = r_p \tan(\frac{\pi}{N}) \tag{4.15}$$

The small-angle approximation was applied to simplify the equation 4.15 further. This assumption is valid when π/N is very small and therefore is applicable with large

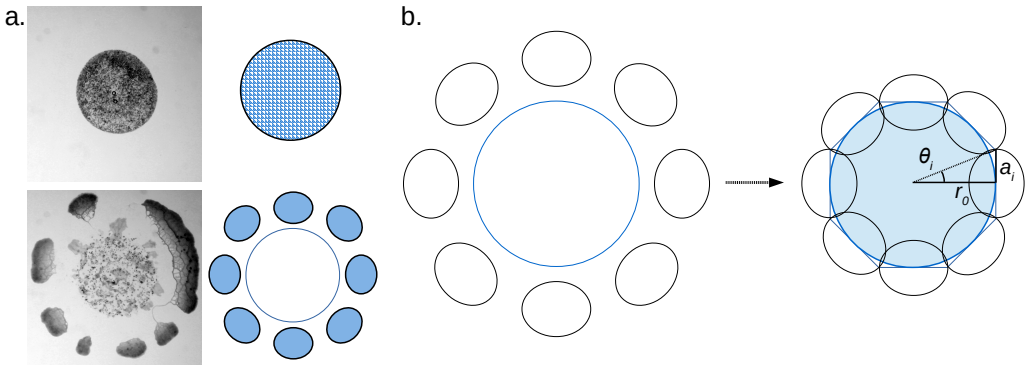

Figure 4.42: Simplification of the satellite growth pattern. Pictures show the initial patch filled with microplasmodia and fully detached satellites at the pause state (Panel (a)). The patch was represented by a perfect circle, and all satellites were assumed to be of identical size and shape. To maximize the searched area, the size of satellites was maximized within certain constraints (Panel (b)). The constraint was set as a crowding effect on the patch circumference, which defined the number and size of satellites based on the size of the patch.

N. The deviations caused by this approximation is later evaluated in a scaling equation (Figure 4.43). With the help of this approximation, we arrive at a scaling equation

$$N = \frac{\pi^2 R}{C}, \tag{4.16}$$

where R is the aspect ratio, which describes a relationship between the coverage of the microplasmodia and the number of satellites produced. This can be rearranged to scaling on the area of satellites per coverage with equation 4.14, which results in

$$\frac{A_s}{A_p} = \frac{C^2}{\pi^2 R}. \tag{4.17}$$

The two scaling equations describe the number, the size, and the shape of a satellite, based on the density of the microplasmodia at the initial state. Based on equation 4.16, the number of satellites produced is expected to decrease as the coverage increases, whereas based on equation 4.17, the size of satellites, normalized by the patch size, would increase with C.

To evaluate the margin of error resulting from the small angle approximation in the cases of low N, the equation 4.16 was compared with a scaling equation without the approximation, which can be numerically solved (Figure 4.43). When both solutions were compared in the scaling equation, the differences were minimal. Only when N was below 10 and C larger than 0.6, noticeable differences were observed. Since all of our experiments were below $C = 0.5$, and the differences were minimal, the approximation did not significantly alter the scaling.

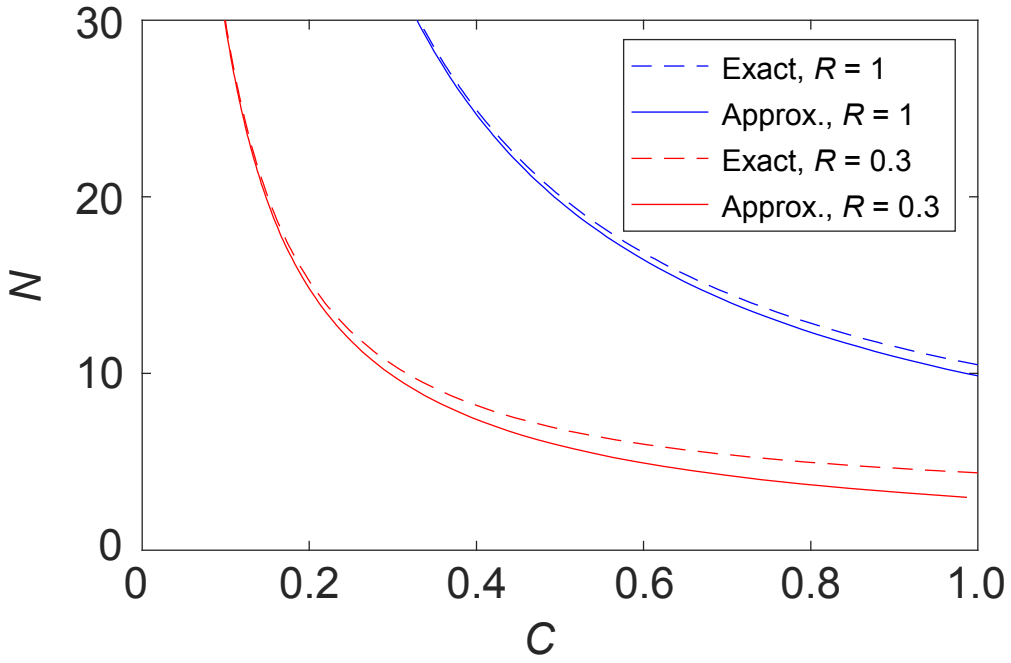

Figure 4.43: Comparison between the exact solution and the small angle approximation in the scaling equation according to equation 4.16. Two aspect ratio values were arbitrarily picked to show the effects of high and low N. In $N > 10$, only a small deviation between the approximation and the exact solution occurred. The deviations became larger in low N. However, all of the experimental data were in regions where $C < 0.5$, and therefore within regions where deviations were small.

Model evaluation and satellite collision

The scaling relationship based on the maximization principle was compared to empirical data. Only a small subsection of the satellite data was used to ensure that all parameters influencing satellite growth were kept identical. There was some suspicion that the aspect ratio R decreased as A_s/A_p increased. This notion is also supported by figure 4.34, where only the larger satellites fall below the hypothetical circular minimal distance. However, no explicit relationship between the two could be derived due to a large variance in the data (Figure 4.35). Therefore, R was measured from the data, and the mean and the range of two standard deviations of the aspect ratio were used to characterize the spread of the data.

The scaling relationship based on the maximization principle showed some similarities with the observed size of satellites, as the exponential increase was accurately captured (Figure 4.44, panel (a)). Moreover, although all data lie just outside of two standard deviations, the data reproduce the shape of the theoretical curve, suggesting that the simplified model captures certain features of the data well, but is missing a factor or offset integrating further information. Therefore, only the magnitude of increase would need to be adjusted, rather than significantly modifying the model. However, there were no obvious correlations between the scaling and observed number of satellites per cover-

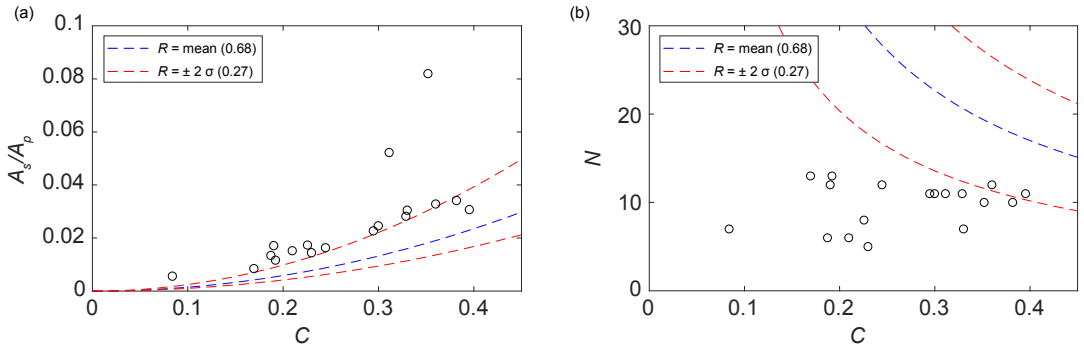

Figure 4.44: The scaling relationship between coverage and satellites. Scaling relation with the area (Panel (a)) matched the general exponential increase of the A_s/A_p, but most data were located just outside of two standard deviations (Red line). The number of satellites produced did not resemble the scaling derived from maximizing principle (Panel (b)). Only very few data points were present within the range of two standard deviations, near C of 0.4, and the predicted trend was not seen in the data.

age (Figure 4.44, panel (b)). The data fell well below the predicted scaling, especially in low C.

To further refine the scaling, experiments, as well as our assumptions during the derivation of the scaling, were reviewed. At the boundary condition of the derivation, it was assumed that all satellites were crowded at the border of the patch, contacting but remaining as separate entities. However, in most of the cases, the collision between two satellites caused fusion (Figure 4.45). This collision and the resultant fusion had two effects: first, it increased A_s/A_p, and moreover, it decreased N. Therefore, the collision factor k was introduced in the scaling equations (Equation 4.16 and 4.17) to adjust N and A_s, leading to the revised equation

$$\frac{A_s}{A_p} = k \times \frac{C^2}{\pi^2 R}. \tag{4.18}$$

k, in this case, represents how much larger the satellites are compared to the theoretical size calculated from equation 4.17. Further, the inverse of k is used to calculate how many satellites are lost due to collision:

$$N = \frac{1}{k} \times \frac{\pi^2 R}{C} \tag{4.19}$$

k was calculated from fitting the data.

Introduction of the collision factor k altered the scaling relationship only in the magnitude of the increase, and not the shape of the curve. k of 1.7 lowered the scaling for the satellite sizes so that thereafter, the data agreed well with the scaling (Figure 4.46, panel (a)). The collision factor also adjusted the scaling of N, and data from the coverages greater than 0.3 was within the range of the scaling equation. However, the data from

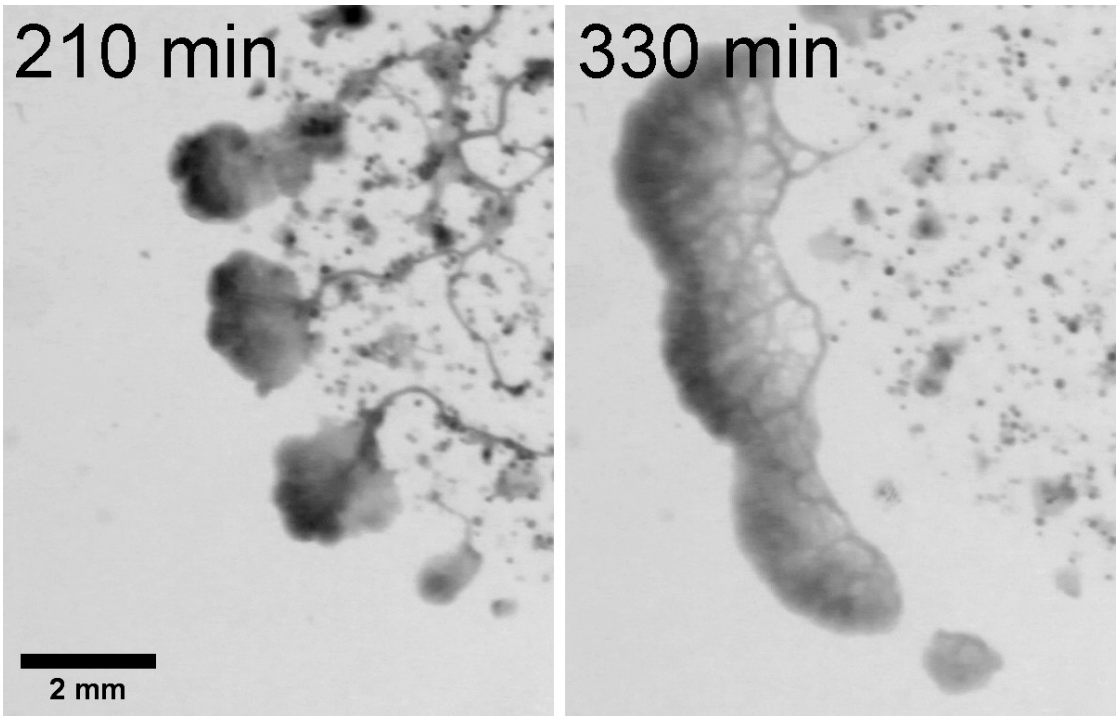

Figure 4.45: Collision of satellites. The left image shows 4 protrusions, which would have resulted in 4 separate satellites. However, they have contacted and fused with one another, forming only 2 satellites. The satellite formed from 3 protrusions is much larger and more elongated than the satellite from a single protrusion.

lower coverages still deviated from the predicted scaling (Figure 4.46, panel (b)).

Diffusion and fusion probability

While the collision factor k allowed the scaling equation to fit better for A_s/A_p, there were still some fundamental deviations observed in the scaling of N. The scaling predicts that a very large number of satellites is produced in low C. However, in practice, low coverages result in no satellites. Also, it was clear that a single microplasmodium did not move away from the patch by itself when it did not form satellites in a fusion process. Satellites were always larger than the microplasmodia, and therefore fusion must occur to bring sufficient biomass to form satellites. Assuming that microplasmodia are evenly distributed, the distance between the microplasmodia decreases as the coverage increases. Since microplasmodia must come into physical contact with each other before fusion can occur, they must travel, at least, to the nearest microplasmodium to form a mesoplasmodium. Moreover, satellites protrude at a fixed time after inoculation (Figure 4.5), limiting the time that microplasmodia can move and fuse.

Intuitively, then, mesoplasmodia are more likely to form in higher C, since they microplasmodium travel smaller distances to meet their nearest neighbours. In lower coverages, a microplasmodium may not be able to meet another microplasmodium, which leads

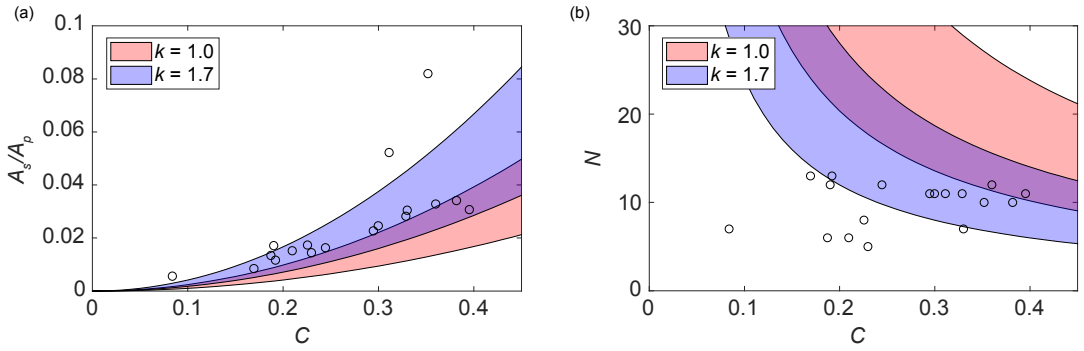

Figure 4.46: The scaling relationship between coverage and satellites with the collision factor k. The area shaded with red indicates the raw scaling, and the blue shade indicates the scaling equations with collision factor. The boundaries were set with two standard deviations of the aspect ratio. The satellite size was in very good agreement with the scaling, with k of 1.7 (Panel (a)). It also improved the fit of N, where many of the data now lies within the range of the scaling equation (Panel (b)). However, points in low C were still below the number predicted by the scaling.

to a failure in forming satellites. To calculate the average distance between microplasmodia, a hypothetical ideal distribution of microplasmodia was constructed (Figure 4.31). Then, the distance between the microplasmodia s was calculated from the coverage C and its own diameter d (Equation 4.6).

Next, the likelihood for the microplasmodia to cross the distance of s was considered. The motility of microplasmodia was assumed to be a free diffusion without any drift. Then, we focused on the distance between the two nearest microplasmodia, s, to simplify the problem into one-dimension. Since this normal diffusion was assumed, the probability distribution was a Gaussian curve centred at 0. In 1-D, the corresponding cumulative distribution function (CDF) was an error function. Using the CDF, the probability of microplasmodia travelling a minimum distance is:

$$P(s) = erfc(\frac{s}{\sqrt{4Dt}}) \tag{4.20}$$

$P(s)$ represents the probability that two microplasmodia will come into contact as a function of the distance between the microplasmodia, s, with a given diffusion coefficient D and time t. Then, we combined equation 4.20 with equation 4.6 to arrive at a probability of fusion based on coverage,

$$P(C) = erfc(\frac{1}{\tilde{l}}(\frac{1}{\sqrt{C}} - 1)) \tag{4.21}$$

with,

$$\tilde{l} = \frac{\sqrt{4Dt}}{d}.$$

In equation 4.21, $P(C)$ represents the probability of two microplasmodia coming into contact. We assume this probability to be equal to the probability of satellite formation, as the fusion of two microplasmodia is considered as an initiation and a crucial first step in forming a satellite. The fusion probability was plotted against C with several $\tilde{l}$ values (Figure 4.47).

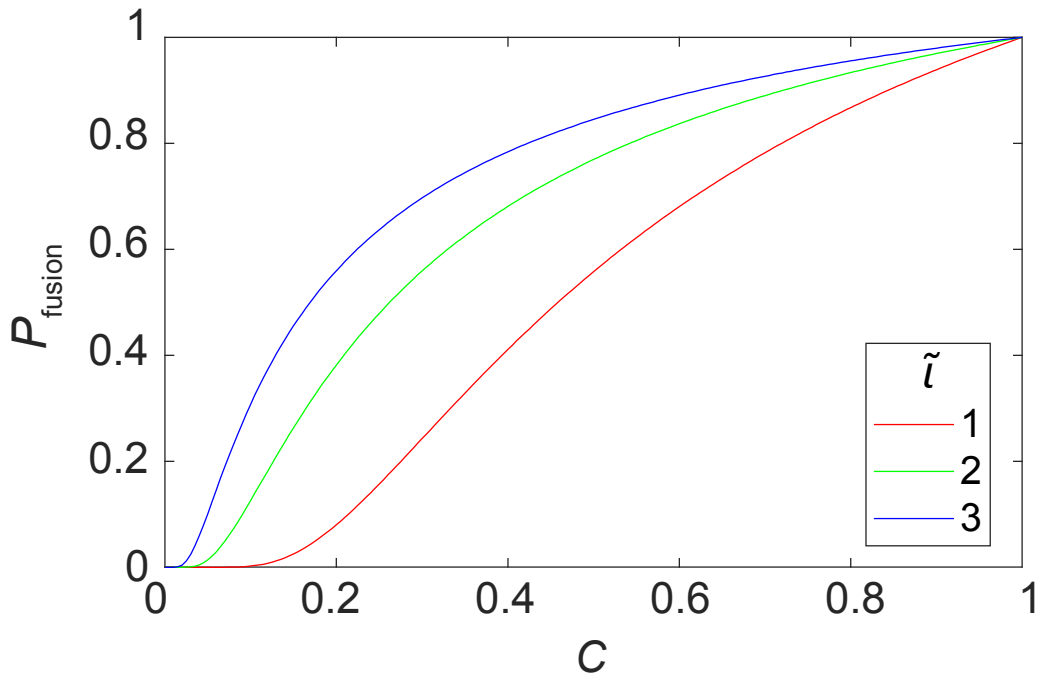

Figure 4.47: Fusion probability of microplasmodia based on coverage and scaled length of travel. The $\tilde{l}$ represents the scaled diffusion length over the diameter of the microplasmodium. The probability converged to 1 as the coverage increases. Moreover, larger values of $\tilde{l}$ resulted in higher fusion probabilities in general.

As expected, the fusion probability converges to 1 as the coverage reaches 1 since all microplasmodia are in contact with each other (Figure 4.47). The general trend of the fusion probability was a saturating curve. The unitless factor $\tilde{l}$ represented the mean distance travelled by the microplasmodia via diffusion, scaled by microplasmodial diameter. A higher value of $\tilde{l}$, therefore, meant that microplasmodia travelled further, and thus more likely to encounter other microplasmodia. As evident in the figure, higher $\tilde{l}$ values resulted in a higher probability of fusion, especially evident in lower C.

Diffusion: a consideration of the narrow escape problem

The ideal scenario presented in figure 4.31 can also be interpreted as a narrow escape problem (NEP). In the NEP, the probability of a particle to hit a small window in a given area is considered. In our case, each neighbouring microplasmodium can be considered as a 'window' that the centre microplasmodium must hit in order to escape from the free

space.

Based on the work by Basnayake et al. [117], it was found that the relative window size with respect to the boundary determined the magnitude of the narrow escape effect. The authors considered only the cases where the escape of the particle was unlikely, and therefore their solution was in the form of an exponential function. This meant that the NEP cases can only be evaluated in low fusion probabilities where the relationship is exponential.

We considered two extreme cases in terms of window sizes in the NEP to see whether the comparison can be realized since the size of the escape window was the key factor. In the limit of very large windows, the entire circumference of the free diameter can be considered an escape window (See figure 4.31). This, experimentally, would be the case of very high coverage where microplasmodia are very close to each other. This case can be approximated by one-dimensional diffusion since the direction of diffusion is irrelevant; any step in any direction is towards a neighbouring microplasmodium. In the other extreme of very small windows, the direction of travel becomes relevant, since the neighbouring microplasmodia are sparsely distributed. In this case, the fusion probability with one-dimensional diffusion causes overestimation, as a microplasmodium must diffuse at specific directions to find neighbouring microplasmodia. Therefore, the exponential regions of the fusion probabilities in low C is focused, since this is the region where the difference would be noticed due to the effect of the NEP. Moreover, it was predicted that the solution from NEP would result in lower probabilities in general, compared to its one-dimensional fusion probabilities.

The survival probability $S(t)$ of a particle in a 2D environment, when the escape is not likely is [117]:

$$S(t) \approx 1 - \frac{\sqrt{2}\pi t}{2\log(\frac{1}{\epsilon})s_2^2} e^{-\frac{s_2^2}{4t}} \tag{4.22}$$

where ϵ is the ratio of the window size with respect to the boundary of the free space, and s_2 is the nearest distance between the particle and the window. The fusion probability $P(t)$ is simply $1 - S(t)$.

To convert ϵ with respect to C, we consider a free space with a radius of $2r_f$. Then, the perimeter of this arena is $4\pi r_f$, with $6d$ as window size due to the ideal lattice placement of microplasmodia depicted in figure 4.31. Assuming that the distribution is homogeneous, the definition of coverage can be written for a free area centred around a microplasmodium:

$$C \approx \frac{4 \times \pi(\frac{d}{2})^2}{\pi(2r_f)^2} = \frac{d^2}{4r_f^2} \tag{4.23}$$

Here, it is assumed that the microplasmodia on the border of the arena contribute half of their area for coverage. This leads to an overestimation of coverage, especially

in small $2r_f$. However, we are concerned with, as is with equation 4.22, cases where microplasmodia are not likely to fuse. In such cases, $2r_f$ must be large, and therefore the errors caused by this assumption become negligible. Utilizing this new definition, the ϵ can be expressed in terms of C. Then, we substitute $\tilde{l}$ in, to compare both fusion probabilities:

$$P(t) \approx \frac{\sqrt{2}\beta^2\tilde{l}^2}{8\log(\frac{2\pi}{3\sqrt{C}})}e^{-\frac{\beta^2}{\tilde{l}^2}} \tag{4.24}$$

with

$$\beta = \frac{1}{\sqrt{C}} - 1.$$

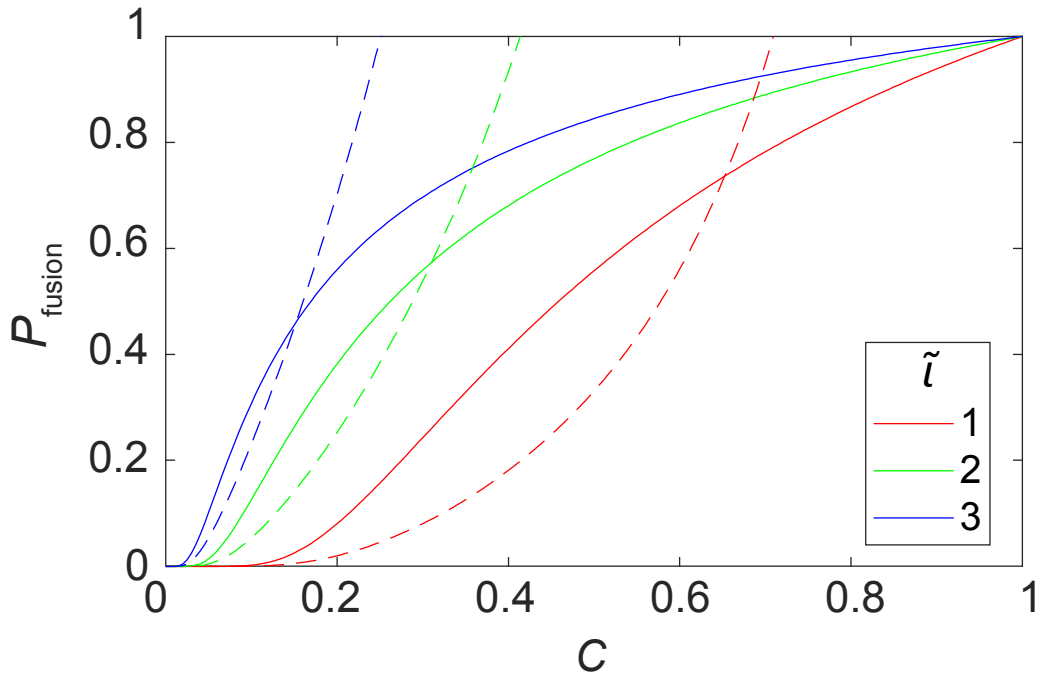

Figure 4.48: Comparison of fusion probability between the one dimensional diffusion and application of narrow escape problem. Solid lines indicate the fusion probability used in the scaling, and dashed lines indicate the fusion probability based on the NEP. Legends indicate $\tilde{l}$ values. The NEP is approximated for cases where the escape (in our case, the fusion) was unlikely, and therefore exponential. The narrow escape showed lower probabilities than a one-dimensional diffusion, as expected, in lower coverages and low $\tilde{l}$. The NEP effects were also greater in low $\tilde{l}$.

As expected, the fusion probability P_{fusion} based on NEP showed an exponential increase. Within the relevant parameter space, it quickly went out of bounds, and due

Table 4.10: Parameters calculated from fitting are shown in figure 4.49, and from experimental measurements.

Parameters	Data used	Measured	From fit	Standard Error
k	A_s/A_p	1.36	2.712	0.228
k	N	1.36	1.301	0.212
$\tilde{l}$	N	1.73	2.041	0.303

to the approximation, the fusion probability did not converge to 1. In general, NEP exerts the strongest effect in low C, and the fusion probabilities based on NEP was lower than the simple diffusion model, which was consistent with the expectation (Figure 4.48). Also, the effect was more prominent in lower $\tilde{l}$.

If P_{fusion} from NEP is lower than our original model (Equation 4.21), one can assume that the window size impacts the fusion and therefore the scaling needs to be adjusted accordingly. For example, the effect of the NEP was pronounced when $\tilde{l} = 1$ where the effect was seen until $C \approx 0.5$, affecting all of the experimental data. However, as $\tilde{l}$ becomes larger, the effects of NEP, as well as the region where this effect is seen, becomes smaller. At $\tilde{l} = 3$, effects were only visible below $C = 0.1$ and their influence was minimal. Therefore, the motility of the microplasmodia determines how much effect the NEP exerts on the fusion probability. The fusion probability in one-dimension is applied to the scaling equations first, and the resulting fit of $\tilde{l}$, as well as experimental determination of $\tilde{l}$ is used later to determine the validity of this assumption

Combining the models and fitting the data

The fusion probability $P(C)$ (Equation 4.21) was introduced to the scaling equation, along with the collision factor to see how the scaling relationship was altered. To do so, the length scale $\tilde{l}$ was determined from the experimental data along with k. $\tilde{l}$ could not be estimated from A_s/A_p, as the application of the fusion probability in the scaling of the area always made the fit worse, causing $\tilde{l}$ to diverge to infinity during fitting. Therefore, N was used to estimate k and $\tilde{l}$ first. Subsequently, $\tilde{l}$ from fitting N was used in estimating k from A_s/A_p. The values from the best fit were: $\tilde{l}$ of 2.04, k of 1.30 and 2.71 for N and A_s/A_p, respectively (Table 4.10). The resulting scaling equation was plotted with the data (Figure 4.49).

After collision and fusion probabilities were included, the scaling accurately predicted the number of satellites N produced per coverage C (Figure 4.49, panel (b)). The main impact of the application of fusion probabilities was that the scaling relationship at $C = 0$ became 0, rather than diverging for low C. The N peaked around a C of 0.15, and slowly decreased as C increased. Almost all data lie within the area defined by two standard deviations.

An exponential increase in A_s/A_p was also in line with the scaling, although the fit appeared slightly worse than the scaling with only the collision factor (Figure 4.49, panel (a)). The general shape of the curve was kept, even with fusion probabilities applied.

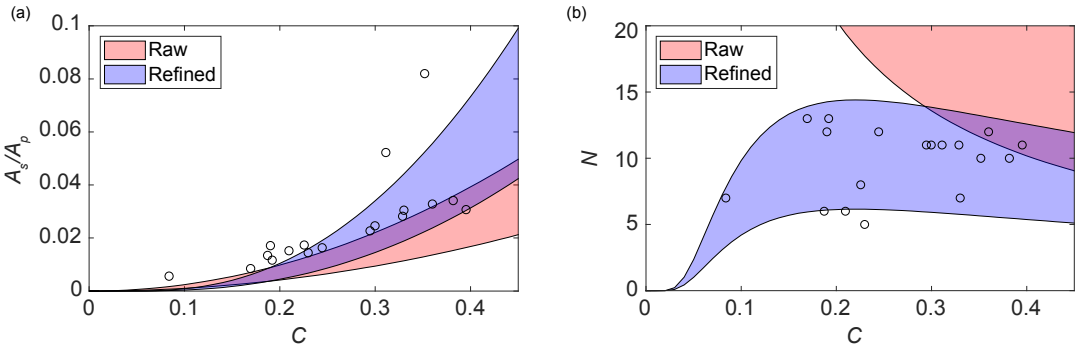

Figure 4.49: Scaling relationships of satellites, with fusion probabilities of microplasmodia and collision of satellites accounted for. The area shaded with red indicates the raw scaling, and the blue shade indicates the refined scaling with collision factor and fusion probability. The exponential increase of the satellite size was captured by with the refined scaling equation with collision factors and fusion probabilities (Panel (a)). The refined scaling also accurately matched the number of satellites produced, with a gradual decrease in the number of satellites after a rapid increase per coverage (Panel (b)). The parameters for the fit are described in table 4.10

.

However, there were some deviations in the low coverage where the size of the satellite was underestimated.

To note, two different k were utilized instead of one, and therefore a further investigation into the collision factor is needed. The k of 1.30 was used for the scaling for N, but this value would result in the scaling for A_s/A_p to lie below the experimental data. This deviation is discussed later, along with the assumption of the equal height between satellites and microplasmodia (Section 5.5: discussion).

$\tilde{l}$ of 2.04 suggested that the NEP impacts the fusion probability up to $C \approx 0.3$ Therefore, the predicted scaling may be lower than what was represented in figure 4.49. No further modification was performed for the fusion probability, as the differences between the fusion probabilities were considered minor. However, the theoretical differences of the predicted fusion probabilities were noted. Larger sets of data may show deviations that require the NEP to alter the scaling.

Experimental verification of parameters

To validate our model of the scaling relationship in satellite growth, parameters were measured experimentally. $\tilde{l}$ can be calculated based on equation 4.21, and the parameters therein can be obtained experimentally. The diffusive properties of the microplasmodia were discussed in section 4.7.6 and the D value obtained was used accordingly (Figure 4.30). The fusion probability was considered in 1-dimension (Equation 4.21) as a function of the distance between two microplasmodia. Since both microplasmodia diffused, the diffusion coefficient was doubled to account for the change in the reference frame.

The parameter t was a part of defining a typical diffusion length of a microplasmod-

ium before fusion. Therefore, to determine it experimentally, one would need to observe a time-series data until the fusion event was observed. However, the fusion event is difficult to monitor by eye, as the precise moment of membrane disintegration and fusion could not be easily recognized. To alleviate this issue, the exponential decay of the object dynamics were utilized (Equation 4.3).

Since the exponential decay model accurately described the number of object dynamics, and these objects are microplasmodia, this can be considered as a reflection of the fusion rate. Using the decay rate, a mean lifetime of microplasmodia was calculated (Table 4.6). This value was used as a t to calculate $\tilde{l}$.

The diffusion coefficient of microplasmodia in satellite growth was 24.1 μm^2/min, and the mean diameter of these microplasmodia was (51.0 $\pm$ 3.1 µm). t was measured from the decay rate of the number of objects (Figure 4.17), which was 40.5 minutes. With these values, $\tilde{l}$ of 1.73 was obtained. This value is close to our estimation (2.04) (Table 4.10).

To estimate the collision factor k, protrusions of satellite growth were manually observed, and the deviation of protrusion numbers and the final number of satellites was noted. Then, k was calculated as:

$$k = \frac{N_{\text{protrusions}}}{N_{\text{observed}}} \tag{4.25}$$

k from the experiment was 1.36, which was consistent with the value obtained from fitting N (1.30) (Table 4.10).

4.10 Summary

The satellite growth of *P. polycephalum* was observed from microplasmodia on a solid agar substrate. In this growth, motile bodies named satellites are formed and radially expanded away from the initial spot of inoculation. Satellite growth is temporally coordinated, and this can be seen both visually (Figure 4.5) and also from measuring the area covered over time (Figure 4.19). This type of growth has not been documented outside of the laboratory of Prof. Dr. Hans-Günther Döbereiner. Therefore, an investigation into how and why this alternative growth occurs was commenced as a part of this doctoral study.

Based on results from the master's thesis by the author, a hypothesis on the satellite growth of *P. polycephalum* was established. In master's thesis, it was revealed that the age of the microplasmodia at the start of the experiment, as well as lack of glucose, were two crucial factors in inducing the satellite growth (Section 4.4). Therefore, it was hypothesized that this satellite growth is a foraging pattern induced by prolonged starvation. Moreover, since this is a foraging pattern, the satellite growth is interpreted in

a similar line of OFT, where the survival chance of the organism is maximized. Since satellites move away from their initial spot, it was assumed that the search area is maximized (Section 4.5).

This hypothesis resulted in two different models describing the satellite growth pattern. First, the distance travelled by satellites (d) was described based on chemotaxis (Section 4.8). The correlation between the d and the patch area (A_p) was noted, and this was described with a saturating function with a threshold. Then, a hypothetical signal molecule was imagined that diffused out of the patch, which effectively 'pushed out' the satellites. This hypothesis is supported by a qualitative observation that the satellites actively avoid a spot inoculated with the old medium, without touching the boundary of the spot (Figure 4.11). This mechanism could also explain why the satellite expands away from the patch radially. A diffusion front was simulated based on Gaussian convolution, and the diffusion coefficient of the hypothetical signal molecule was calculated. Not only the model best described the correlation between d and A_p over other models tested but the diffusion coefficient of the hypothetical signal molecule was also similar to other biological molecules that are used for signalling purposes in other organisms. Therefore, the satellite growth is caused by a signal molecule, and the diffusion of this molecule controls the radial expansion as well as the distance travelled by satellites.

The second model assumed, as in OFT, that the search area is maximized to optimize the possibility of energy gain (Section 4.9). Then, the optimal number of satellite (N) and the size (A_s) are predicted with scaling equations based on the coverage (C), which describes the amount of biomass in a patch. The scaling predicted that the satellite size should increase as coverage increases, and the number of satellites to decrease as the coverage increases. However, while the observed A_s was consistent with the prediction, N did not agree with the scaling. Therefore, the scaling was modified based on empirical observations that deviate from the assumptions used to derive the scaling equations.

First, it was assumed that the satellites may come into contact with each other without fusion, but this was not the case. Therefore, a collision factor k was included in the scaling to accommodate fusion between satellites. Second, it was assumed that all microplasmodia fuse to form satellites without restriction. However, since satellites are formed within a fixed time, there was a possibility that the microplasmodia could not meet and fuse one another.

This possibility was explored by modelling a fusion probability of a microplasmodia based on coverage, assuming that the microplasmodia diffuse freely. The tracking of microplasmodia and calculating the mean squared displacement (MSD) revealed that microplasmodia indeed diffuse freely in a short time scale (Section 4.7.6). Assuming an idealized distribution of microplasmodia, the distance between microplasmodia was calculated based on C. Then, the probability of fusion was calculated, with a scaled length of $\tilde{l}$.

The refined scaling equation accurately predicted the distribution of empirical data (Figure 4.49). Moreover, both k and $\tilde{l}$ could be experimentally calculated, and matched

the values obtained from the fit (Table 4.10). Therefore, satellite growth maximizes the search area. Furthermore, this supports the original hypothesis that satellite growth is a foraging pattern of *P. polycephalum*, a strategy employed in nutrient-depleted conditions.

In summary, we have established a model to describe a general relationship between the initial biomass and the subsequent satellite production, based on the maximization principle. While the model lacks somewhat in precision, it was constructed with simple and generalized assumptions and sufficiently explains the trends in the size and number of satellites produced. The model is based on the hypothesis that satellite growth is a foraging strategy under starvation, and to maximize the search area. The unicellular organism, in a fragmented state, produced a new foraging pattern that has not been documented before. Our report suggests that even a simple organism is capable of complex optimization behaviour, without specialized and dedicated organs for information processing.

Part IV

Discussion

Chapter 5

Discussion

5.1 Evaluation on the main hypothesis

In the main hypothesis (Section 4.5), the satellite growth was considered a foraging strategy induced by the lack of nutrients. This hypothesis was based on previous observation from the Author's Master's thesis, where the lack of glucose, as well as the age of the microplasmodia, were two factors crucial in the satellite formation. In this section, the two factors, the age and the glucose, are evaluated based on the results stated in this work. This, in turn, will be used to discuss the validity of the main hypothesis.

Previously, it was established that the presence of glucose was inhibitory to the satellite formation. This notion is further supported by figure 4.9, where the addition of the nutrient suppressed the satellite growth. However, the growth pattern did not revert back to a network, and a small number of satellites still formed. Moreover, the conditions used to induce satellite growth contained all other nutrients except glucose. When the experiment was performed with an agar without any nutrients, the migratory pattern of the microplasmodia was distinct from the satellite growth (Figure 4.8).

Several experiments were performed with agar plates with varying concentration of glucose concentration, in an attempt to better describe the inhibitory effect. However, these experiments were difficult to evaluate for two main reasons.

1. The overall success of the satellite induction was below 60%. Therefore any negative observation could not be directly attributed to the effect of the glucose.

2. The onset of the secondary satellites, which protrudes and detaches later than usual (See figure 4.13, row (d), red arrow), hindered the accurate description of the satellite pattern.

Therefore, while enough evidence was gathered to support the positive correlation between the lack of glucose and the satellite onset, the nature of the relationship remains elusive. It is not clear whether the glucose, above certain concentrations, completely inhibits the satellite growth and induces network growth, or gradual suppression of migration and formation of fragments occurs as the concentration increases. The author conjectures that it is a gradual suppression, based on the observation such as figure 4.9

that the addition of nutrients after inoculation only suppressed the distance travelled and number of fragmented bodies.

The age of microplasmodia, counted from the inoculation of the fresh liquid culture, was also an important indication on satellite onset. It appeared that there was a sharp transition from network to satellite growth after a certain age when only the probability of the onset is considered (Figure 4.12). However, upon closer inspection, the transition between the network and the satellite growth was more gradual.

First, the formation of satellites may involve a temporary network that is quickly disintegrated (Figure 4.7). The summed image of many satellite growths exhibited a residual network visible, sometimes connecting all the satellites. Therefore, it is possible that satellite growth is based on network architecture, where certain aspects of the *P. polycephalum* growth is accentuated to the extreme to lose the vein and cause disconnection.

Second, the network and satellite growth may coexist. The best example is given in figure 4.13, where the growth outcome was investigated in detail based on the microplasmodial age. The first three rows (a-c) exhibits a possible transition route from a network with extending growth fronts to a satellite. A network is visible until 6 hours in a row (c), even though this network is invisible in 9 hours. Therefore, many evaluations, which focused on the pause state to extract many of the properties of the satellite growth, may have missed the underlying network properties.

Nonetheless, there are many satellite growths, especially originating from older microplasmodia, that does not exhibit any of the network properties (Figure 4.6, Figure 4.13, row (d)). In these examples, there are no indications to suggest that satellite growth is a variation of network growth. Therefore, it is possible that *P. polycephalum* possesses two growth modes, and these two growths may be co-exhibited during the transition.

Therefore, the age of microplasmodia is also a crucial factor in the onset of satellite growth. However, as was the case with glucose, the exact relationship between the age of microplasmodia and the satellite growth is unclear. Moreover, the observations suggest two possible root mechanisms for satellite formation:

- The satellite growth is based on network growth, where certain aspects of the network growth are accentuated. The gradual transition from a network to a satellite growth is expected, and the satellite is a fragmented growth front
- The satellite growth is a distinct growth pattern from network growth, but two growths can co-exist and produce a mixed outcome. In this case, the properties of the network growth gradually disappear during the transition, and the satellite properties eventually dominate, which are distinct from the network.

Since evidence gathered from the dissertation does not refute the notions initially used to construct the hypothesis, the main hypothesis is held valid.

5.2 Cause of the satellite growth

P. polycephalum is known to utilize its slime as an external memory, and shows a strong preference in exploring areas that are not marked by the slime [95]. Since the liquid culture becomes highly viscous due to the slime production, we first suspected the slime itself as an inducer of the alternative growth. Experiments were performed with supernatants from the microplasmodia that produced satellites. However, although this supernatant was capable of influencing the trajectory of satellites that were already formed (Figure 4.11), it did not induce the new growth mode when it was applied to younger microplasmodia. Therefore, the external signal alone was not sufficient to alter the growth mode.

The result from the diffusion analysis suggests that satellite growth, at least in part, is induced by chemotaxis. It is known that cyclic AMP (cAMP) plays a significant role in motility and pattern formation in *Dictyostelium discoideum*, a close relative of *P. polycephalum* [118]. cAMP is a known chemoattractant for *P. polycephalum* [119], and has been implicated in motility of *P. polycephalum* network [120]. How cAMP and other molecules influence the growth pattern of *P. polycephalum*, especially satellite growth, is an interesting topic that should be further investigated.

However, the young microplasmodia could not be induced into satellite growth. Experiments were attempted with microplasmodia younger than day 5, and adding a slime extracted from microplasmodia aged 6, and produced a satellite pattern. Both incubation of microplasmodia with old slime up to 30 minutes, as well as adding them after inoculation have resulted in network growth. Therefore, the cause is likely both the age and the nutrient condition of the surroundings, and both conditions need to be met to induce the satellite.

5.2.1 Age of microplasmodia

The term 'age' was utilized to indicate the time elapsed after microplasmodia has been inoculated into a fresh culture. However, microplasmodia are known to be immortal as long as nutrients are supplied [77]. Therefore, the age here describes the state of the microplasmodia based on starvation rather than the total number of nuclear division. This is evident from experiments from the Master's Thesis, where the change in the incubation temperature of the microplasmodia influenced the age of microplasmodia that produced satellites. Specifically, a lower temperature resulted in a slower rate of growth, and the satellites were produced with older satellites compared to the higher temperature of incubation (Figure 4.4).

It is known that starvation is one of the factors involved in sporulation [29]. However, without appropriate additional signals, *P. polycephalum* transforms into dormant spherules. These inactive particles were often seen in the satellite experiments, as many microplasmodia did not fuse and remained stationary. Given sufficient time, these microplasmodia also resuscitated, these did not for satellites but networks. Therefore, whatever the pathway utilized for the satellite growth appears to reset once the microplasmodia undergoes a spherulation. Sporulation was never observed during the satellite experiments.

Although microplasmodia from the same culture should consist of identical genetic materials, their internal states may differ. This was also noted previously that the oscillation of the microplasmodia from the same fragment was different until they fused [78]. Therefore, the individual differences in microplasmodia may result in some fragments to undergo dormancy quicker than the other. How the individual microplasmodia would behave without the other, and what the behavioural spectrum of individual microplasmodia would be an interesting topic. It is expected that the individual microplasmodium would exhibit amoeboid motility, without the fixed direction of movement and constantly changing morphology, as evident from figure 4.8. How these behaviour change based on the age may hint at a motility and control mechanism of foraging.

5.2.2 Availability of nutrients

The concentration of glucose was measured as a benchmark for the availability of nutrients, as it was used both in the liquid and solid medium as a primary carbon source (Table 4.3, 4.1). However, other nutritional levels were not monitored in detail. In the liquid culture, the fall of the biomass corresponded to the depletion of the glucose, and this was used as the indication that microplasmodia were starving. However, no attempts were made to probe the internal state of the microplasmodia to find any markers that would indicate the level of starvation.

Moreover, the main experiments were performed with agar plates that lacked only glucose but contained the rest of the nutrients. When young microplasmodia were transferred to these plates, extensive network growth was observed, and *P. polycephalum* maintained its vitality for several days. Therefore, it was evident that the slime mould was capable of surviving without glucose. Moreover, all satellites after the pause state eventually proceeded to form a network and remained vital.

Therefore, it is suspected that the microplasmodia look for readily usable nutrient such as glucose first when they are starved. In an extreme starvation scenario such as the ones utilized in the satellite growth, the organism quickly evaluated the environment based only on the presence of the primary carbon source. The re-evaluation of the environment appears to occur during the pause state, which then the satellite state is terminated.

5.3 Detailed supposition of the internal state during the satellite growth

Based on the evidence gathered during the thesis, the internal state and possible mechanisms are hypothesized from the beginning to the end of the satellite growth. The description follows the phases described in figure 4.5.

1. Before the initial state

Microplasmodia are suspended in medium, starved, and the signal molecule is accumulated in the medium. They are approximately 6 days old from the point of inoculation Some microplasmodia have already committed to the spherulation. The total Biomass is significantly reduced, and the average size of microplasmodia is smaller compared to 3 days ago when the peak mass was achieved. At this point, the growth pattern is not committed, as these microplasmodia would for a network if they are placed on an agar plate with glucose.

2. Initial state and pre-protrusion phase

   Microplasmodia are placed on an agar plate without glucose, and the signal molecule is transferred along with microplasmodia. Initially, due to the residual liquid, microplasmodia are suspended and do not make solid contact with an agar. It is also known that the endocytotic activity is reduced as a microplasmodia [69], and therefore the detection of the lack of glucose is delayed. Moreover, it is thought that the actin network is required for microplasmodial motility, and these would only form after approximately 1 hour [71]. Therefore, we suspect the following:

   - Microplasmodia in the first hour after inoculation likely has the same internal state as the ones just before the initial state.
   - Therefore, any influence induced in the first hour will have an impact on the growth pattern, as the information about the environment is not established.

   After one hour, microplasmodia start moving. Microplasmodia that forms non-satellites (i.e. networks) diffuse freely, as seen from figure 4.30 for up to an hour. However, the motility of the microplasmodia in the satellite growth was distinct from the ones that formed networks. Therefore, the motility is already influenced by the environment, and the information about the environment is already detected by the microplasmodia. This information, in turn, determines the outcome of the collective growth. This is the earliest possible point that the commitment to satellite growth could occur. Whether this commitment occurs in microplasmodial level, or at mesoplasmodial level is unclear. If future experiment determines that the commitment occurred before protrusion, then it would suggest that the foraging decision to form satellite likely occurred as microplasmodia.

3. Protrusion state

   Previously, the occurrence of the protrusion was thought to indicate satellite growth. This was proven to be false, as protrusion may still retain properties of the network, as seen in figure 4.13, row (b). Mesoplasmodia are formed and information from individual microplasmodia are likely synchronized. Therefore, the author suspects that based on the level of information, a growth pattern is determined. The growth pattern is not binary as previously indicated, but a combination of properties from network and satellite growth. If information towards the satellite properties is strong, i.e. more microplasmodia commited on the satellite growth than the network growth, then the satellite is produced. If not, a network is formed. Based

on the strength of the information, the growth is modulated. This hypothesis can explain residual vein formation from the satellite growth, the coexistence of the network and satellite growth, as well as the radially migrating growth fronts such as the ones in the figure 4.13, row (a). Moreover, this hypothesis allows two different satellites to posses different property due to the statistical fluctuation.

Future experiments that show that either the commitment of the growth is around the protrusion state, or change the behaviour of the subset of satellites would support this notion.

4. Post-protrusion phase

   It appears that the satellite during the post-protrusion phase do not survey the environment, since the environment is capable of maintaining a network growth, and migration would have reduced the competition as well as the concentration of the signal molecule. Nonetheless, the satellite migrates until the pause state, and the distance is the parameter that was influenced, not the time of migration (Section 4.8). Therefore, it is suspected that the internal state of the satellite is the same as the moment that the satellite growth was committed, with some internal clock.

5. Pause state

   At a pause state, the satellites appear to survey the environment again, as the outcome of growth differs before and after this state. This is supported by the observation of multiple different types of growth pattern after the pause state. It is suspected that the starvation level of the organism remains the same, if not worse. Satellites would have spent energy for motility, although one cannot remove the possibility that the satellite actively gathered nutrients from agar as it propagated. At this stage, the concentration signal is below the threshold level and cannot be detected, and the plasmodial mass is also larger. Therefore, the lack of the signal molecule induces the satellite to transition into a network growth.

5.4 Discussion on diffusion length

In equation 4.9, $\Delta A/K$ determines the position of the saturating curve. By definition from equation 4.8, ΔA cannot be smaller than 0, since A_p cannot be smaller than A_T. The slope of the curve is M when A_p equals A_T, and decreases thereafter as A increases. If $\Delta A/K$ is much larger than 1, the curve is in the asymptotic region. However, in our case, K, A_T and A_p are on the same order of magnitude. Therefore, $\Delta A/K$ remains relatively small and δ still responds well with increasing A_p. This is also evident by the fact that the theoretical maximum distance travelled by a satellite should be equal to M plus b (Table 4.8), which is approximately 6 mm. The fit remains well below 5 mm, showing that the curve is not close to saturation. Therefore, further tests can be done

with a larger A_p in saturating regions to further support our hypothesis.

Distance travelled by satellites was analyzed with respect to their own size as well as their patch of origin. Analysis with the satellite size revealed that the shape of the satellite can be simplified to a circle to describe the minimal displacement for small satellites. Since the distance d is measured from the border of the patch to the centroid of the satellite, the radius of the satellite is, in fact, the minimum distance that a satellite must travel to separate itself from the patch. In small satellites, there are no restrictions on morphology. However, the larger satellites fall below this line, which means that they cannot be circular but are instead oval to achieve a minimal separation to be recognized as a satellite. Therefore, there is a restriction of morphology as the size increases. It would be interesting to investigate whether there is a distinct correlation between the area of satellites and their shape, such as an aspect ratio.

The distance travelled showed saturating increase as the patch area increased. Moreover, in small patches, the distance travelled appeared constant. The model based on diffusion of a signal molecule was able to describe both trends, with a diffusion coefficient that is within the range of other small biological molecules such as single amino acids and monosaccharides. The result therefore strongly suggests the presence of a signal molecule crucial for the satellite growth.

As to the cause of a large variance seen in the dataset (Figure 4.34, panel (b)), we consider the event of satellite formation as a whole to be a series of stochastic events, each compounding the variance of the others. First, the microplasmodia must come together to form mesoplasmodial bodies within the patch. Based on the analysis on mean squared displacement and the step length distribution, microplasmodia perform a random walk on a short time scale (10 min) but may be repulsed by each other (See section 4.7.6). Therefore, the formation of these mesoplasmodia is driven via chance encounters. Then the satellites protrude from the patch border, which could be observed anywhere between 120 to 240 minutes (Figure 4.5). Finally, the detachment time of the satellite from the patch also shows a large variance. Therefore, satellites have different travel time, even if they are originating from the same patch.

The most probable scenario is, that satellite propagation is a combination of internal and external factors. Internal factors likely dictate the phases of the mesoplasmodial growth, such as protrusion and pause state (Figure 4.5), while the external factors, such as a chemotactic molecule diffusing through the agar, determine how far satellites travel. We find that the free fit of the data and the results from numerical solutions are in such a good agreement that it is highly unlikely that they are coincidental, and the diffusion coefficient from this analysis is in line with the diffusion coefficients of small molecules. We hope to substantiate this with experimental verification in the subsequent investigation, as well as to identify the compound responsible for satellite growth.

In this study, the effects of chemotaxis and the threshold phenomenon were used to describe satellite growth. The model was successful in capturing the overall trend of distance travelled by satellites d as a function of the patch area A_p. Several assumptions

were made to construct this model. The concentration of the signal is assumed to be equal throughout the experiments. This was helpful in describing a general trend of satellite displacement. However, patches were resuspended with different volumes of water, and therefore the concentration would not be constant. Also, the velocities of satellites were not investigated in detail. Since all satellites move for about the same time due to their coordination of phases (Figure 4.5), it would mean that the satellites that travel farther have a higher velocity. It would be interesting to see if the satellites demonstrate constant velocity until they stop, or if it is faster when they initially detach from the patch. Higher spatial and temporal resolution is necessary to look at the properties of satellite motility in detail.

5.5 Discussion on scaling

To calculate the fusion probability, the microplasmodia were modelled as a freely diffusing particle. The MSD of the microplasmodia from satellites showed a saturating growth, where the trajectory was linear for 10 minutes (Figure 4.30, panel (a)). This is in contrast to our assumption that the microplasmodia diffuse freely. Moreover, the calculated value of $\tilde{l}$ suggested that describing the process as a narrow escape problem is appropriate (Figure 4.48) However, the estimation of motility from these movements was still consistent with the theoretical fit of the scaling. Therefore, this shows that the underlying mechanism is still driven with a stochastic probability distribution, and it is consistent, or close enough to free diffusion, such that one can provide a general description of the process of satellite formation.

The length scale $\tilde{l}$ calculated using the diffusion coefficient from microplasmodia was in good agreement with the value from the theoretical fit (Table 4.10). This supports the notion that the first fusion is the most important event in satellite formation, and that the stochastic nature of diffusion modulates the number of satellites produced.

Around 30-40 minutes, there appeared to be a disintegration of a membrane and the plasmodium leaking out of the membrane, causing an area of a microplasmodium to increase (Figure 4.26). Leaked biomass made contact with other biomass from microplasmodia and reorganized as mesoplasmodia. These observations are in contrast to our previous findings. *P. polycephalum*, during network formation, diffused and hit other fragments as microplasmodia [75]. However, the satellite growth occurs in shorter time scale than the network, as reflected by the slowest growth of the area, as well as the slowest decay rate of the number of objects (Figure 4.16, Table 4.6).

This process needs to be examined in detail, to determine whether the membrane temporarily disappears or it is a process of cell spreading. Either way, this suggests that the height of microplasmodia is lowered, and this may explain the discrepancies in satellite size, where satellites are lower in height compared to the microplasmodia.

The height of a satellite, measured by a transmission electron microscopy, provided values of 200 to 300 µm [107], which is significantly higher than the microplasmodial

diameter. However, the intensities of satellites in greyscale images were generally weaker than the microplasmodia. It is unclear how and why these inconsistencies arose, but they may prove to be a useful hint in elucidating the biological mechanism behind satellite construction. Moreover, the difference in height between the microplasmodia and satellite may be crucial in converging the collision factor k. If the satellite is lower in height than the microplasmodia, then satellites should be larger than our prediction, as the same volume of biomass would cover a greater area. Moreover, if the height of the satellite is altered after the protrusion and detachment, the scaling for the area of a satellite can be modified without affecting the crowding boundary condition. Therefore, the reorganization of the plasmodial mass from microplasmodia to satellite should be investigated in detail, as well as an accurate measurement of the height of these structures needs to be made.

Tracking was stopped once microplasmodia fused, to ensure that the diffusion coefficient from larger components was not mixed in. Since we focused on the first contact, it was necessary to ensure that only the motility of the single microplasmodium was measured. It is unclear what happens between the first fusion of microplasmodia and the protrusion of satellites from the patch circumference. The microplasmodia may change their movement type after fusion. It is clear that satellites exhibit a directed motion and not a random walk, and therefore it would be interesting to observe when this directionality arises within the mesoplasmodia. Previously, it was suggested that the directionality of satellites is caused by a diffusing signalling molecule [23], and perhaps the mesoplasmodia are required to reach a critical size to recognize a chemical gradient.

Not all microplasmodia in the patch fused and formed satellites, even though they were not dormant and exhibited motility. Several attempts have been made to identify the set of microplasmodia that would eventually form a satellite without success. Further experiments are planned with lower coverages of microplasmodia and higher resolution to elucidate and pinpoint the onset of the satellite development.

In very low coverages, no satellites were formed. Since no single microplasmodia moved on their own out of the patch, there must be a minimum size for a satellite to attain its motility. (However, see figure 4.8 for exceptions) Therefore, in theory, some coverages cannot form satellites, which is not reflected in our model. The lack of data at low coverages may be in part contributed by the stochastic nature of satellite formation after the first fusion event. Lower than predicted N around the C of 0.2 may be the indication of this stochasticity (Figure 4.49, panel (b)). More experimental data is required to show whether satellite formation becomes unstable in low coverages.

The collision event may occur in the patch, around the border of the patch during crowding, and even after satellites are detached. The collisions between satellites would be very difficult to detect if they occurred inside the patch. Currently, two different k were estimated for each model for N and A_s, respectively. This indicates that either A_s or N is overestimated experimentally. It is more likely that our assumption on the same height between all states of *P. polycephalum* is wrong, and our measurement for A_s is off. Empirical measurement of satellite and microplasmodial mass would reveal whether

they have the same area to mass ratio. It is also possible that the satellites grew and increased their biomass in the course of the experiment, although the relatively constant area of the satellite during propagation makes this unlikely.

It is important to note that the number of satellites produced is only dependent on the coverage, while the satellite size depends on the coverage as well as the size of the patch. This means that larger patches must have a larger 'catchment area' for a satellite to gather more biomass compared to the coverage patches with smaller areas have. However, on a microscopic scale, the organism is much more likely to be able to estimate the local density of biomass, rather than the global distribution. We have not measured whether the speed of microplasmodia depends on the patch size, and we do not consider this to be a likely scenario. Some mesoplasmodia have been observed in the centre of the patch that could not move out of the patch from the initial spot. More experiments with larger patch size may help in understanding whether the patch size has an additional effect on satellite production.

Chapter 6

Outlook

P. polycephalum has proven to be a unique and suitable model organism to study and probe various biophysical questions. In particular, the connection between the macroscopic scale behaviour and the microscopic properties that correlates with the macroscopic behaviour has been investigated and documented [25, 85, 121]. In this work, the biophysical investigation continued into the realm of foraging, where the response of a single-celled organism under starvation was analyzed in both anomalous diffusion and maximizing principle (Sections 4.8 and 4.9). It is in the author's opinion that the slime moulds will only continue to prove useful to researchers investigating complex patterns and behaviours by providing a platform of a well-established and relatively simple biological system.

The recent publication of *P. polycephalum*'s genome [60] will no doubt open many avenues of investigations that were not previously accessible. It is not practical to discuss all the possible methods of genome manipulation, pathways that can be probed, as well as genome mining techniques to reveal details of *P. polycephalum*. Instead, the outlook will be limited to the possibilities that stem from the work performed in this thesis, especially the satellite growth which was induced by starvation.

The satellite growth provides a unique opportunity to study, probe and understand a foraging behaviour in a simple model organism. Moreover, the decision-making processes, as well as information processing and integration, can be studied in multiple levels, since the unique properties of *P. polycephalum* allow an agent to be merged and divided at will, without losing their vitality. The proposed investigations and possible outcomes that may result from these outlooks are divided into different categories, but all interconnected in describing and understanding the behaviour of a unicellular organism. The knowledge accumulated from this model organism is not limited to the realm of unicellular organisms, but aid in modelling behaviours of complex organisms.

6.1 Biochemical investigation

The goal of the proposed biochemical investigation is to identify biochemical agents responsible for the alternative foraging pattern in *P. polycephalum*. The slime mould alters

its behaviour based on its age as well as nutritional condition. Therefore, internally, there should be a difference in genetic expression that causes the growth pattern to alter. Moreover, the thesis revealed that there is an external signal molecule responsible for satellites to expand away from the patch (Section 4.8). Identification of these biochemical components furthers our understanding of how the simple organism manipulates itself to best respond to environmental and internal stress. Moreover, the identification of similar systems present in other organisms provides a wider understanding of how living organisms evolved to survive in nature.

6.1.1 Identification of the signal molecule

In the thesis, the signalling pathway and the hypothetical signal molecules were extensively discussed mainly based on its diffusive properties. A clear understanding of these pathways and the chemicals will not only further the knowledge of the slime mould but also in other organisms as well. Although unicellular, *P. polycephalum* exhibited certain characteristics that could be considered 'cognitive' [32,122]. Therefore, it is possible that by understanding how the slime mould behaves, we may take a glimpse at how other animals make complex decisions.

The chemicals involved in initiating the satellite growth from *P. polycephalum* is of great interest, as it plays a crucial role in determining the appropriate survival strategy of the organism. Based on the works in this thesis, it is expected that there are external as well as internal signals associated with alternative growth. Identification of these factors allows one to test the capacity of the emergency-response program enclosed in a unicellular organism. Moreover, the nature of the chemicals themselves may reveal how the response system is controlled.

As revealed most clearly from the diffusion length analysis in section 4.8, a signal molecule influences the distance the satellites travel. Identification and isolation of this molecule can be done by extracting and separating molecules from the spent medium, focused specifically on the liquid media where microplasmodia produced satellites. Since one expects the signal molecule to be secreted, and produced as a response to starvation, it would not be present in the fresh medium, but abundant when microplasmodia form satellites. Liquid chromatography with various detection methods, such as UV detector or mass-spectrometry, can be used to create profiles of peaks, each peaks representing similar class molecules (For example, see [123]). This allows quick screening to identify which peaks appear as the age of the culture advances.

Then, the spent media can be divided into aliquots, based on their retention time corresponding to the peaks in the liquid chromatography result. Each aliquot can then be tested on other satellite experiments, to see whether the repulsion between the aliquot and the satellite is observed. This type of test is commonly referred to as an activity-based screening, where the desired effect, repulsion between the chemical and the organism, is monitored and selected while others are discarded. Once the repulsion is confirmed, then the identification of the active ingredient from the target aliquot may begin. The target aliquot can be further divided into sub-aliquots via liquid chromatography. This helps

to identify whether there are more than one compounds in the target aliquot that were not separated from the first chromatography, and also remove other impurities. Once the pure solution of the molecule that shows a repulsive effect to a satellite is obtained, then the structure of the molecule can be solved via mass-spectrometry and/or nuclear magnetic resonance.

Identification of the signal molecule opens a new avenue of bioinformatics research. The structure of the molecule can be cross-checked with other known molecules and identify homology. Then, the known functions, as well as the mechanism of function of these other similar molecules can be used to infer how the signal molecule of *P. polycephalum* functions. The homology search, which finds DNA and/or protein sequences that are similar to the query sequence, may also reveal whether the signal molecule belongs in a class of known signalling molecules. If the signal molecule is a homologue to a known signal molecule, then the mechanism of function, as well as receptor type for the signal molecule, would be identified. Then these receptor proteins can be identified via genome mining from the genome of *P. polycephalum*, and marked as a key component in the satellite growth as well as foraging behaviour. Moreover, the signalling cascade of the homologous system from other organisms would help in understanding and identifying how the signal molecule controls foraging behaviour. Furthermore, identification of interacting partners and other proteins within the regulatory network gives additional targets to influence the growth mode of *P. polycephalum*.

There are extensive studies on signal molecules on the cellular slime mould, *D. discoideum* [118, 124]. In particular, the cyclic AMP (cAMP) is a known chemoattractant to the cellular slime mould and can be used to create various spiral patterns [125]. The receptors and the pathways the receptor triggers are well-established, along with regulatory elements for gene expression of response. cAMP was considered a possible candidate as the hypothetical signal molecule, but the preliminary experiments failed to elicit a response from *P. polycephalum*. Clear identification of the signal molecule will help identification of analogues and possible receptors. Then, these candidates can be used to compare with the studies in *D. discoideum* to see the similarities, and to identify key points of subsequent experiments. Moreover, the search for the similarities should not be limited to the slime moulds, but the higher animals. It is possible that the pathways for responding to starvation-related stress is highly conserved, and therefore remain in other species that are not genetically similar to the slime mould. This would then strengthen the argument that the slime mould is a strong and appropriate model organism to study basal cognitive capacities at a cellular level.

6.1.2 Identification of internal signalling pathway into the satellite growth

There were almost always left-over microplasmodia that did not fuse to become a satellite but remain in the patch. However, there were no visible differences between the microplasmodia that formed a satellite from the ones that do not. It is assumed that the internal signalling pathway, as well as the gene expression, would show the difference and therefore can be used as a marker to indicate whether a microplasmodium would

form a satellite. Since the construction of mesoplasmodia finishes, at the latest, at the protrusion state, the gene expression profile of the protrusion is compared with a gene expression profile of another plasmodium, but one destined to a network. A similar type of decision-making occurs in a slime mould during sporulation. When a slime mould receives appropriate signals, the organism commits to sporulation by activating pathways that are designated for differentiation and sexual reproduction. These pathways, as well as the temporal commitment to this development, has been extensively and elegantly investigated by Prof. Wolfgang Marwan [27].

To compare the internal differences between the microplasmodia, a large number of samples are required to correctly identify the markers of the satellite growth. These markers may be a rise in a particular protein concentration, and/or increased expression of a gene. In either case, an expression profile is established from a large number of samples to characterize the typical distribution and concentration of genes and gene products (For example, see [126]). It is expected that these expression profiles will differ between microplasmodial state, network growth, and satellite propagation. Therefore, at some point, the change is made so that the expression commits to the satellite from a microplasmodial state.

To capture when the commitment is made, as well as to identify what molecules are responsible for this commitment, the expression profiles are compared between two groups. It is hypothesized that there would be specific gene products designated for the satellite propagation, which will be expressed in significantly higher quantities during the satellite growth compared to the network growth. Therefore, this key molecule is identified by comparing the gene expression profile between the satellite and network growth. This can be done by reverse transcriptase polymerase chain reaction (rt-PCR), which detects the messenger RNAs (mRNAs) in the cell. One can read off these mRNAs to identify the gene product, and quantify how much mRNA is present in the cell, indicating the expression level of the target gene product (For example, see [127]).

Then, the expression profile of the microplasmodia is examined in higher temporal resolution, to pinpoint when the key molecule for the satellite growth begins to increase, marking the commitment to the satellite growth over the network growth. The function of the gene product can also be speculated based on the DNA sequence and known homologues via bioinformatic techniques. Furthermore, possible signalling pathways that are involved with the key molecule may be revealed. One can obtain these gene products via overexpression in bacterial hosts with plasmids containing the desired gene products. Then, these proteins can be re-introduced into the slime mould to see whether the behaviour can be altered. While it is difficult to introduce exogenous agents into the slime mould due to the slime layer, it is nonetheless possible with microinjection techniques [107].

Identification of these external and internal factors controlling the foraging behaviours of the slime mould during starvation advances our understanding on basic decision-making processes, and capabilities of a unicellular organism to store sufficient strategies to best adapt and survive during uncertainty. Moreover, the type of network constructed

based on interacting components of the external and internal signals and how each connection is regulated provides further avenues to investigate and compare the decision-making mechanism of a unicellular organism to the complex organisms.

6.2 Biological investigation

The goal of the biological investigation is to generate a quantitative description of the foraging pattern of *P. polycephalum*. The slime mould exhibited alternative growth patterns based on environmental conditions. It is reasoned, based on optimal foraging theory, that these patterns are not random but effective solutions to maximize the chance of survival and propagation of progenies. To determine why these patterns are utilized under different conditions, one must understand what is different between the two growths. Moreover, since these patterns originate from seemingly identical fragments called microplasmodia, the behaviour of these small fragments are also of great interest.

By understanding the subtle differences of behaviours, one can gain deeper insights into the capacities of a single cell organism to adapt and survive. The different strategies exhibited by the slime mould can also be compared to other animals that possess distinct modes of foraging in different environmental conditions. Moreover, the slime mould's unique ability to fuse and merge while maintaining its unicellular gives a different perspective on collective behaviour, which may serve as the model organism to study such effects.

6.2.1 Distinction between a satellite and network growth

It was discussed previously [98] that since the fragmentation increases the number of organisms, it is advantageous for survival in adverse conditions. It was also considered during the main hypothesis since the organism has been starved for an extended period, the fragmentation not only increases the search area efficiency but also a survival probability if the nutrient found during the search is not sufficient to maintain the entire body of the plasmodium.

It remains to be determined whether the satellite and the network growth are the two extreme ends of a survival strategy, or two distinct strategies, possibly involving different internal mechanisms. The growth pattern between the network and the satellite growth requires detailed investigation, to see how the growth transition from one mode to the other. As described in the proposed biochemical investigation, the author speculates the difference in the gene expression determines the outcome of the growth between the satellite and the network growth. During sexual reproduction, the slime mould *P. polycephalum* also undergoes drastic morphological changes, forming hyphae and spores. While in both cases, the survival strategies are based on environmental and internal signals, the outcome is different. The commitment to sexual reproduction does not have an intermediate phenotype between the network and the spores, while the satellite growth shows a gradual transition of phenotypes (Figure 4.13).

This suggests that at least one of the signals that the slime mould incorporates into determining the survival strategies is not an on-off switch, but rather a fine-tuning knob that modulates the characteristics of its morphologies. Based on the evidence in the thesis, this signal is based on the relative age of the microplasmodia used in the experiments. However, the 'age' of microplasmodia and its effect on the growth morphologies were also influenced by the growth conditions of the microplasmodia. Therefore, understanding how *P. polycephalum* perceives the surrounding environment, as well as what type of information the slime mould considers important, will help us, in turn, to understand how these survival strategies are formed.

One of the difficulties in performing the satellite experiments was that the same batch of the microplasmodia could not be re-used. Under the experimental protocols described (Section 4.2), the act of extracting microplasmodia from a liquid culture irreversibly disrupted their growth, altering the outcome of the subsequent experiments performed with the same batch. Therefore, to accurately understand and observe how the growth of microplasmodia is affected by age in finer temporal resolution, duplicate liquid cultures must be prepared, each dedicated for a specific time point of data. This could not be performed during the author's thesis due to the lack of cultivation and observation equipment suited for large-scale experiments. The recent acquisition of the larger shaking cultivation unit, as well as low-cost DYI observation unit developed in the lab, would make the proposed experiment possible.

Two characteristics of interest during the growth from the microplasmodia are abandonment and loss of network characters. The abandonment is the phenomenon where the formation of larger structures causes the initial inoculation spot to be vacated (Figure 4.13). As the age progresses, even the network growth tended to quickly move away from the initial location. The concept of the motility in *P. polycephalum* network was previously discussed with the network structure formation [128]. However, during the satellite transition, this appears to be either accelerated, or the formation of the structure itself is fundamentally altered.

The loss of network characters refers to the residual vein-like structures sometimes evident during the satellite growth (Figure 4.7). Some satellites retained the network-like structures posterior to the direction of travel. The internal veins observed in the satellite were probed via electron microscopy, but no solid structural basis could be found within the satellite [107]. However, other satellites, especially in smaller ones, these structures are less visible and the morphology almost resembles that of a fish keratocyte (For example, see [129]).

The large-scale observation with various ages of the microplasmodia will help to identify when these characteristics appear and disappear. Moreover, larger dataset helps to remove statistical variations inherent in biological systems. These, in turn, will help us to better distinguish and define what the satellite growth is and when it occurs over the network growth. Abandonment likely occurs due to the lack of nutrients, or accumulation of negative stimulus. Therefore, an accurate description of the abandonment describes the *P. polycephalum*'s behavioural tendency under stress. It is unclear whether and how

the network characteristics are involved in responding to stress. However, there has been a thorough description of different network morphologies under different conditions [109]. In this study, the slime mould reduced the contact area between its body and the agar surface when they were placed on unfavourable conditions. Therefore, careful observations on when and how the network characteristics disappear may reveal other details of the behaviour of the slime mould.

Based on these outcomes, a detailed chart can be constructed, describing when the network properties decline and disappear and when the satellite characteristics emerge. Based on this timing, one can also elucidate at what point the satellite growth becomes beneficial over the network growth. This may be related to the internal energy storage of the microplasmodia, or strength of the signal molecule described in the section 6.1.1. The foraging strategy of the *P. polycephalum* under starvation then can be better described based on this transition.

6.2.2 Influence of other nutrients on the satellite motility and morphology

The stable morphology of the satellites was not maintained when the same microplasmodia were inoculated on a water-only agar (Figure 4.8). The growth pattern of *P. polycephalum* on this condition is also of great interest, as the motility and the fragmentation properties of the satellite growth are kept, but the stable morphology and the direction are lost. It would be interesting to investigate how the lack of other nutrients influence the construction of the initial mesoplasmodia, as well as how much of the satellite characteristics are maintained under a harsher condition.

The experimental protocol described in this thesis only deprived the slime mould of the carbon source. Therefore, how *P. polycephalum* reacts to the lack of other nutrients, such as proteins and other minerals required for growth needs to be tested. To investigate this, different compositions of agar plates can be prepared, each lacking specific nutrients. The experiments would compare the growth of microplasmodia from different growth conditions to the satellite growth observed based on the growth condition described in this thesis. It is hypothesized that the glucose is the main factor in causing the satellite formation, therefore the lack of protein source or other micronutrients would not cause the satellite formation, as long as glucose is present in sufficient quantities. In these cases, different morphologies of network growth are expected.

When other nutrients are absent along with glucose, the changes in the satellite growth itself is expected. The author suspects that the protein plays a role in maintaining the stable morphology and direction of the satellite during propagation, as it is required to form new proteins to sustain its motility. It is also possible that other minerals present in smaller quantities impact the motility. If this is the case, the impact of the mineral can be further investigated, and other instances where the direction of cell motility is impacted by such minerals may be referenced. Also, in an evolutionary sense, this may reveal what type of environment the *P. polycephalum* was subjected to, and how the organism developed effective foraging strategies using limited sensory capacities.

It remains to be seen whether the stable morphology is the hallmark of the satellite growth, or only the fragmentation and the radial abandonment of the initial position is crucial in the alternative foraging strategies. Larger sets of examples are required to determine what are the characteristic foraging patterns of *P. polycephalum* in these different nutritional compositions. Analysis on these patterns will lead to understanding how a single cell organism alters its behaviour to based on the ever-changing environment.

6.2.3 Behavioural description of microplasmodia

The satellite growth starts from smaller components fusing to create a larger component, and therefore the collective movement, as well as the behaviour of microplasmodia, is also of great interest. The behaviour of microplasmodia before the satellite growth appears to be completely different, as individual microplasmodium does not have a stable morphology nor direction of movement. The environment an individual microplasmodium senses must also be different from the ones sensed by larger mesoplasmodia. Moreover, based on the behaviour of microplasmodia, the growth of *P. polycephalum* is determined between network and satellite. In this thesis, microplasmodial movement was described based on the step length and the turn angle (Section 4.7.6), but much higher spatial resolution and larger sets of data are required to better describe how the microplasmodia behave.

Three key aspects of microplasmodial behaviour are:

1. Is there a behavioural difference between a single isolated microplasmodium and a microplasmodium with other neighbours?

2. What is the behavioural difference between microplasmodia that forms networks and microplasmodia that forms satellites?

3. How does the size of a plasmodium affect the behaviour?

The answer to the first question is currently unclear, although the author suspects that it strongly depends on the perception length of the microplasmodia. As evident from the figure 4.32, the motility of microplasmodia are influenced when they are near one another. However, it is unknown what other aspects of microplasmodia behaviour are influenced when microplasmodium are grouped near each other. To make matters more complicated, microplasmodia in contact with another microplasmodium may or may not fuse.

Nonetheless, both the satellite and the network growth begins from microplasmodial state. Therefore, there must be a noticeable difference in microplasmodial behaviour between the two growths. The microplasmodia in the satellite growth are shown to diffuse at a higher rate (Figure 4.30), but this does not fully explain why the microplasmodia form multiple bodies instead of one. Moreover, the mesoplasmodia from the network growth almost always resembled veins and nodes, while the satellite mesoplasmodia were

more globular and spread out.

To describe these differences, higher temporal and spatial observations of microplasmodia are required, as well as better image processing and analysis techniques. First, a baseline behaviour of microplasmodia is established by observing the microplasmodia in isolation up to 5 hours after inoculation, to compare with microplasmodia in the satellite growth before the migration phase. Various characteristics should be noted and measured quantitatively, including and not limited to: size, frequency of oscillation, the amplitude of fluctuation from oscillation, motility, etc. How these characteristics are influenced by different factors, such as the age of microplasmodia, as well as the presence and/or absence of nutrients, should be charted and explored in detail.

Then, the microplasmodia from the same culture are used to observe how they behaviours collectively. Same characteristics are observed to determine whether there is a significant difference in behaviour between an isolated and a group of microplasmodia. This will then identify characteristics that are altered based on the interaction between the microplasmodia.

To answer the second question, one needs to compare single and collective movement of microplasmodia between the satellite and network growth. The difference may arise at an individual level, in which case the characteristics noted above will be cleary different between a network-bound microplasmodium and a satellite-bound microplasmodium. However, if there are no significant differences at an individual behaviour, then the difference must arise at a collective level. This leads to the investigation of collective behaviours, with additional parameters such as coverage and area covered by the microplasmodia. Based on the characteristics identified from comparing the isolated and collective microplasmodia, detailed description is given to collective behaviour such as the synchronicity of the oscillation, direction of movement, and fusion probability. These characteristics of the collective behaviour are compared between the network and satellite growth, to determine how the two growths could appear from seemingly the same initial conditions.

To tackle the third question, a different type of description, as well as advanced image processing is required to handle complex shapes and sizes. Microplasmodia are relatively small and generally round and therefore their boundaries are clear and movement easily tracked. However, mesoplasmodia have irregular shape and many pseudopods, and the boundary between these and the agar may be difficult to identify, especially with slime layers present. Various contrast-enhancing techniques, as well as methods to improve the acquired image quality, should be utilized, including a stronger illumination. The slime mould is known to avoid light and alter its behaviour, therefore care should be taken to ensure that the stronger illumination does not affect the satellite and network growth.

Then, the mesoplasmodial fragments from the first two experiments are observed in detail, noting additional characteristics such as the size and shape parameters. It is expected that the mesoplasmodia in network growth shows irregular shape and sizes, with no preferential direction of travel, while the mesoplasmodia in the satellite growth shows

the globular shape and similar direction of travel.

Based on these three observations, one can describe the behaviour of the *P. polycephalum* from microscopic to the macroscopic level, as well as the individual and collective behaviour connecting different phases of the growth. This will help researchers understand which parameters of behaviour is important in different growths, and how one characteristic in microscopic behaviour may impact the outcome and behaviour of the mesoplasmodia. Moreover, the connection of behaviours between micro- to macroscale provides a unique opportunity to design and model other agent-based and swarm intelligence models where a large number of participants or agents are present.

6.3 Biophysical investigation

The goal of the biophysical investigation is to generate a model to explain the behaviour of *P. polycephalum*. The slime mould is a simple single-celled organism without neurons to process information, and it does not possess dedicated sensory units to perceive information. Nonetheless, the organism was capable of possessing alternative growth patterns in response to stress. Therefore, it was reasoned that the organism utilizes physical laws to alter its growth patterns. Then, its patterns and movements can be modelled with relatively simple physical laws. The satellite growth experiment can be simplified, and a set of rules introduced to mimic the movement of the microplasmodia. By adjusting the parameters of the rules of movement, one can better understand why from the same set of fragments, two different growth patterns can emerge. Based on the importance of parameters, one gains a deeper understanding of how a biological system is programmed to store different repertoire of patterns.

6.3.1 Simulating a microplasmodial distribution in a patch

An accurate description of the behaviour helps to build a model of the organism to predict different outcomes. These models help to obtain desired results by identifying key elements of the experimental design. Many of the results from the biochemical and biological investigations can be used as a parameter to model the growth of *P. polycephalum* from microplasmodia to satellites. Microscopically, the fusion process between microplasmodia to create mesoplasmodia is of great interest, as this process directly influences whether the growth becomes satellite or network. The diffusion process of microplasmodia are not completely free during the satellite growth (Figure 4.30), and therefore it is assumed that there is an interaction between the microplasmodia that slows the diffusion down. However, microplasmodia in a network growth diffuse at a relatively constant rate.

To determine how this interaction influences microplasmodial behaviour, one can simulate the initial growth process. In an experiment, microplasmodia with the varying size is placed on agar as a droplet. Then, these microplasmodia land randomly in a circular patch where droplet was placed. In a simulation, the microplasmodia can be approximated as a circle with varying radii. The random landing of microplasmodia can be mimicked either by picking random spots and drawing circles with appropriate radii,

or a sequential adsorption method [116]. The latter method avoids overlap between the microplasmodia, making a field with only perfect circles, while the first method results in various irregular shapes caused by an overlap.

In an experiment, the size of microplasmodia changes based on the age of the culture. Preliminary observations showed that the microplasmodia were the largest when they were aged between 3 to 4 days, then the size decreased until they became dormant. The simulation can implement different sized circles to represent microplasmodia with varying age. Moreover, the density, or the area covered by the microplasmodia, is controlled by the number of circles drawn in a field.

Preliminary results showed that even with these simple processes or randomly placing circles in a field, one can create images of the patch of microplasmodia at the initial condition that appear very similar to the experimental image. The simulated image can be adjusted to match properties to different experimental images at initial conditions, including the coverage, the average size and the size distribution of microplasmodia, and the distance distribution between the nearest objects. These techniques allow many different initial conditions to be explored, including some that are difficult to produce in an actual experiment.

6.3.2 Modelling the microplasmodial diffusion

Simulating patch images at initial conditions will allow investigators to probe various scenarios of microplasmodial growth without needing extensive experimental dataset. Moreover, the simulation of microplasmodial movement will reveal what properties are involved in the movement of *P. polycephalum*, and how many mechanisms are needed to accurately describe the microplasmodial movement. To this end, the experimental data is used to first analyze the properties of these movements. Some of the analysis techniques are already introduced and used to generate statistics on the movement, including the diffusion coefficient, step length and turn angle (See section 4.7.6). Proposed investigations in section 6.2.3 will also provide insight on how the microplasmodia behaves.

The simulated image from the proposed investigation above is used as a starting point for the diffusion simulation. Each object is considered as an individual agent that moves after each time step. The simulation then uses the next image as a basis for the next time step, each time step representing one experimental observation. Then, these simulated time-series images are compared with experimental data, both visually and quantitatively, to determine whether the microplasmodia behaviour was successfully mimicked.

There are several notable characteristics that need to be reflected in the simulation. First, in an experiment, only a proportion of the microplasmodia in a patch showed active movement. This activity also appeared to be dependent on the age of the microplasmodia, with younger microplasmodia exhibiting a higher proportion of activity. Moreover, some inactive microplasmodia may have a delay after inoculation, and only begin to move after some time. These can be accounted for by assigning an active and inactive agent, and delayed agent who can move after a certain time. The proportion of

activity can also be controlled, to match the experimental data in question.

Second, when microplasmodia collide with one another, two microplasmodia may fuse and become one larger mesoplasmodium, or it may not fuse and remain as two microplasmodia. Currently, it is unclear what dictates whether the fusion occurs or not between the two microplasmodia. In younger microplasmodia that commits to network growth, the fusion readily occurred and percolation occurred fully to one largest component [75]. However, this was generally not the case in older microplasmodia and this was evident in most satellite growths where some microplasmodia were left behind the patch. It was first thought that they were inactive due to the lack of nutrients, but closer observations showed that they exhibited the same motility as the fusing microplasmodia that formed satellites. *P. polycephalum* has different fusion types, and only the plasmodia with the same fusion types can fuse [80]. However, the microplasmodial culture is prepared from a fragment from a single plasmodium, therefore it was considered that all microplasmodia shared the same fusion type and capable of fusing.

Also, the fusion event was difficult to measure from experimental data, as the segmentation technique was not accurate enough to distinguish between two microplasmodia in contact and fused microplasmodia. Therefore, the simulation can probe multiple rates of fusion to determine which probabilities result in the most similar outcome to the experimental observation. The fusion probability can be incorporated into the simulation, by assigning a probability to either merge or not when two agents collide.

As shown in the thesis, the network growth and the satellite growth not only differed in the diffusion coefficient but also the trajectory of the mean squared displacement (MSD) (Figure 4.30). The trajectories of the microplasmodia during the satellite growth showed a saturating increase, and its asymptote appeared to be the mean distance between the microplasmodia at initial condition (Figure 4.32). This strongly suggests that there is a long-range interaction between the microplasmodia, at least in the satellite growth. This repulsive effect can be added to the simulation by monitoring the distance between the nearest microplasmodia. Once the nearest distance between the two agents crosses the threshold, the probability of turning away from each other is increased. This threshold length, as well as the probability shift, determines how strong the repulsive effect will be during the simulation.

Once the fusion probability, the activity of microplasmodia and the long-range interaction length and strength are assigned, then the microplasmodial movement can be simulated. The diffusion coefficient, determined experimentally, should be scaled appropriately and be incorporated into the simulation to establish a reasonable speed of movement. For a random diffusion, after each time step, an agent is moved to a random direction with an appropriate step length. Other parameters can be used to further refine this diffusion movement, including the step length distribution and the turn angle of microplasmodia. Then, the simulated time-series are compared to the experimental data. One of the characteristics that can be compared is the rate of decay or the mean lifetime of microplasmodia (τ)(equation 4.3). An accurate simulation should mimic the population dynamics of the microplasmodia in both network and satellite growth. The

size distribution of mesoplasmodia can also be compared between the simulation and the experimental data.

These three parameters, fusion probability, the motile activity and the long-range interaction, is adjusted to determine their respective effects alone. This, in turn, will determine which effects drive different foraging pattern to emerge, and how the experimental setup should be adjusted to test this theory. The author suspects that only diffusion speed plays a crucial role in the foraging decision. The repulsion effect may be attributed to the slime layer around the microplasmodia and is therefore expected to be present in network growth, given enough experimental data. The fusion probability may play a role in influencing the growth pattern, but it likely has a stronger influence in the foraging efficiency rather than the foraging pattern. The lower probability of fusion between microplasmodia likely contributes to the overestimation of the coverage, as these fragments are counted as active biomass at initial conditions, but not transferred to the satellite bodies.

If the simulation is successful in reproducing the statistics of growth from the experimental data, then it strongly suggests that the complex pattern formation and decision-making of the *P. polycephalum* do not require complex mechanisms. The simulation does not dictate how the organism should move as a whole, but only controls the behaviour of individual agents. Therefore, this connects to collective behaviour and collective intelligence, where higher capacities are exhibited from a group which are not present in individuals who compose of the group [130]. The model also opens a new avenue of study in pattern formation, and how small differences at initial conditions result in different patterns, in a biological platform.

6.3.3 Modelling the radial expansion

The satellite, by definition, is larger than the microplasmodia. In the satellite growth, only the satellites moved at a coordinated manner, while unfused microplasmodia, although oscillating and motile, remained in the patch. Therefore, it was suspected that there is a minimal length required for a cell to determine a chemical gradient. The chemical that causes this migration is the suspected signal molecule that diffuses through the agar plate, which has been already simulated (Figure 4.37). If only a larger mesoplasmodium can react to the signal molecule, this may result in different behavioural patterns between the microplasmodia and mesoplasmodia.

Smaller motile fragments have been observed in water only agar (Figure 4.8). These were smaller than the average satellites, did not maintain stable direction and its shape constantly changed as it crawled agar. These smaller motile fragments were also seen during the satellite growth, although these were rare and did not travel as far as the satellites. Therefore, it was suspected that the stable morphology, as well as a certain size threshold, helps *P. polycephalum* to move as a satellite.

Moreover, all the satellite experiments followed a defined temporal progression (Figure 4.5) This suggested that not only the microplasmodia need to fuse and form mesoplas-

modia along the border of the patch before the protrusion state, but some mesoplasmodia may wait along the border until rest of the satellites are formed. It was suggested in the thesis that there is an internal timer that sets off the satellites to detached and propagates, but it is unclear whether this mechanism is also coupled to the gradient sensing mechanism.

To test whether a similar phenomenon can be replicated, the microplasmodial diffusion simulation described above is further adjusted. Mainly, the simulation introduces a repulsion force from the centre of the field. This repulsion is only felt by the mesoplasmodia above a certain size. When microplasmodia fuse and grow above this threshold size, the probability of direction is skewed away from the centre of the field, causing them to crowd along the borders. The repulsion effect between the agents remains, preventing rapid aggregation and fusion of mesoplasmodia at the borders. At the end of the simulation, the number and the average size of mesoplasmodia, as well as the time it took for fragments to travel to the border is noted. These values are then compared with the experimental results from the scaling studies based on the initial coverage of the microplasmodia (Figure 4.49)

The successful simulation of this process provides insight into the interaction between the mesoplasmodia and external field. Also, correct implementation of the simulation can help establish the minimum coverage required to produce the satellite growth, as well as the minimum satellite size that reacts to the external field. Moreover, the simulation can be used to generate outcomes that are neither network nor satellite, but something unique. Then, based on the differences in the parameter, one can speculate how such a growth strategy might be useful, and attempt to replicate with the slime mould. Altogether, the successful outcome of the simulation will be useful in assessing how the *P. polycephalum* controls the foraging strategy. Also, the decision of a unicellular organism can be compared to that of a complex organism based on the parameters of the simulation.

Bibliography

[1] Charles Darwin. *On the Origin of Species*. John Murray, London, November 1859.

[2] Joseph Grinnell. The Niche-Relationships of the California Thrasher. *The Auk*, 34(4):427–433, October 1917.

[3] Jeremy M Wolfe. When is it time to move to the next raspberry bush? Foraging rules in human visual search. *Journal of Vision*, 13(3):10–10, January 2013.

[4] Eric L Charnov. Optimal foraging, the marginal value theorem. *Theoretical Population Biology*, 9(2):129–136, April 1976.

[5] Yuuki Y Watanabe, Motohiro Ito, and Akinori Takahashi. Testing optimal foraging theory in a penguin-krill system. *Proceedings of the Royal Society B: Biological Sciences*, 281(1779):20132376, January 2014.

[6] Peter Nonacs. State dependent behavior and the Marginal Value Theorem. *Behavioral Ecology*, 12(1):71–83, January 2001.

[7] Sophie Bertrand, Arnaud Bertrand, Renato Guevara-Carrasco, and François Gerlotto. Scale-Invariant movements of fishermen: The same foraging strategy as natural predators. *Ecological Applications*, 17(2):331–337, March 2007.

[8] Gandhimohan M Viswanathan, Sergey V Buldyrev, Shlomo Havlin, M G E da Luz, E P Raposo, and H Eugene Stanley. Optimizing the success of random searches. *Nature*, 401(6756):911–914, October 1999.

[9] David A Raichlen, Brian M Wood, Adam D Gordon, Audax Z P Mabulla, Frank W Marlowe, and Herman Pontzer. Evidence of Lévy walk foraging patterns in human hunter-gatherers. *Proceedings of the National Academy of Sciences of the United States of America*, 111(2):728–733, January 2014.

[10] Marina E Wosniack, Marcos C Santos, Ernesto P Raposo, Gandhimohan M Viswanathan, and Marcos G E da Luz. The evolutionary origins of Lévy walk foraging. *PLOS Computational Biology*, 13(10):e1005774, October 2017.

[11] Ya-Ping Tang, Eiji Shimizu, Gilles R. Dube, Claire Rampon, Geoffrey A Kerchner, Min Zhuo, Guosong Liu, and Joe Z. Tsien. Genetic enhancement of learning and memory in mice. *Nature*, 401(6748):63–69, September 1999.

[12] Natalia Caporale and Yang Dan. Spike Timing–Dependent Plasticity: A Hebbian Learning Rule. *Annual Review of Neuroscience*, 31(1):25–46, July 2008.

[13] Xing Fu, Patrick Giavalisco, Xiling Liu, Gareth Catchpole, Ning Fu, Zhi-Bin Ning, Song Guo, Zheng Yan, Mehmet Somel, Svante Pääbo, Rong Zeng, Lothar Willmitzer, and Philipp Khaitovich. Rapid metabolic evolution in human prefrontal cortex. *Proceedings of the National Academy of Sciences of the United States of America*, 108(15):6181–6, April 2011.

[14] Arthur Prindle, Jintao Liu, Munehiro Asally, San Ly, Jordi Garcia-Ojalvo, and Gürol M. Süel. Ion channels enable electrical communication in bacterial communities. *Nature*, 527(7576):59–63, November 2015.

[15] Brian J Ford. Cellular intelligence: Microphenomenology and the realities of being. *Progress in Biophysics and Molecular Biology*, 131:273–287, December 2017.

[16] Toshiyuki Nakagaki, Hiroyasu Yamada, and Agota Toth. Maze-solving by an amoeboid organism. *Nature*, 407(6803):470, 2000.

[17] Anthony Trewavas. The foundations of plant intelligence. *Interface Focus*, 7(3):20160098, June 2017.

[18] Michael Crossley, Kevin Staras, and György Kemenes. A two-neuron system for adaptive goal-directed decision-making in Lymnaea. *Nature Communications*, 7(1), September 2016.

[19] František Baluška and Arthur Reber. Sentience and Consciousness in Single Cells: How the First Minds Emerged in Unicellular Species. *BioEssays*, 41(3):1800229, March 2019.

[20] Tanya Latty and Madeleine Beekman. Speed-accuracy trade-offs during foraging decisions in the acellular slime mould Physarum polycephalum. *Proceedings of the Royal Society B: Biological Sciences*, 278(1705):539–545, February 2011.

[21] Richard P Heitz. The speed-accuracy tradeoff: history, physiology, methodology, and behavior. *Frontiers in Neuroscience*, 8, June 2014.

[22] Tanya Latty and Madeleine Beekman. Irrational decision-making in an amoeboid organism: transitivity and context-dependent preferences. *Proceedings of the Royal Society B: Biological Sciences*, 278(1703):307–312, January 2011.

[23] Jonghyun Lee, Christina Oettmeier, and Hans-Günther Döbereiner. A novel growth mode of *Physarum polycephalum* during starvation. *Journal of Physics D: Applied Physics*, 51(24):244002, June 2018.

[24] Paul Williams, Klaus Winzer, Weng C Chan, and Miguel Cámara. Look who's talking: communication and quorum sensing in the bacterial world. *Philosophical transactions of the Royal Society of London. Series B, Biological sciences*, 362(1483):1119–1134, July 2007.

[25] Christina Oettmeier, Klaudia Brix, and Hans-Günther Döbereiner. Physarum polycephalum —a new take on a classic model system. *Journal of Physics D: Applied Physics*, 50(41):413001, October 2017.

[26] Cornelis J Weijer. Dictyostelium morphogenesis. *Current Opinion in Genetics and Development*, 14(4):392–398, 2004.

[27] Wolfgang Marwan and Christine Starostzik. The sequence of regulatory events in the sporulation control network of Physarum polycephalum analysed by time-resolved somatic complementation of mutants. *Protist*, 153(4):391–400, December 2002.

[28] Tanya Latty and Madeleine Beekman. Food quality affects search strategy in the acellular slime mould, Physarum polycephalum. *Behavioral Ecology*, 20(6):1160–1167, August 2009.

[29] Wolfgang Marwan, Arumugam Sujatha, and Christine Starostzik. Reconstructing the regulatory network controlling commitment and sporulation in Physarum polycephalum based on hierarchical Petri Net modelling and simulation. *Journal of theoretical biology*, 236(4):349–65, October 2005.

[30] Tanya Latty and Madeleine Beekman. Slime moulds use heuristics based on within-patch experience to decide when to leave. *Journal of Experimental Biology*, 218(8):1175–1179, April 2015.

[31] Audrey Dussutour, Tanya Latty, Madeleine Beekman, and Stephen J Simpson. Amoeboid organism solves complex nutritional challenges. *Proceedings of the National Academy of Sciences of the United States of America*, 107(10):4607–4611, March 2010.

[32] Romain P Boisseau, David Vogel, and Audrey Dussutour. Habituation in non-neural organisms: evidence from slime moulds. *Proceedings of the Royal Society B: Biological Sciences*, 283(1829):20160446, April 2016.

[33] Vincenzo Bonifaci, Kurt Mehlhorn, and Girish Varma. Physarum can compute shortest paths. *Journal of theoretical biology*, 309:121–133, September 2012.

[34] Atsushi Tero, Seiji Takagi, Tetsu Saigusa, Kentaro Ito, Dan P Bebber, Mark D Fricker, Kenji Yumiki, Ryo Kobayashi, and Toshiyuki Nakagaki. Rules for biologically inspired adaptive network design. *Science*, 327(2010):439–442, 2010.

[35] Chris R Reid, Hannelore MacDonald, Richard P Mann, James A R Marshall, Tanya Latty, and Simon Garnier. Decision-making without a brain: how an amoeboid organism solves the two-armed bandit. *Journal of The Royal Society Interface*, 13(119):20160030, June 2016.

[36] Thomas W Schoener. Theory of Feeding Strategies. *Annual Review of Ecology and Systematics*, 2(1):369–404, November 1971.

[37] John Maynard Smith. Optimization theory in evolution. *Annual Review of Ecology, Evolution, and Systematics*, 1978(1978):31–56, 1978.

[38] Graham H Pyke. Optimal Foraging Theory: A Critical Review. *Annual Review of Ecology and Systematics*, 15(1):523–575, January 1984.

[39] Graham H Pyke, H Ronald Pulliam, and Eric L Charnov. Optimal Foraging: A Selective Review of Theory and Tests. *The Quarterly Review of Biology*, 52(2):137, June 1977.

[40] John Maynard Smith and G A Parker. The logic of asymmetric contests. *Animal Behaviour*, 24(1):159–175, February 1976.

[41] John Maynard Smith. The Theory of Games and the Evolution of Animal conflicts. *Journal of Theoretical Biology*, 47:209–221, 1974.

[42] F Bartumeus and J Catalan. Optimal search behavior and classic foraging theory. *Journal of Physics A: Mathematical and Theoretical*, 42(43):434002, October 2009.

[43] John R Krebs, John C Ryan, and Eric L Charnov. Hunting by expectation or optimal foraging? A study of patch use by Chickadees. *Animal Behaviour*, 22:953–964, 1974.

[44] Michael F Shlesinger, George M Zaslavsky, and Joseph Klafter. Strange kinetics. *Nature*, 363:31–37, May 1993.

[45] Andy M Reynolds. Current status and future directions of Lévy walk research. *Biology Open*, 7(1):bio030106, January 2018.

[46] Michael F Shlesinger, B J West, and Joseph Klafter. Lévy dynamics of enhanced diffusion: Application to turbulence. *Physical Review Letters*, 58(11):1100–1103, March 1987.

[47] Rosario N Mantegna and H. Eugene Stanley. Stochastic Process with Ultraslow Convergence to a Gaussian: The Truncated Lévy Flight. *Physical Review Letters*, 73(22):2946–2949, November 1994.

[48] M Levandowsky, J Klafter, and B S White. Swimming Behavior and Chemosensory Responses in the Protistan Microzooplankton as a Function of the Hydrodynamic Regime. *Bulletin of Marine Science*, 43(3):758–763, 1988.

[49] Kyriacos C Leptos, Jeffrey S Guasto, J P Gollub, Adriana I Pesci, and Raymond E Goldstein. Dynamics of Enhanced Tracer Diffusion in Suspensions of Swimming Eukaryotic Microorganisms. *Physical Review Letters*, 103(19), November 2009.

[50] Gandhimohan M Viswanathan, V Afanasyev, Sergey V Buldyrev, E J Murphy, P A Prince, and H Eugene Stanley. Lévy flight search patterns of wandering albatrosses. *Nature*, 381(6581):413–415, May 1996.

[51] Gabriel Ramos-Fernandez, José L. Mateos, Octavio Miramontes, Germinal Cocho, Hernan Larralde, and Barbara Ayala-Orozco. Lévy walk patterns in the foraging movements of spider monkeys (Ateles geoffroyi). *Behavioral Ecology and Sociobiology*, 55(3):223–230, January 2004.

[52] Tomohiro Shirakawa, Takayuki Niizato, Hiroshi Sato, and Ryota Ohno. Biased Lévy-walk pattern in the exploratory behavior of the Physarum plasmodium. *Biosystems*, 182:52–58, August 2019.

[53] Fernando A Oliveira, Rogelma M S Ferreira, Luciano C Lapas, and Mendeli H Vainstein. Anomalous Diffusion: A Basic Mechanism for the Evolution of Inhomogeneous Systems. *Frontiers in Physics*, 7, February 2019.

[54] Gandhimohan M Viswanathan, E P Raposo, and M G E da Luz. Lévy flights and superdiffusion in the context of biological encounters and random searches. *Physics of Life Reviews*, 5(3):133–150, September 2008.

[55] S J Gould and R C Lewontin. The spandrels of San Marco and the Panglossian paradigm: a critique of the adaptationist programme. *Proceedings of the Royal Society of London. Series B. Biological Sciences*, 205(1161):581–598, September 1979.

[56] G A Parker and John Maynard Smith. Optimality theory in evolutionary biology. *Nature*, 348(6296):27–33, November 1990.

[57] Sina M Adl, Alastair G B Simpson, Christopher E Lane, Julius Lukeš, David Bass, Samuel S Bowser, Matthew W Brown, Fabien Burki, Micah Dunthorn, Vladimir Hampl, Aaron Heiss, Mona Hoppenrath, Enrique Lara, Line le Gall, Denis H Lynn, Hilary McManus, Edward A D Mitchell, Sharon E Mozley-Stanridge, Laura W Parfrey, Jan Pawlowski, Sonja Rueckert, Laura Shadwick, Conrad L Schoch, Alexey Smirnov, and Frederick W Spiegel. The Revised Classification of Eukaryotes. *Journal of Eukaryotic Microbiology*, 59(5):429–514, September 2012.

[58] Susannah M Porter, Ralf Meisterfeld, and Andrew H Knoll. Vase-shaped Microfossils from the Neoproterozoic Chuar group, Grand Canyon: A Classification guided by modern testate amoebae. *Journal of Paleontology*, 77(3):409–429, May 2003.

[59] Thomas Cavalier-Smith, Anna Maria Fiore-Donno, Ema Chao, Alexander Kudryavtsev, Cédric Berney, Elizabeth A Snell, and Rhodri Lewis. Multigene phylogeny resolves deep branching of Amoebozoa. *Molecular Phylogenetics and Evolution*, 83:293–304, February 2015.

[60] Pauline Schaap, Israel Barrantes, Pat Minx, Narie Sasaki, Roger W Anderson, Marianne Bénard, Kyle K Biggar, Nicolas E Buchler, Ralf Bundschuh, Xiao Chen, Catrina Fronick, Lucinda Fulton, Georg Golderer, Niels Jahn, Volker Knoop, Laura F Landweber, Chrystelle Maric, Dennis Miller, Angelika A Noegel, Rob Peace, Gérard Pierron, Taeko Sasaki, Mareike Schallenberg-Rüdinger, Michael Schleicher, Reema Singh, Thomas Spaller, Kenneth B Storey, Takamasa Suzuki, Chad Tomlinson, John J Tyson, Wesley C Warren, Ernst R Werner, Gabriele Werner-Felmayer, Richard K Wilson, Thomas Winckler, Jonatha M Gott, Gernot Glöckner, and Wolfgang Marwan. The Physarum polycephalum Genome Reveals Extensive Use of Prokaryotic Two-Component and Metazoan-Type Tyrosine Kinase Signaling. *Genome Biology and Evolution*, 8(1):109–125, January 2016.

[61] Anna Maria Fiore-Donno, Sergey I Nikolaev, Michaela Nelson, Jan Pawlowski, Thomas Cavalier-Smith, and Sandra L Baldauf. Deep Phylogeny and Evolution of Slime Moulds (Mycetozoa). *Protist*, 161(1):55–70, January 2010.

[62] Jim Clark. The myxamoebae of Didymium iridis and Physarum polycephalum are immortal. *Mycologia*, 84(1):116–118, 1992.

[63] Israel Barrantes, Jeremy Leipzig, and Wolfgang Marwan. A next-generation sequencing approach to study the transcriptomic changes during the differentiation of Physarum at the single-cell level. *Gene Regulation and Systems Biology*, 2012:127–137, 2012.

[64] H Sauer, K Babcock, and H Rusch. Sporulation in Physarum polycephalum: A model system for studies on differentiation. *Experimental Cell Research*, 57(2-3):319–327, October 1969.

[65] Juliet Bailey. Building a plasmodium: Development in the acellular slime mould Physarum polycephalum. *BioEssays*, 19(11):985–992, November 1997.

[66] John W Daniel and Harold P Rusch. The pure culture of Physarum polycephalum on a partially defined soluble medium. *Journal of General Microbiology*, 25(1901):47–59, 1961.

[67] Edmund Guttes, Sophie Guttes, and Harold P Rusch. Morphological observations on growth and differentation of Physarum polycephalum grown in pure culture. *Developmental Biology*, 3(C):588–614, 1961.

[68] Wolfgang Gawlitta, Klaus V Wolf, Hans-Ulrich Hoffmann, and Wilhelm Stockem. Studies on microplasmodia of Physarum polycephalum - I. Classification and locomotion behavior. *Cell and Tissue Research*, 209(1):71–86, 1980.

[69] Klaus V Wolf and Wilhelm Stockem. Studies on microplasmodia of Physarum polycephalum: Endocytotic activity, morphology of the vacuolar apparatus and defecation mechanism. *Protoplasma*, 99(1-2):125–138, 1979.

[70] Klaudia Brix, Jörg Kukulies, and Wilhelm Stockem. Studies on microplasmodia of Physarum polycephalum - V. Correlation of cell surface morphology, microfilament organization and motile activity. *Protoplasma*, 137(2-3):156–167, 1987.

[71] Klaudia Brix and Wilhelm Stockem. Studies on microplasmodia of Physarum polycephalum. VII. Adhesion-dependent changes in the organization of the fibrillar actin system. *Cell Biology International Reports*, 11(7):529–536, 1987.

[72] Jörg Kukulies, Klaudia Brix, and Wilhelm Stockem. Studies on microplasmodia of Physarum polycephalum - VI. Functional analysis of a cortical and fibrillar actin system by use of fluorescent-analog cytochemistry. *Cell and Tissue Research*, 250(1):125–134, 1987.

[73] Christiane Ohl, Klaudia Brix, and Wilhelm Stockem. Studies on microplasmodia of Physarum polycephalum. Quantitative analysis of contractile activities and microfilament organization. *Cell and Tissue Research*, 264:283–291, 1991.

[74] Jean-Paul Rieu, Hélène Delanoe-Ayari, Seiji Takagi, Yoshimi Tanaka, and Toshiyuki Nakagaki. Periodic traction in migrating large amoeba of Physarum polycephalum. *Journal of The Royal Society Interface*, 12(106):1–10, 2015.

[75] Adrian Fessel, Christina Oettmeier, Erik Bernitt, Nils C Gauthier, and Hans-Günther Döbereiner. Physarum polycephalum Percolation as a Paradigm for Topological Phase Transitions in Transportation Networks. *Physical Review Letters*, 109(7):078103, August 2012.

[76] Kyoko Ogawa, Hisae Maki, Mamiko Sato, Hiroshi Ashihara, and Takako S Kaneko. Accumulation of noncrystalline cellulose in Physarum microplasmodia. *Protoplasma*, 250(5):1105–1113, October 2013.

[77] Fu-Sen Hu, Jim Clark, and Tim Lott. Recurrent Senescence in Axenic Cultures of Physarum polycephalum. *Microbiology*, 131(4):811–815, April 1985.

[78] R. Vimala Nair. Periodic events and cell cycle regulation in the plasmodia of Physarum polycephalum. *Journal of Biosciences*, 20(1):105–139, January 1995.

[79] Ryo Kobayashi, Atsushi Tero, and Toshiyuki Nakagaki. Mathematical Model for Rhythmic Protoplasmic Movement in the True Slime Mold. *Journal of Mathematical Biology*, 53(2):273–286, August 2006.

[80] R T M Poulter and Jennifer Dee. Segregation of factors controlling fusion between plasmodia of the true slime mould *Physarum polycephalum*. *Genetical Research*, 12(1):71–79, August 1968.

[81] Soichiro Tsuda, Klaus-Peter Zauner, and Yukio-Pegio Gunji. Robot control with biological cells. *Bio Systems*, 87(2-3):215–23, March 2007.

[82] Atsushi Tero, Kenji Yumiki, Ryo Kobayashi, Tetsu Saigusa, and Toshiyuki Nakagaki. Flow-network adaptation in Physarum amoebae. *Theory in Biosciences*, 127(2):89–94, May 2008.

[83] Chris R Reid and Madeleine Beekman. Solving the Towers of Hanoi - how an amoeboid organism efficiently constructs transport networks. *The Journal of Experimental Biology*, 216(Pt 9):1546–51, 2013.

[84] Liping Zhu, Masashi Aono, Song-Ju Kim, and Masahiko Hara. Amoeba-based computing for traveling salesman problem: long-term correlations between spatially separated individual cells of Physarum polycephalum. *BioSystems*, 112(1):1–10, April 2013.

[85] Daniel Schenz, Yasuaki Shima, Shigeru Kuroda, Toshiyuki Nakagaki, and Kei-Ichi Ueda. A mathematical model for adaptive vein formation during exploratory migration of Physarum polycephalum : routing while scouting. *Journal of Physics D: Applied Physics*, 50(43):434001, November 2017.

[86] Toshiyuki Nakagaki, Makoto Iima, Tetsuo Ueda, Yasumasa Nishiura, Tetsu Saigusa, Atsushi Tero, Ryo Kobayashi, and Kenneth Showalter. Minimum-Risk Path Finding by an Adaptive Amoebal Network. *Physical Review Letters*, 99(6):068104, August 2007.

[87] Silvano Martello and Paolo Toth. *Knapsack problems: algorithms and computer implementations*. Wiley-Interscience series in discrete mathematics and optimization. J. Wiley & Sons, Chichester ; New York, 1990.

[88] Brigitte Tenhumberg, Mike A. Keller, Hugh P Possingham, and Andrew J Tyre. Optimal patch-leaving behaviour: a case study using the parasitoid Cotesia rubecula: Patch leaving behaviour. *Journal of Animal Ecology*, 70(4):683–691, December 2001.

[89] Andra Thiel. How to measure patch encounter rate: decision-making mechanisms in the parasitic wasp Asobara tabida. *Animal Cognition*, 14(1):73–82, January 2011.

[90] John M C Hutchinson, Andreas Wilke, and Peter M Todd. Patch leaving in humans: can a generalist adapt its rules to dispersal of items across patches? *Animal Behaviour*, 75(4):1331–1349, April 2008.

[91] Tanya Latty and Madeleine Beekman. Food quality and the risk of light exposure affect patch-choice decisions in the slime mold Physarum polycephalum. *Ecology*, 91(1):22–27, 2010.

[92] Chris R Reid, Madeleine Beekman, Tanya Latty, and Audrey Dussutour. Amoeboid organism uses extracellular secretions to make smart foraging decisions. *Behavioral Ecology*, 24:812–818, 2013.

[93] Tuyen T M Huynh, Trung V Phung, Steven L Stephenson, and Hanh T M Tran. Biological activities and chemical compositions of slime tracks and crude exopolysaccharides isolated from plasmodia of Physarum polycephalum and Physarella oblonga. *BMC Biotechnology*, 17(1), December 2017.

[94] J Justin McCormick, Judith C Blomquist, and Harold P Rusch. Isolation and Characterization of an Extracellular Polysaccharide from Physarum polycephalum. *Journal of Bacteriology*, 104(3):1110–1118, 1970.

[95] Chris R Reid, Tanya Latty, Audrey Dussutour, and Madeleine Beekman. Slime mold uses an externalized spatial "memory" to navigate in complex environments. *Proceedings of the National Academy of Sciences of the United States of America*, 109(43):17490–17494, October 2012.

[96] York Winter and Kai Petra Stich. Foraging in a complex naturalistic environment: capacity of spatial working memory in flower bats. *Journal of Experimental Biology*, 208(3):539–548, February 2005.

[97] Yasutaka Kakiuchi and Tetsuo Ueda. Fragmentation of the plasmodium into equally sized pieces by low temperatures in the true slime mold Physarum polycephalum: A new morphogenesis. *Protoplasma*, 206(1-3):131–136, March 1999.

[98] Yasutaka Kakiuchi, Tetsuo Takahashi, Akio Murakami, and Tetsuo Ueda. Light Irradiation Induces Fragmentation of the Plasmodium, a Novel Photomorphogenesis in the True Slime Mold Physarum polycephalum: Action Spectra and Evidence for Involvement of the Phytochrome. *Photochemistry and Photobiology*, 73(3):324–329, 2001.

[99] Lewis Greenspan. Humidity fixed points of binary saturated aqueous solutions. *Journal of Research of the National Bureau of Standards Section A: Physics and Chemistry*, 81A(1):89, January 1977.

[100] Johannes Schindelin, Ignacio Arganda-Carreras, Erwin Frise, Verena Kaynig, Mark Longair, Tobias Pietzsch, Stephan Preibisch, Curtis Rueden, Stephan Saalfeld, Benjamin Schmid, Jean-yves Tinevez, Daniel James White, Volker Hartenstein, Kevin Eliceiri, Pavel Tomancak, and Albert Cardona. Fiji: an open-source platform for biological-image analysis. *Nature Methods*, 9(7):676–82, July 2012.

[101] H T Banks and Michele L Joyner. AIC under the framework of least squares estimation. *Applied Mathematics Letters*, 74:33–45, December 2017.

[102] Michael Snipes and D. Christopher Taylor. Model selection and Akaike Information Criteria: An example from wine ratings and prices. *Wine Economics and Policy*, 3(1):3–9, June 2014.

[103] Eric-Jan Wagenmakers and Simon Farrell. AIC model selection using Akaike weights. *Psychonomic Bulletin & Review*, 11(1):192–196, February 2004.

[104] M H Zwietering, I Jongenburger, F M Rombouts, and K van't Riet. Modeling of the bacterial growth curve. *Applied and Environmental Microbiology*, 56(6):1875–1881, June 1990.

[105] John W Daniel, Karlee L Babcock, Alice H Sievert, and Harold P Rusch. Organic Requirements and Synthetic Media for Growth of the Myxomycete Physarum Polycephalum. *Journal of Bacteriology*, 86(2):324–31, August 1963.

[106] Kenji Matsumoto, Seiji Takagi, and Toshiyuki Nakagaki. Locomotive Mechanism of Physarum Plasmodia Based on Spatiotemporal Analysis of Protoplasmic Streaming. *Biophysical Journal*, 94(7):2492–2504, April 2008.

[107] Christina Oettmeier, Jonghyun Lee, and Hans-Günther Döbereiner. Form follows function: ultrastructure of different morphotypes of *Physarum polycephalum*. *Journal of Physics D: Applied Physics*, 51(13):134006, April 2018.

[108] Adrian Fessel. *Topological dynamics of small degree networks*. Dissertation, Universität Bremen, Bremen, December 2018.

[109] Atsuko Takamatsu, Eri Takaba, and Ginjiro Takizawa. Environment-dependent morphology in plasmodium of true slime mold Physarum polycephalum and a network growth model. *Journal of Theoretical Biology*, 256:29–44, 2009.

[110] Abraham. Savitzky and Marcel J E Golay. Smoothing and Differentiation of Data by Simplified Least Squares Procedures. *Analytical Chemistry*, 36(8):1627–1639, July 1964.

[111] Edward J Schantz and Max A Lauffer. Diffusion Measurements in Agar Gel. *Biochemistry*, 1(4):658–663, July 1962.

[112] Tetsuo Ueda, Kazuyuki Terayama, Kenzo Kurihama, and Yonosuke Kobatake. Threshold phenomena in chemoreception and taxis in slime mold Physarum polycephalum. *The Journal of General Physiology*, 65(2):223–234, February 1975.

[113] J Crank. *The Mathematics of Diffusion*. Oxford University Press, Oxford, second edi edition, December 1975.

[114] Joachim Weickert. *Anisotropic Diffusion in Image Processing*, volume 256. Teubner-Verlag, Stuttgart, March 1998.

[115] Martin Dworkin and Kenneth H Keller. Solubility and diffusion coefficient of adenosine 3':5'-monophosphate. *The Journal of Biological Chemistry*, 252(3):864–5, February 1977.

[116] Jens Feder. Random sequential adsorption. *Journal of Theoretical Biology*, 87(2):237–254, November 1980.

[117] Kanishka Basnayake, Claire Guerrier, Zeev Schuss, and David Holcman. Asymptotics of extreme statistics of escape time in 1,2 and 3-dimensional diffusions. *Journal of Nonlinear Science*, September 2018. arXiv: 1711.01330.

[118] Carol L Manahan, Pablo A Iglesias, Yu Long, and Peter N Devreotes. Chemoattractant signaling in dictyostelium discoideum. *Annual Review of Cell and Developmental Biology*, 20:223–253, 2004.

[119] Randall L Kincaid and Tag E Mansour. Cyclic 3',5'AMP phosphodiesterase in Physarum polycephalum. II. Kinetic properties. *Biochimica et Biophysica Acta - General Subjects*, 588(3):342–350, 1979.

[120] N B Matveeva, V A Teplov, A R Nezvetsky, T G Orlova, and S I Beylina. Involvement of cyclic adenosine monophosphate in the control of motile behavior of Physarum polycephalum plasmodium. *Biophysics*, 57(5):644–650, 2012.

[121] Shun Zhang, Robert D Guy, Juan C Lasheras, and Juan C del Alamo. Self-organized mechano-chemical dynamics in amoeboid locomotion of Physarum fragments. *Journal of Physics D: Applied Physics*, 50(20):204004, May 2017.

[122] Jordi Vallverdú, Oscar Castro, Richard Mayne, Max Talanov, Michael Levin, Frantisek Baluška, Yukio Gunji, Audrey Dussutour, Hector Zenil, and Andrew Adamatzky. Slime mould: The fundamental mechanisms of biological cognition. *Biosystems*, 165:57–70, March 2018.

[123] Christopher T Calderone, Stefanie B Bumpus, Neil L Kelleher, Christopher T Walsh, and Nathan A Magarvey. A ketoreductase domain in the PksJ protein of the bacillaene assembly line carries out both alpha- and beta-ketone reduction during chain growth. *Proceedings of the National Academy of Sciences of the United States of America*, 105(35):12809–14, September 2008.

[124] Peter J M Van Haastert and Peter N Devreotes. Chemotaxis: signalling the way forward. *Nature Reviews Molecular Cell Biology*, 5(8):626–634, August 2004.

[125] E Pálsson and Edward C Cox. Origin and evolution of circular waves and spirals in Dictyostelium discoideum territories. *Proceedings of the National Academy of Sciences of the United States of America*, 93(3):1151–1155, 1996.

[126] Iyyappan Rajan, Remitha Rabindran, N Nithya, T Lakshmipriya, P R Jayasree, and P R M Kumar. Assessment of cell cycle phase-specific effects of zerumbone on mitotically synchronous surface cultures of Physarum polycephalum. *Protoplasma*, 251(4):931–941, January 2014.

[127] Britta Werthmann and Wolfgang Marwan. Developmental switching in Physarum polycephalum : Petri net analysis of single cell trajectories of gene expression indicates responsiveness and genetic plasticity of the Waddington quasipotential landscape. pages 1–35, 2017.

[128] Adrian Fessel, Christina Oettmeier, and Hans-Günther Döbereiner. Structuring precedes extension in percolating Physarum polycephalum networks. *Nano Communication Networks*, April 2015.

[129] Juliet Lee, Akira Ishihara, Julie A Theriot, and Ken Jacobson. Principles of locomotion for simple-shaped cells. *Nature*, 362(6416):167–171, March 1993.

[130] Chris R Reid and Tanya Latty. Collective behaviour and swarm intelligence in slime moulds. *FEMS Microbiology Reviews*, (July):1–9, August 2016.